UDC: 61 ISSN 1409-9837

ZAMM

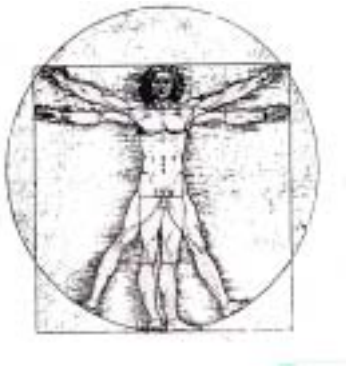

MAAM

ACTA MORPHOLOGICA

PUBL I KAC I JA NA ZDRU@EN I ETO NA ANATOM I I MORF OLOZ I NA MAKEDON I JA

PUBLICATION OF MACEDONIAN ASSOCIATION OF ANATOMISTS AND MORPHOLOGISTS

Vol.9(1) 2012

ACTA MORPHOLOGICA
Medical journal
of
Macedonian Association of Anatomists and Morphologists (MAAM)

Published
Twice a year

Print
Printing office"Ilko"-Gostivar

Corresponding address
Institute of Anatomy, Medical Faculty, 50 Divizija 6, Skopje, R.Macedonia
Tel/fax:++389 2 3125304
e-mail:acta_morphologica@yahoo.com

CONTENT

ACTA MORPHOLOGICA is ***available on***

UDK: 611.133.33

ANATOMY OF MIDDLE CEREBRAL ARTERY

Papazova Marija, Zhivadinovik J, Trpkovska B, Dodevski A
Institute of Anatomy, Medical Faculty, Skopje, R. Macedonia

Abstract

Cerebral circulation, especially arterial, in recent decades has attracted the interest of anatomsits and clinicians. The importance of the cerebral arterial system is due to the exceptional importance of the organ that it supplies and the fact that cerebrovascular pathological processes are the leading place primary cause of morbidity and mortality.

The aim of this study was to determine the morphological and topographic characteristics of the middle cerebral artery: shape, position, diameter, length; the number, types and distribution of its branches and the correlation of these vessels with adjacent brain structures.

The examination was made on 50 specimens of human brain fixed in 10% formalin. The shape, postion, diameter and length of the middle cerebral artery were assessed, as well as the number, types and distribution of branches and correlation with adjacent brain structures.

We present the obtained results and the most common variations.

The importance of the *MCA* is a result of the significance of the structures it supplies.

Key words: middle cerebral artery, anatomy, vascularisation

Introduction

Cerebral circulation, especially arterial, in recent decades has attracted the interest of anatomsits and clinicians. The importance of the cerebral arterial system is due to the exceptional importance of the organ that it supplies, and to the fact that cerebrovascular pathological processes are at the leading place as the primary cause of morbidity and mortality.

The aim of this study was to determine the morphological and topographic characteristics of the middle cerebral artery:

- shape, position, diameter, length;
- number, types and distribution of branches;
- correlation with adjacent brain structures.

Material and methods

Macroscopical investigations of morphological and topographic characteristics of the middle cerebral artery were performed in the laboratory of the Institute of Anatomy, applying inspecion and disection methods.

The examination was made on 50 specimens of human brain fixed in 10% formalin. The arachnoidea from the base and lateral sides of the brain was removed, and careful inspection and dissection of the trunk and branches of middle brain artery were made. Precautions were taken to avoid disruption of the normal topographical relationships.

The shape, position, diameter and length of the middle cerebral artery were assessed, as well as the number, types and distribution of branches and correlation with adjacent brain structures.

All data for the artery and its branches are illustrated semischematically on uniform drawings obtained by crossing the orriginal picture of the base of the brain and the external side of brain hemisphere.

Results

The analysis of a. cerebri media made on 50 specimens of human brain showed that this artery was the most developed branch of a. carotis interna, with the usual distribution and correlations with adjacent brain structures (Fig.1).

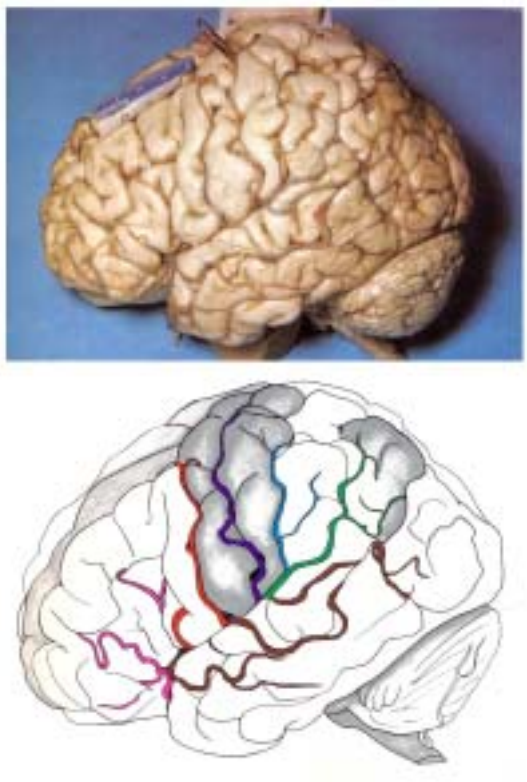

Fig. 1. Leptomeningeal branches of MCA at the lateral surface of brain
PF (rose), PrC (red), CA (violet), AP (blue), ANG (green), TO, AT, MT, PT (brown)

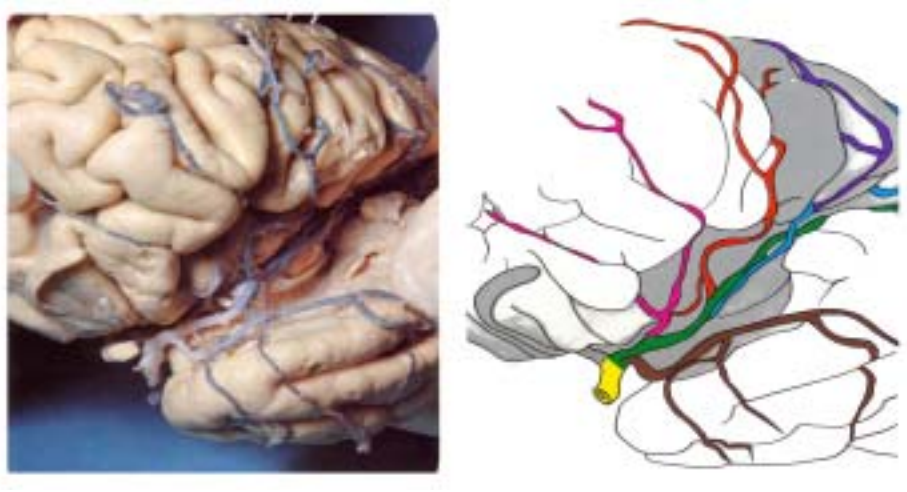

Fig. 2. M_1 and M_2 segments of MCA and insuloopercular branches

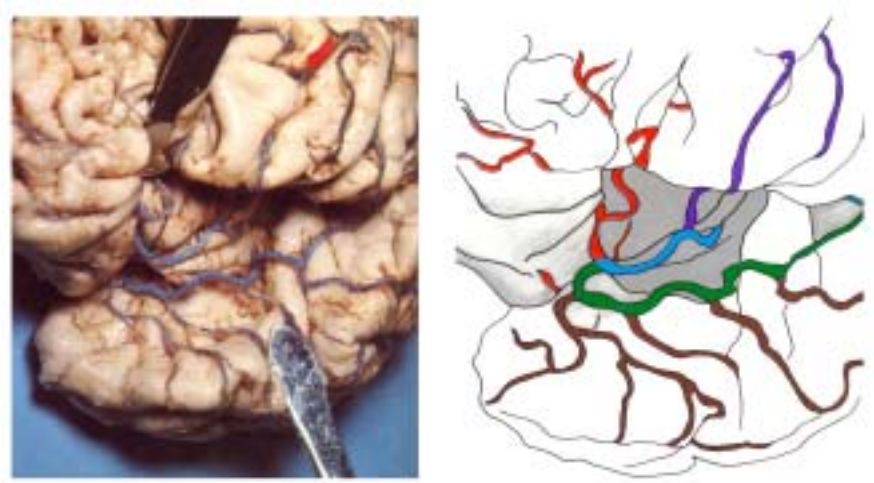

Fig. 3. Three terminal branches of MCA
CA (violet) originates from PrC (red), and AP (blue) from ANG (green)

The average diameter of the proximal segment M_1 ranged from 2.4 to 4 mm, and the average length was 15 mm; and the average diameter of the distal segment M_2 ranged from 2.2 to 3.9 mm.

The ending of the distal segment M_2 was singular in 15% of cases. In 52% of cases it was divided in two terminal branches, dorsal and ventral (Fig.2) and in 24% of cases in three terminal branches (dorsal, ventral and medial) (Fig.3). There were four terminal branches (dorsal, ventral and two medial) in 9% of cases.

The average diameter of the dorsal terminal branch was 2.0 mm, and its average length was 10.5 mm in cases with terminal bifurcation. The average diameter of the ventral terminal branch was 2.1mm, and the average length 10.0 mm.

The average diameter of the dorsal terminal branch was 1.5 mm, and its average length was 13.1 mm in cases with terminal trifurcation. The average diameter of the medial branch was 2.0 mm, and the average length 14.0 mm. The average diameter of the ventral terminal branch was 2.1mm, and the average length 10.0 mm.

The terminal branches in cases with terminal tetrafurcation were radially distributed, and their average diameter varied from 0.7 to 0.9 mm.

The following branches of the MCA were identified:

- a. prefrontalis was singular in 50% of the cases, and it was double in the remaining;
- a. centralis was double in 50% of the cases. Its diameter was from 0.7 to 1.8 mm (1.1mm);
- a. parietalis anterior‘s diamter ranged from 0.6 to 1.7 mm (1.4 mm) and it was singular;
- a. parietalis posterior originated directly from the trunk in 7% of the specimens, and from neighboring branches in 93%. The diameter of the artery was from 0.9 to 1.7 mm (1.4 mm);
- a. gyri angularis‘ diameter ranged from 0.7 to 2.0 mm (1.6 mm). This was the most developed branch of MCA in 80% of the analyzed specimens;
- a. temporooccipitalis was formed independently in 60% of cases and the rest 40% were divisions of a common

trunk with a. gyri angularis. Its diameter was 0.7 - 2.2 mm (1.2 mm);
- a. temporalis posterior's diameter ranged from 0.5 to 2.1 mm (1.2mm);
- a. temporalis media diameter ranged from 0.7 to 1.4mm (1.1mm), and a. temporalis anterior from 0.6 to 1.3 mm (0.9mm).

A duplication of the MCA was registered in 0.7 – 2.7% of cases.

Accessory middle brain artery (a. cerebri media accessoria) was present in 0.3-2.7% of cases.

Discussion

Anatomy of middle cerebral artery

The middle cerebral artery (a. cerebri media; middle cerebral artery - *MCA*) is the most developed terminal branch of the a. carotis interna. *MCA* extends on the base of the brain and then enter the insuloopercular part through the proximal part of the Sylvius sulcus.There it gives rise to the largest number of leptomeningeal branches, which come to the surface through the sulcus of Sylvius and are distributed throughout the lateral side of the hemisphere. The MCA has two main segments, proximal and distal (1,2,3).

The Proximal segment (M_1) runs from the a. carotis interna to the limen of the insula, between the temporal and the frontal lobes.

The intermediate part, between the proximal and the distal part, is named as the knee of the MCA.

There are 2 to 21 perforant branches *(aa. lenticulostriatae)*; their diameter being between 80 to 900 μm. They originate directly from the M_1 segment or from the leptomeningeal branches. They run into the brain parenhima through the openings of the substantia perforata anterior. The perforanted branches are usually divided into medial (thin) and more developed lateral branches. One of the most developed lateral branches is the Charcot artery (arteria haemorrhagiae cerebri). The lenticulostrial arteries most commonly supply: the rostrodorsal part of the head and the largest part of the body of the nucleus caudatus, the whole putamen (except for the ventrorostral part), the lateral segment of the globus palidus (except for the ventrorostral part), the dorsal part of the capsula interna (i.e. the dorsal part of the crus anterius and genu, as almost the whole dorsal part of crus posterior) (4).

A. orbitofrontalis lateralis continues either as singular or with a common trunk along with the first perforal artery. The latter is the most proximal of all and it supplies the lateral part of the gyri orbitales.

A. temporalis originates either from the M_1 or from a. temporalis anterior. It supplies the temporal pole and sometimes the ventral part of the uncus.

The *distal segment (M_2)* extends from the limen of the insula to the terminal point of the MCA. From the main trunk of M_2, leptomeningeal branches arise, singulary or together with common trunk and diverge throughout the insula. At the level of the marginal sulcuses of the insula they change the course making anses, surround certain parts of the operculum and finally, through the sulcus of the Sylvius come out to the surface. The described vessels are called insuloopercular arteries. On the lateral carotid arteriograms they could be seen forming the so called triangle of the Sylvius, which is a projection of the insula. The lower vertex of the triangle is formed by the knee of the MCA, at the level of the insula. The frontal vertex is formed by the most rostral upper insuloopercular artery ansa. The back vertex is the so called point of the Sylvius, which is located on the level at the most caudal part of the insula, i.e. the most medial part of the gyrus temporalis transversus. The expansive intracranial processes can dislocate and deform the parts of the Sylvius triangle.

The following leptomeningial branches can be recognized (1, 3, 5):

A. prefrontalis (PF) - originates from the common trunk together with a. orbitofrontalis medialis and a. precentralis. It supplies the largest part of the lateral prefrontal cortex, premotor field and the Broca zone.

A. precentralis (*PrC)* - usually is a singular branch, located in or near by the groove that carries the same name. It supplies one part of the Broca zone, the caudal part of the pre-motor cortex, the frontal eye field and part of the primary motor cortex.

A. centralis (*CA)* - arises either singular or with common trunk with the neighboring branches. It is usually located in sulcus centralis or in its proximity. It usually supplies the deep part and walls of the sulcus centralis, the caudal part of the gyrus precentralis and the rostral part of the gyrus postcentralis.

A. parietalis anterior – passes through or near the sulcus postcentralis. It supplies the caudal part of the gyrus postcentralis and rostral part of the gyrus supramarginalis.

A. parietalis posterior – is one of the most important branches of the *MCA*. It is located in the dorsocaudal part of the gyrus supramarginalis and terminates in the sulcus intraparietalis, supplying these structures.

A. gyri angularis ANG - is the most caudal and usually the longest, singular branch of the *MCA*. It passes transversaly throughout the temporal part of the gyrus supramarginalis or throughout the most caudal part of the gyrus temporalis superior. It usually terminates in gyrus angularis divided in two branches, which usually end in the gyri occipitales laterales and supplies all these structures; sometimes supplying the most caudal part of the stria at the level of the occipital pole.

A. temporooccipitalis (*TO)* - is a strong and longer branch of the MCA, which extends obliquely caudally and ventrally through the caudal third of gyrus temporalis medius et inferior and terminates at gyri occipitales laterales.

A. temporalis posterior (*PT)* - extends into the caudal parts of gyrus temporalis superior, medius et inferior.

A. temporalis media et anterior (MT, AT) - supplies the rostral parts of all three temporal gyri.

Variations of the middle cerebral artery

The variations of the a. cerebri media are very rare compared to the other brain vessels. An isolated aplasia of this blood vessel has not been noted. The fenestration is also very rare and it is usually found in the M_1 segment. The most common variations are accessory arteries and duplications of *MCA* (1, 5, 6). When there is a duplication of the MCA, two vessels (dorsal and ventral) arise from a. carotis interna. All temporal branches usually arise from the ventral *MCA*, and the leptomeningeal branches from the dorsal one. The perforant branches originate from both arteries.

The accessory cerebral artery (a. cerebri media accessoria) originates from the proximal segment of the *ACA*. It runs caudally and laterally and accompanies a. cerebri media. The accessory *MCA* usually gives rise to the lateral orbitofrontal branch, one perforant branch, and several perforant vessels.

Clinical anatomy of the middle cerebral artery

The importance of the *MCA* is due to the importance of the structures it supplies. The majotity of strokes originate in the territory of the *MCA*. The term occlusion encompasses all causes of regional arterial failure other than aneurysms (4, 7, 8,9). The embolism and lacunar strokes are more frequent in the later years of life.

Embolism

The embolus can be stuck in different parts of each artery, the trunk, the proximal and distal division or in the cortical branches.

The trunk

Occlusion of the trunk affects both, central and cortical branches, inducing contralateral hemiplegia, extensively expressed contralateral loss of sensitivity and directing of the eyes to the side of the stroke. The left-sided lesions are usually associated with a global aphasia and the right sided with a contralateral loss of sensitivity. Many patients die in coma, caused by the compression of the middle brain due to the edematous zone of the stroke. In some patients the situation rapidly improves in a few days.

Proximal divisions

The embolus in the upper divisions causes contralateral paresis (weakness) and a cortical type of loss of sensitivity of the face and arm, followed by a disarticulation, caused by the damages of the supranuclear pathways involved in the articulation. The left sided lesions are usually followed by a Broca aphasia, and the right sided with a contralateral disorder.

Distal divisions

The embolus in the lower divisions causes contralateral homonim hemianopia, and sometimes a state of confusion and disturbance which is a result of the infringement of the lymph pathway in the temporal lobe. The left sided lesions are usually followed by Werniske aphasia, alexia and sometimes by a ideomotor apraxia.

Embolism of the branches

The following isolated changes are caused by the embolus stuck in one of the cortical branches.

A. orbitofrontalis

Elements of the prefrontal syndrome can be present.

A. precentralis

Broca aphasia (left sided), monotone speech patterns (right sided).

A. centralis (Rolando)

Contralateral loss of the motor function or the sensitive function of the whole face and the left arm.

A. parietalis posterior

Contralateral disturbance (especially in the right sided lesions), tactile anomia.

A. giri angularis

Contralateral homonim hemianopia; alexia with a left sided lesion.

Aa. temporales posterior et media

Werniske aphasia (left-sided lesion), sensitive aprosodia (right sided lesion).

Lacunar strokes

The lacunar strokes should be considered when the clinical data point to a small lesion (7, 10). The most common are:

Clear motor hemiparesis, caused by the lacunar stroke in the corona radiate or capsule interna. The weakness is usually manifested in the lower part of the face and arm and there are sensitive and cortical disorders.

Clear sensitive syndrome, caused by the lacunar stroke in the ventral back nucleus of the thalamus. There is a strong disorder of the tactile recognition of the contralateral extremity, together with the sensitive ataxia.

Syndrome of dysarthria and clumsy arm movementcaused by the lacuna between the fibers which come down towards or in the genu capsulae internae. These have corticonuclear descendent fibers, which pass toward the contralateral motor nucleus of the pons or the medulla oblongata and fibers from the premotor cortex, which takes part in the contralateral manual control. The dominant signs are dysarthria which is a result of paresis of the lips, tongue and jaw muscles and clumsiness in arm movements.

Haemorrhage

Cerebral haemorrhages are usually caused by one of the aa. lenticulostriatae of MCA (8,9), due to prior systemic hypertension. The most common location is putamen with spreading in the anterior and posterior crus of capsula interna. Haematomas may be small as pease or as a golf ball. Large hemorrhages rupture into the lateral ventricle and is usually fatal within 24 hours. Typical clinical sign is a severe, sudden headache with loss of consciousness in several minutes. The eyes tend to move to the side of the lesion. The awakening is followed by a complete flaccid hemiplegia (except for the upper face). Tendon reflexes are absent on hemiplegical side, and the Babinski sign is present. After the stroke that affects the left capsula interna, right-handed people frequently have initial clumsiness on the left hand. Studies made by functional magnetic resonance imaging suggest that in healthy right-handed left motor cortex is more active during

the left-hand movement, than is during the right motor cortex in the movement of the right hand. In other words, the left motor cortex has a higher level of bilateral control. The final result of capsular stroke is spastic hemiparesis with hemihypesthesia (reduced sensitivity). The typical position while walking is: the elbow and finger in flexion, and the leg moves forward with circumduction because of antigravitation tonus of the muscles. During early rehabilitation, immobilizing of the hand is necessary to avoid subluxation of the shoulder (partial subluxation).

The middle cerebral artery is an essential component of the cerebral vascular system with great morphological and clinical significance resulting from the importance of the structures which it supplies as well as from the polymorphism of the pathological processes that affect this artery.

References

1. Papazova M, Lazarova D, Zhivadinovik. Vaskularizacija na mozokot. UKIM, Skopje, 2011.
2. Duvernoy HM, Delon S, Vannson JL. Cortical blood vessels of the human brain. Brain Res Bull 1981; 7:519-30.
3. Lee RM.Morphology of cerebral arteries. Pharmacol Ther. 1995;66(1):149-73.
4. Vitoseviæ Z, Cetkoviæ M, Vitoseviæ B, Joviæ D, Rajkoviæ N, Millisavljeviæ M. Blood supply of the internal capsule and basal nucleiSrp Arh Celok Lek. 2005;133 (1-2):41-5.
5. Scremin IU. Cerebral vascular system. 2nd ed. Amsterdam: Elsevier; 2004.
6. Mohr JP, Lazar RM, Marshall RS, et al. Middle cerebral artery disease. In : Barnett HJM, Mohr JP, Stein BM, et al, eds. Stroke: pathophysiology, diagnosis and menagment. 3rd edn. New York: Churchill Livingstone; 1998: 427-80.
7. Amarenco P, Caplan LR, Pessin MS. Vertebrobasilar oclusive disease. In: Barnett HJM, Mohr JP, Stein BM, et al, eds. Stroke: pathophysiology, diagnosis and menagment. 3rd edn. New York: Churchill Livingstone; 1998: 513-98.
8. Mohr JP, Pessin MS. Middle cerebral artery disease. In : Barnett HJM, Mohr JP, Stein BM, et al, eds. Stroke: pathophysiology, diagnosis and menagment. 3rd edn. New York: Churchill Livingstone; 1998: 481-502.
9. Shibuya M. Brain angiogenesis in developmental and pathological processes: therapeutic aspects of vascular endothelial growth factor. FEBS J. 2009 Sep;276(17):4636-43. Epub 2009 Jul 31. Review.
10. Wardlaw JM. What causes lacunar stroke? J Neurol Neurosurg Psychiatry 2005; 76:617-9.

UDK: 611.127

ANATOMICAL FEATURES OF RIGHT ATRIUM

Zhivadinovik Julija, Lazarova-Tosovska D, Papazova M, Matveeva N, Dodevski A
Institute of Anatomy, Medical Faculty, Skopje, R. Macedonia

Abstract

The anatomy of the inside surface of the right atrium became more interesting with the development of ablation techniques for treatment of atrioventricular nodal reentry tachycardia (AVNRT).

The aim of this study was to present the dimensions of the ostium of the coronary sinus, the tricuspid valve anulus and the triangle of Koch, and to describe the arrangement of the superficial atrial muscle fibers in and around the area of the triangle of Koch.

The examination was made on 100 human hearts obtained after autopsies of patients who died from no cardiac reasons. The diameter of the orifice of the coronary sinus, the circumference of the tricuspid valve anulus and the dimensions of the triangle of Koch (sides a, b, c and the area) were measured and the arrangement of the superficial, subendocardial muscle fibers was analyzed.

The mean values of the lenght of the side a was 26.1 $\pm$ 3.0 mm, side b 20.2 $\pm$ 3.6 mm and side c 24.5 $\pm$ 2.5 mm. The mean value of the area of the triangle of Koch was 256, 2 $\pm$ 6.7 mm^2.The mean value of the diameter of the ostium of the coronary sinus was 9.3 $\pm$ 1.8 mm.The mean value of the length of the tricuspid leaflet was 107.8 $\pm$ 10.3 mm. We presented the usual pattern and the variations of atrial subendocardial muscle fibers orientation.

Key words: right atrium, triangle of Koch, coronary sinus, tricuspid valve

Introduction

The anatomy of the inside surface of the right atrium became more interesting with the development of ablation techniques for treatment of atrioventricular nodal reentry tachycardia (AVNRT) (1, 2).

The interior surface of the right atrium consists of three parts: a smooth-walled venous component, posteriorly, leading anteriorly, to the vestubule of the tricuspid valve and the auricule. The smooth-walled venous part receives the opening of the venae cavae and coronary sinus. The wall of the vestibule has a ridged surface and that of the auricle is trabeculated (3).

The *superior vena cava (vena cava superior - SVC)*, that returns the blood from the upper half of the body, opens into the upper and back part of the atrium, the direction of its orifice being downward and forward. Its opening has no valve.

The *inferior vena cava***,** larger than the superior, returns the blood from the lower half of the body, and opens into the lowest part of the atrium, near the atrial septum. Its orifice is directed upward and backward, and, along its lateral, or right margin it is guarded by a flap-liked valve of varyng size, the *valve of the inferior vena cava* (*Eustachian valve*). The valve is a fold of endocardium. It is semilunar in form, its convex margin being attached to the anterior margin of the orifice; its concave margin, which is free, ends in two cornua, of which the left is continuous with the anterior edge of the limbus of oval fossa while the right is lost on the wall of the atrium. In the fetus this valve is of large size, and serves to direct the blood from the inferior vena cava, through the foramen ovale, into the left atrium. In the adult it occasionally persists, and may assist in preventing the reflux of blood into the inferior vena cava; more commonly it is small, and may present a cribriform or filamentous appearance.

The *coronary sinus (sinus coronarius - SC)* opens into the right atrium, between the orifice of the inferior vena cava, the oval fossa and the vestibule of the atrioventricular opening. It returns the majority of blood from the heart itself and is it is often guarded by a thin, semicircular valve, the *valve of the coronary sinus (valve of Thebesius*). The upper part of this valve joins with the Eustachian valve and from this commissure, a tendinous structure, called the *tendon of Todaro*, runs forward to the sinus septum (the septum between the sinus septum and the oval fossa), and inserts into the central fibrous body..

The *foramina venarum minimarum (foramina Thebesii*) are the orifices of minute veins (*venaecordis minimae)*, which return blood directly from the muscular substance of the heart.

Antero-inferior in the right atrium is the large, oval vestibule leading to the orifice of the tricuspid valve.

A triangular zone (*the triangle of Koch*) is found between the attachment of the septal leaflet of the tricuspid valve, the anteromedial margin of the orifice of the coronary sinus, and the round, collagenous, palpable, subendocardial tendon of Todaro. The triangle indicates the site of the atrioventricular node and its atrial connections.

Anterosuperior to the insertion of the tendon of Todaro, the septal wall is the atrioventricular component of the membranous septum, intervening between the right atrium and subaortic outlet of the left ventricle. The atrial wall bulges anterosuperiorly above the membranous septum. This area is the aortic mound (torus aorticus) and marks the location of the non-coronary sinus of the aorta with its enclosed valvar cusp.

The *fossa ovalis* is an oval depression on the septal wall of the atrium, and corresponds to the the foramen ovale in the fetus. It is situated at the lower part

of the septum, above and to the left of the orifice of the inferior vena cava.

The *limbus fossae ovalis* (*annulus ovalis*) is the prominent oval margin of the fossa ovalis. It is most distinct above and at the sides of the fossa; below, it is deficient. A small slit-like valvular opening is occasionally found, at the upper margin of the fossa, leading upward beneath the limbus, into the left atrium; it is the remains of the fetal aperture between the two atria.

The *intervenous tubercle* (*tuberculum intervenosum; tubercle of Lower*) is a small projection on the posterior wall of the atrium, above the fossa ovalis. It is distinct in the hearts of quadrupeds, but in men is scarcely visible. It was supposed by Lower to direct the blood from the superior vena cava toward the atrioventricular opening.

The right atrium, in and around the triangle of Koch, can be divided into four areas with relativevly similar orientation of the superficial muscle fibers (4). The variability in the arrangement of these fibers may be one of the factors influencing the route for impulses entering the AV node, which is located beneath the intersection of sinus septal, vestibular and anterosuperior areas. The posterorinferior area located behind and beaneath the orifice of the coronary sinus, contains mostly longitudinaly oriented fibers that extend from pectineate muscles to the isthmus between the orifice of the coronary sinus and the septal leaflet of the tricuspid valve. The sinus septal (SS) area is made up of circumferential fibers that run between the orifices of coronary sinus and inferior vena cava, encircling the oval fossa. The fibers in the vestibular (V) area provide a continuation of the P fibers toward the AV node, but also turn in a spiral pattern around the orifice of the coronary sinus as well as anteroposteriorly to join the SS fibers. Anterosuperior (A) area generaly contains two groups of superficial fibers: circumferential fibers passing in front of the oval fossa, and longitudinal fibers protruding over the AV node.

The **aim** of this study was to present the dimensions of the ostium of the coronary sinus, the tricuspid valve anulus and the triangle of Koch, and to describe the arrangement of the superficial atrial muscle fibers in and around the area of the triangle of Koch.

Material and methods

The examination was made on 100 human hearts obtained after autopsies of patients who died from no cardiac reasons. The hearts were removed intact, together with the proximal parts of the great arteries and veins, and fixed in 10% formaldehyde, for at least 72 hours. The right atrium was opened through an incision between the superior and inferior caval venous orifices, and then by extending an incision perpendicular to the first along the lateral wall of the atrium into the right appendage.

The diameter of the orifice of the coronary sinus, the circumference of the tricuspid valve anulus and the dimensions of the triangle of Koch were measured by caliper. The numeric values of the triangle of Koch were determined by measuring its sides (a, b, c): side a is the length of the tendon of Todaro, side b is the distance from the tendon of Todaro to the septal leaflet of the tricuspid valve (at the right angle to the leaflet) passing through the coronary sinus and side c is the distance from the insertion of the side b to the central fibrous body, along the septal leaflet of the valve. The area of the triangle is calculated as P = b x c/ 2.

For analyzing the arrangement of the superficial muscle fibers, the right atrium was divided into four areas: posteroinferior (P), sinus septal (SS), vestibular (V) and anterosuperior (A) (Fig.1). Atrial endocardium was carefully peeled, and inspected using magnifying glass (x10). The orientation of the fibers was described as: horizontal (parallel to the AV junction), longitudinal (parallel to the interatrial groove at the right angle to the AV junction) and oblique (oblique to the AV junction).

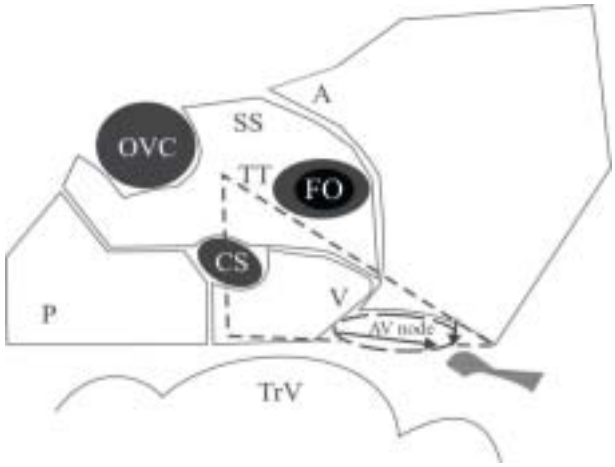

Fig. 1. Right atrium divided into four areas: posteroinferior (P), sinus septal (SS), vestibular (V) and anterosuperior (A)

Results

The results obtained for the dimensions of the triangle of Koch have shown that the mean value of the length of side a was 26.1 ± 3.0 mm, of side b 20.2 ± 3.6 mm and of side c 24.5 ± 2.5 mm. The mean value of the area of the triangle of Koch was 256. 2 ± 6.7 mm^2.

The mean value of the diameter of the ostium of the coronary sinus was 9.3 ± 1.8 mm.

The mean value of the length of the tricuspid leaflet was 107.8 ± 10.3 mm.

The analysis of the arrangement of the atrial subendocardial muscle fibers yieldedthe folowing results:

In the posteroinferior (P) area superficial, sudendocardial muscle fibers had longitudinal orientation in 91%, oblique orientation in 6% and horizontal in 3% of the specimens.

In the vestibular (V) area 95% of specimens had horizontal orientation of the subendocardial fibers, 3% had oblique and 2% longitudinal fiber orientation.

In the sinus septal (SS) area 94% of specimens had horizontal fiber orientation, 5% oblique and 1% longitudinal orientation.

In anterosuperior (A) area two types of fiber orientation (oblique and horizontal) were present in 90% of cases. In 7% of specimens the endocardial fibers had longitudinal and in 3% oblique orientation of muscle fibers.

Discussion

Authors who perform electrophysiological procedures of radiofrequent catheter ablation (Mc Guire), consider that the triangle has uniform size among patients and they analyze the triangle in boundaries that are significantly smaller than the anatomically accepted ones (5). These data present values obtained indirectly using mathematical formula, during electrophysiological procedures or under direct vision during surgical procedures for cure of supraventricular tachycardia. These authors were interested in the part of the anatomically accepted area of the triangle of Koch alone, since AV node tissue and slow and fast conducting pathways, are located near the apex of the triangle, 1 cm in front of the orifice of the coronary sinus, which is within the scope of this measuring. The results obtained with the postmortal measuring of the anatomical boundaries of the triangle of Koch in our study, are in agreement with published data, and have demonstrated differences in the area of the triangle among patients (5, 6).

During electrophysiological procedures the ostium of the coronary sinus (OCS) provides a useful route for mapping and ablation of left-sided accessory pathways. In addition, the OCS is an electrophysiologically active structure. Previous studies have demonstrated the capability of spontaneous depolarization and slow conduction in the smooth muscle of the CS, providing inherent automaticity (7, 8). Also, the atrial myocardial sleeve that covers the proximal CS provides the ability for conduction and automaticity, forming an electrical connection between the two atria. Studies have shown that this connection is of clinical importance as it may be a source of arrhythmias such as atrial fibrillation (9). Active myocardium within the CS may serve either as a source for abnormal automaticity generating a focal tachycardia or as a part of a reentrant circuit. In patients with atrial fibrillation, CS myocardium may also initiate recurrent atrial fibrillation. Since the CS is one of the connections between the right and left atria, with Bachmann's bundle forming the other important connection, reentrant tachycardia involving the CS muscle and both atria are sometimes seen in patients with marked atrial enlargement, especially after a surgical maze procedure.

Marked changes in fiber orientation in the zone of intersection of fibers from SS, V and A areas (at the apex of the triangle of Koch) could account for discontinuity in the spread of the excitatory wave front (2, 10, 11, 12). In our study 91% of examined specimens had the usual architecture of the subendocardial atrial muscle fibers, and most variations were in area A (longitudinal fiber orientation in 7% of the specimens), which was in agreement with the literature. Privious studies have shown that conduction of the impulses within the muscular walls of the atriums reflect the arrangement of well developed muscular bundles. Experimentaly were demonstrated two broad bands of atrial approaches to the AV node, one from the inferior region beneath the orifice of the coronary sinus (V area), and the other from the SS area (2, 6, 10). These approaches reflected the geometry of the right atrium produced by the orifices of the caval veins, the coronary sinus, and the oval fossa.

The relationship between the above described gross morphologic picture of the atrial approaches and the compact AV node is of enormous importance. The orientation of the superficial muscle fibers correlated with the known patterns of activation. Propagation of impulses in a direction parallel to muscle fibers is faster than propagation in a direction at right angles to the fiber (anisotopic conduction). Thus, the variability in the orientation of the fibers in the approaches may influence the input of impulses to the AV node. The variation of changes in orientation from one area to another, or within the same area, may potentiate reentrant circuit.

References

1. Janse MJ et al. AV Nodal Reentry.Part I. J Cardiovas Electrophysiol 1993; 4 (5): 561-72.
2. Anderson RH, Webb S. Clinical Anatomy of the Atrial Septum With Reference to Its Developmental Components. Clin Anat 1999; 12:362-74.
3. Gabella G. Chapter 10 Cardiovascular System. In: Gray's Anatomy. New York: Churchill Livingstone; 1995.
4. Sanchez-Quintana D. et al. Architecture of the Atrial Musculature In and Around the Triangle of Koch: Its Potential relevance to Atrioventricular Nodal Reentry. J Cardiovas Electrophysiol 1997; 8 (12): 1396-407.
5. McGuire MA. et al. Dimensions of the Triangle of Koch in Humans. Am J Cardiol 1992 ;70(7): 829-30.
6. Zhivadinovik J. Morfologija i klinichko znacenje na triagolnikot na Koh.- [Doktorska disertacija]. Skopje: Medicinski fakultet 2008.
7. Silver MA, Rowley NE. The Functional Anatomy of the Human Coronary Sinus. Am Heart J 1988; 115: 1080- 4.
8. Karaca M et al. The Anatomic Barriers in the Coronary Sinus: Implications for Clinical Procedures. J Intervent Cardiac Electrophysiol 2005;14: 89-94.

9. D'Cruz IA, Shirwany A. Update on Echocardiography of Coronary Sinus Anatomy and Physiology. Echocardiography 2003; 20:87-95.

10. Sanchez-Quintana et al. The Terminal Crest: Morphological Features Relevant to Electrophysiology. Heart 2002; 88:406-11.

11. Dobosz PM, Kolesnik A, Aleksandrowicz R, Ciszek. Anatomy of the Valve of the Coronary (Thebesian Valve). Clin Anat 1995; 8(6): 438-9.

12. Habib A, Lachman N, Christensen K, Asirvatham S. The anatomy of the coronary sinus venous system for the cardiac electrophysiologist. Europace 2009; 11:15–21.

Acta morphol. 2012; Vol.9(1):14-19

UDK: 611.831.7/.75:616.316.5-089.87

VARIATIONS OF FACIAL NERVE SURGICAL ANATOMY IN PAROTIDECTOMIES

Popovski Vladimir, Pantchevski G, Iliev A

Clinic for Maxillofacial Surgery, "St Cyril and Methodius" University, Skopje, R. Macedonia

Abstract

Introduction: The anatomy of the facial nerve within the parotid gland is subject to variation and its identification may be further complicated by distortion of its course by tumors, scarring secondary to past inflammatory disease or surgery, or congenital abnormalities. Parotidectomies are without doubt the most demanding form of salivary gland surgery because of the difficulty of avoiding damage to the facial nerve. The relationship of the parotid gland to the facial nerve is of primary surgical importance in parotidectomy procedure. Immediate postoperative dysfunction was frequently encountered (37.1%), but permanent dysfunction was uncommon (3.9%). Regional anatomical peculiarity and evident increasing incidence of parotid gland neoplasm's, create the necessity of competent diagnostic and surgical approach.

Material and methods: We have analyzed the medical records retrospectively, 81 consecutive patients who underwent parotid surgery at our institution in the past 10 years with attention to CT and MRI preoperative findings, operative trunk distance, type of peripheral pattern of facial nerve branching and interconnections.

Results: MRI is superior for determining tumor character and facial nerve involvement. Mean distance from the pointer to the facial nerve trunk and bifurcation was 13 mm, ranging from 12.5 mm and 13.5 mm respectively. Hypoplastic or hyperplastic changes on the main trunk and nerve branches were present in 33% with prevalence in temporal branch. Trifurcation may present with addition of a buccal branches. The frequency of peripheral pattern and connections of the facial nerve were type III (32.1%), type I (27.1%), type IV (23.5%), type II (17.3%), in order of frequency. In every distinctive type subsequent subtype was included.

Conclusion: In most cases, the length of the facial nerve was longer in superficial tumors. It located at more superficial portion than we expected, so we should pay more attention to it during parotid surgery. In type III pattern of peripheral branches of facial nerve, we should identify the anastomosis of buccal and zygomatic branches. Mandibular branch rarely had an anastomosis with the other facial nerve branches in its peripheral distribution.

Key words: parotid gland, parotid neoplasm's, facial nerve, magnetic resonance, parotidectomy

Introduction

The relationship of the parotid gland to the facial nerve is of major surgical importance in parotidectomy procedure. Extratemporal part of the facial nerve exits the cranium via the stylomastoid foramen typically crossing the posterolateral aspect of the styloid process and quickly enters he parotid gland. Through the intraglandular course facial nerve is intimately interwoven with parotid tissue. The first major division of the nerve (pes anaserinus) occurs approximately 1.3 cm from the foramen into temporofacial and cervicofacial branches. Most commonly these divisions and their branches have multiple anastomoses and anatomic studies have demonstrated eight major branching patterns. Skillful knowledge of facial nerve anatomy is crucial to avoid its accidental injury during parotidectomy, maxillofacial fracture reduction, rhytidectomy, and almost any extensive surgery of the head and neck. Reasonable speed and safety in identifying and preserving important anatomical structures are of vital importance for successful surgery in all specialties.

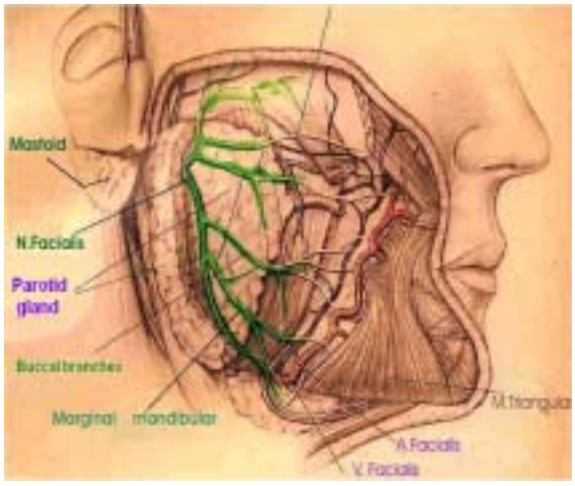

Fig. 1. Intra et extra-glandular facial nerve branching

Parotid gland surgically is often referred to as superficial and deep lobes, but anatomically it is referred to as unilobular gland with numerous processes and no true superficial and deep lobes separated with facial nerve branching[8,11,12]. The variations of facial nerve anatomy encountered during the course of parotidectomy with facial nerve dissection and preservation are analyzed. In most large series[2,3,4], their incidence of variations range from 42-96% with wide diversity of identified patterns.

Fig. 2. Facial nerve relationshp at stylomastoid foramen

The surgical anatomy of the peripheral branches of the facial nerve has been well documented in the literature[1,2,3,14,15]. On the other hand, it is almost mandatory to find significant variations. The identification of the facial nerve in the parotid region during parotidectomy is a paradigmatic procedure. Both the main trunk and peripheral branches must be identified and preserved to prevent permanent aesthetic sequelae and medico-legal actions related to facial paralysis.

Material and methods

Selected is own material from the University Clinic for Maxillofacial Surgery in Skopje, where in the last ten year period, parotid neoplasms surgery was performed 342 patients, of whom 214 were treated with superficial, subtotal or total parotidectomy with preservation of the facial nerve. Completely records for this study we have evaluated in 81 cases comparing preoperative imaging assesment, intraoperative findings and relationship of the dissected and preserved facial nerve with tumor mases. Routine diagnostic algorithm for parotid neoplasms was performed, where tumor detection through initial diagnostics has determining asperity for the kind of tumor pathology required. Magnetic resonance images (MRI) were schematic analyzed about necessary preoperative assessment including the relationship of the facial nerve with the mass lesion and the parotid gland.

In this study, the intraoperative mapping study was done to obtain the exact anatomical data by drawing the exposed facial nerve branches in life size during the operation of parotidectomy. Measurements were made at the end of the procedure by using a caliper. Measuring was performed after tumor and gland tissue extirpation and commodious revelation of the facial nerve and its branches. At the end of the procedure, the correct location of the nerve was double-checked by enlarging the incision to confirm the position of the nerve and the integrity of its branches. Cases with partial or complete resection of the facial nerve were excluded.

Amongst other important entities we have compared the pattern of facial nerve branching, interconnections, positioning and specific characteristics of the trunk and branches. Intraoperatively the meticulous dissection and anlayzes were facilitated by means of the operative magnifyng loupes (6 x magnification).

Fig. 3. Intraoperative findings during parotidectomy procedure

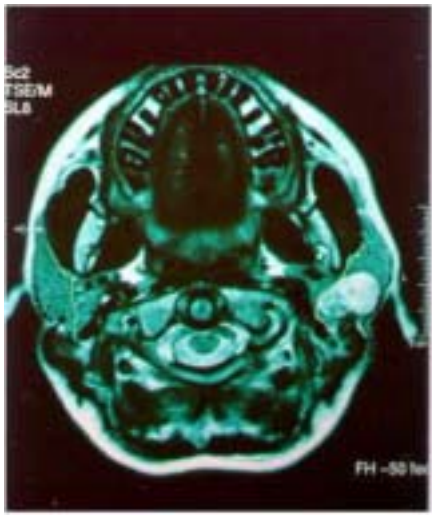

Fig. 4. MRI with facial nerve position and tumor comprehension

Results

We observed differences in the positioning of the facial nerve and the course of the branches of the facial nerve intraoperatively. Special attention was created about facial nerve positioning and changes after the tumor extirpation in parotidectomy procedure.

Fig. 5. Main trunk and greater auricular nerve

The variations in the course and length of the trunk were confirmed in 8 cases (9.8%), while discrepancies of the branching pattern of the facial nerve were observed in 62 cases (76.5%). Regarding the trunk our findings were with differences in the length in range 12.5 to 13.5 mm while average length around 13 mm was confirmed in more than 90% (70 cases). Hypoplastic trunk was apparent in 9.8% (8 cases), ussualy after removal of parotid tumor mass with greater dimmensions. Hiperplastic thrunk was evident in only 3.7% (3 cases). In almost all cases, main trunk was divided into a larger zygomaticotemporal (upper) division and a smaller cervicomandibular or lower division. Only in one case lower division was larger then upper division.

The main trunk is the most consistent portion of the facial nerve. The average length was around 13 mm, ranging from 12.5 to 13.5 mm. The most significant elongation was found in cases after double preparation of facial nerve – usually after removal of deep lobe parotid neoplasm.

Within the parotid gland, there was branching with many individual variations. It was found that the upper division of the facial nerve gives off temporal, zygomatic and buccal branches, whereas the lower division emits marginal mandibular and cervical branches The latter innervate the platysma and may communicate with the cervical plexus.

The four types of branching patterns of the facial nerve with four subtypes were noticeable and are illustrated in Fig. 6 Sema as follows: Type 1: This pattern lacks anastomotic links between the main branches of each division. However, in one subtype, there is splitting and

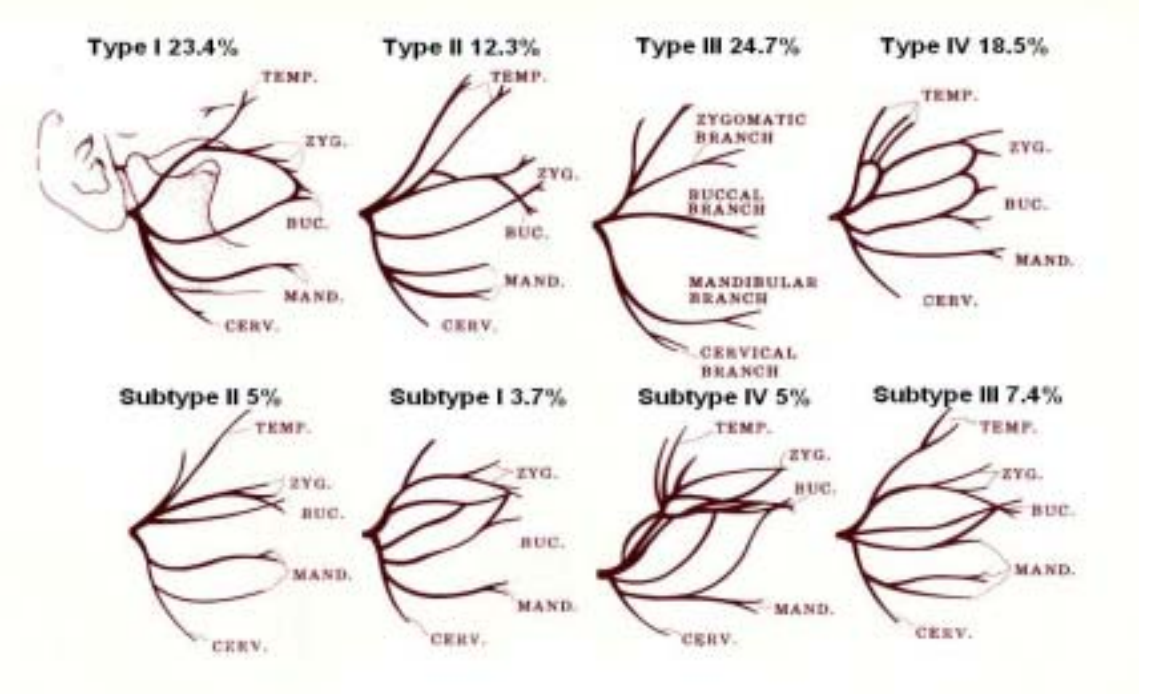

Fig. 6. Facial nerve branching variations-schematic statistic

Fig. 7. Upper division hyperplastic and larger that the trunk

subsequent reunion of the zygomatic branch while in the other, the mandibular branch splits and reunites (Fig. 7). With the subtype comprises 27.1% (19+3 cases). Type 2: In this type, subdivisions of the buccal branch fuse peripherally with the zygomatic branch (Fig. 8). With the subtype comprises 17.3% (10+4 cases).

Fig. 8. Atypical branching of the facial nerve lower division

Type 3: There are major communications between the buccal branch and others with pronounced connections of the upper division in the prevalent subtype III (Figs 9, 10). With the subtype comprises 32.1% (20+6 cases). Type 4: In this type there is a complex branching and anastomotic pattern between the major divisions (Fig. 11). With the subtype IV comprises 23.5% (15+4 cases). Subsequently,

Fig. 9. Facial nerve branching and interconnections after tumor remuval

Fig. 10. Abundant branching and connections of the upper division of the facial nerve

Fig. 11. Rare type of branching pattern with strong zygomatic branch

the facial nerve branches leave the parotid gland and enter the face, where they continue further distally covered by the skin, subcutaneous tissue and facial muscles.

With regard to the connection between branches, it was most in zygomatic to buccal connection (72 cases-88.8%) and least in buccal to mandibular connection (9 cases-11.2%). Overall postoperative transitional palsy was observed in 32% and only 2.7% had prolonged dysfunction of the facial nerve branches up to six months.

Discussion

Productive surgical intervention in case of parotid tumors depends upon good exposure and preservation of facial nerve. This requires a solid understanding of the anatomy of the parotid gland as a basic clinical knowledge for doing surgery safely, including the knowledge of extra temporal anatomy of facial nerve and variations amongst its branches. In this study we aimed to identify the patterns and variability of the branches of the facial nerve. The branches anterior to the parotid gland are very thin and susceptible to surgical or other kind of injuries.

According to our findings bifurcation of the main trunk inside the parotid gland into a temporal and cervical division was the most common configuration. Trifurcation may present with addition of a buccal branch[11]. We have confirmed that in only two cases.

Temporal branch was usually single, the largest in size and richest in divisions[3,8]. This complex nerve may have multiple branches, plexiform configuration, interconnections with itself and with buccal and zygomatic division. Only rarely is hypoplastic, more frequently is hyperplastic. It also presents terminal branches with no connections, but there are from five to seven recognized divisions, consisting of one branch to frontal area, two branches to orbital area, three branches from zygomatic section and two branches to the buccal area. The zygomatic branch is largest and the most important, while the frontal branch is smallest.

The buccal branch from the main stem is present in around 25% of cases[2,8,13]. Always was single and hypoplastic. Mostly connects with the temporal or zygomatic branches.

The cervical branch is subdominant division of two main branches. In rare case it also may be hyperplastic or to have multiple trunks and be plexiform. The marginal mandibular is frequently delicate branch, vulnerable to injury, and connects with other divisions in 12%.

Our findings in this work are consistent to those in the most previous reported studies regarding the extratemporal facial nerve anatomy variations[3,9.10]. First classification of variations was from Katz and Catalano (1987), from their study of the facial nerve's anatomy in 100 patients undergoing parotidectomy, where they observed double trunked nerves in three individuals and cautioned surgeons that unless they were aware of this anomaly, unnecessary damage to the facial nerve could result[8]. Others, in equally large or larger series, have failed to encounter this variant[2,3,5]. The pattern of branching of the facial nerve within the parotid gland is also variable in all previous studies. In relation to the temporal and zigomatic branchs, our results are similar to the Furnas[3]. It is running between the lower part of the ear lobe and the lateral edge of the eyebrow. In accordance with the literature we found in 32.1% connection between the zygomatic and buccal branches. The buccal branches of the facial nerve were noted as having a close relationship with the parotid gland as it crosses anteriorly. In Pogrel *et al*'s study the nerve was found only having one buccal branch in 85% of the cases and the branch or branches coursed inferior and superior to the Stensen's duct in 75% and 25% of the cases, respectively[16]. Saylam et al found variations in 52% of the patients superior, 35% inferior in zygomatic division and mixed patterns in the rest. Erbil *et al* noted that in 90% of all cases both inferior and superior zygomatic branches crossed the facial nerve anteriorly and all buccal branches were inferior to the duct and none of them crossed the duct[17]. Richards et al mentioned that the branches of the facial nerve were always lateral to the parotid duct. In our study, the buccal branches of the facial nerve have both superior and inferior branches which all pass lateral to the parotid duct[18]. The majority of parotid tumors within the gland were located in the body and not in the tail of the parotid gland. This study has the advantage that it was derived from contemporary operative findings rather than cadaver dissections and, as a result, incorporated functional information and the postoperative significance of damage to some of the fine branches.

In conclusion we can corroborate that the facial nerve has a complex pattern of branching which greatly varies between patients. In parotidectomies identification of the main trunk over established landmarks is unconditionally reliant on the exact preoperative planning, but the fine further facial nerve dissection is dependent to the comprehensive knowledge of the branching pattern. In type III and IV pattern of peripheral branches of facial nerve, one should identify the anastomosis of buccal and zygomatic branches. Mandibular branch rarely have an anastomosis with the other facial nerve branches in its peripheral distribution. We are in the opinion that the upgraduated knowledge of courses and relationships of the branches of the facial nerve will actually provide a great benefit in preventing surgical complications and postoperative morbidity in operative procedures including parotidectomy and almost any extensive surgical procedure of the head and neck.

References

1. Cummings CW, Fredrickson JM at all. Otolaryngology – Head and neck surgery. II nd ed. St. Louis-Baltimore-Bosto: Mosby – Year Book; 1993. Vol.II, p.1043-78.

2. Conley J. Salivary Glands and the Facial Nerve. Stuttgart: George Thieme Publishers; 1975. p.313-25.

3. Thawley SE, Panje WR, Batsakis JG. Comprehensive Management of Head and Neck Tumors, Vol.II. Philadelphia:W.B. Saunders Company; 1999. p.1147-72.

4. Pereira JA, Merí A, Potau JM, Prats-Galino A, Sancho JJ, Sitges-Serra A. A simple method for safe identification of the facial nerve using palpable landmarks. Arch Surg. 2004; 139(7):745-7.

5. Seifert G, MiehlkeA, Haubrich J & Chilla R. (1988): Diseases of the salivary glands: pathology, diagnosis, treatment, facial nerve surgery, New York: George Thieme; 1988 p.18-32.

6. Guerrissi J, Gil Miranda M. Intraneural topography of the extratemporal facial nerve: microsurgical nerve reconstruction. J Craniofac Surg. 2007;18(3):578-85.

7. Ptak T, Geyer C. Diseases of the parotid gland. Postgraduate Radiology1995;15(3):119-150.

8. Myckatin TM, Macckinon SE. A review of facial nerve anatomy, Semin Plast Surg. 2004; 18(1):5-12.

9. Kilic C, Kirici Y, Kocaoglu M. Double facial nerve trunk emerged from the stylomastoid foramen and petrotympanic fissure: a case report, J Korean Med Sci. 2010;25(8):1228-30.

10. Popovski V, Iliev A. Extensive craniofacial resections in various malignancies of the maxillofacial region. Pro Otology 2001; I(1): 18-21.

11. Popovski V. Massive Deep Lobe Parotid neoplasms and Parapharyngeal Space Occupaing Lesions: contemporary surgical approaches. Contributions 2007; XXVIII (1): 113-28.

12. Ariyoshi Y, Shimahara M. Determining whether a parotid tumor is in the superficial or deep lobe using magnetic resonance imaging, J Oral Maxillofacial Surg 1998; 56(1):23-6.

13. Gomez DR, Katabi N, Zhung J, Wolden SL, Zelefsky MJ, Kraus DH, Shah JP, Wong RJ (2009): Clinical and pathologic prognostic features in acinic cell carcinoma of the parotid gland. Cancer 2009 May 15;115(10):2128-37.

14. Kosins AM, Hurvitz KA, Evans GR, Wirth GA. Facial paralysis for the plastic surgeon. Can J Plast Surg. 2007;15 (2):77-82.

15. Woltmann M, Faveri R, Sgrott EA. Anatomosurgical study of the marginal mandibular branch of the facial nerve for submandibular surgical approach. Braz Dent J. 2006;17(1):71-4.

16. Pogrel MA, Schmidt B, Ammar A. The relationship of the buccal branch of the facial nerve to the parotid duct. J Oral Maxillofac Surg. 1996; 54(1):71-3.

17. Erbil KM, Uz A, Hayran M, Mas N, Senan S, Tuncel M. The relationship of the parotid duct to the buccal and zygomatic branches of the facial nerve; an anatomical study with parameters of clinical interest. Folia Morphol 2007;66(2):109-14.

18. Richards AT, Digges N, Norton NS, Quinn TH, Say P, Galer C, Lydiatt K. Surgical anatomy of the parotid duct with emphasis on the major tributaries forming the duct and the relationship of the facial nerve to the duct. Clin Anat. 2004; 17(6):463-7.

UDK: 611.711.1

CERVICAL SPINAL CANAL MEASUREMENTS-INDICATORS OF SPINAL STENOSIS

Matveeva N, Lazarova D, Nakeva N, Zivadinovik J, Zafirova B
Institute of Anatomy, Faculty of Medicine, University "Ss Cyril and Methodius", Skopje

Abstract

The aim of this study was to determine normal measurements of the C3-C7 spinal canal, spinal cord and the space available for the cord in anteroposterior plane from MR images and to compare these with previously published data. Measurements were made from 30 MR studies of the cervical spine. We measured the anteroposterior diameters of the vertebral bodies, spinal canal and spinal cord at each vertebral level and computed these diameters to provide two useful numerical values, termed the Torg ratio and the SAC (space available for the spinal cord) value. The Torg ratio was determined by dividing the sagittal spinal-canal diameter by the corresponding sagittal vertebral-body diameter. The SAC was determined by subtracting the sagittal spinal-cord diameter from the corresponding sagittal spinal-canal diameter. The cord varied in average anteroposterior diameter from 7.7 mm SD (0.7) at C3 to 6.7 mm SD (0.7) at C7. The spinal canal varied in average anteroposterior diameter from 15.4 mm SD (1.41) at C3 to 14.7 mm SD (1.38) at C6. The SAC ranged from 7.0mm SD (1.29) to 8.8 mm SD (1.75) and was greatest at C7. The SAC was the least at C4 or C5 in most of the subjects. A Pearson product moment correlation revealed a high level of correlation between the Torg ratio and SAC (r >0.5, P < .01).

Key words: magnetic resonance imaging, cervical spine, spinal stenosis

Introduction

Shape and morphometric aspects of the bony spinal canal reveal level dependency, inter-individual and sex variation, and are particularly susceptible to changes with aging [1]. The cervical spinal canal may become narrowed as a result of a congenital defect (congenital stenosis) or following other changes associated with the vertebral column or its related structures (acquired stenosis). The Torg ratio is widely accepted as an indicator for identifying stenosis. A ratio of less than 0.80 or 0.70 indicates significant spinal stenosis and an increased risk for neurologic injury [2]. Because stenosis is the spinal cord's encroachment in the spinal canal and spinal canal and cord sizes vary among individuals, measurement of the space available for the cord (SAC) may be a useful indicator for identifying stenosis. The aim of this study was to determine normal measurements of the C3-C7 spinal canal, spinal cord and SAC values in anteroposterior plane from MR images of asymptomatic individuals and to compare these with previously published data. The second aim was to examine the relationship between the Torg ratios and the SAC values in order to establish SAC value as an indicator for identifying an increased risk for neurologic injury and spinal stenosis.

Material and methods

Thirty subjects (14 males, 16 females), 26 to 64 years old (mean age 48 years) were analyzed in this study. Subjects who reported a history of cervical spine injury or disease and condition for which MRI was contraindicated were excluded from the study. Sagittal-diameters of the vertebral body, spinal canal, and spinal cord were traced manually and assessed. The sagittal vertebral-body diameter was measured at the midpoint between the superior and inferior endplates. The sagittal spinal-canal diameter was measured as the shortest distance from the midpoint between the vertebral body's superior and inferior endplates to the spinolaminar line.

Fig. 1. Sagital diameter measurements of the spinal cord, spinal canal, and vertebral body
3,6.9,12. 15 = sagittal spinal cord diameter,
2,5,8,11,14 = sagittal spinal canal diameter;
1,4, 7, 10, 13 = sagittal vertebral body diameter.

The sagittal spinal cord diameter was measured at the midline of the vertebral body at the appropriate level. The average of 3 measurements was reported. The Torg ratio was determined by dividing the sagittal diameter of the spinal canal by the sagittal diameter of the vertebral body The SAC was determined by subtracting the sagittal-cord diameter from the corresponding sagittal canal diameter (Figure 1).

1.5-Tesla MRI scanner with body coil was used to collect the data. MRI consisted of a volume 3-dimensional, T2-weighted, fast spin-echo pulse sequence (TR = 3000 ms; TE = 105 ms; FOV = 32 cm; 1.3-mm slice thickness; 256 × 256 matrix; 2 NEX;). This pulse sequence was selected because the 3-dimensional, fast spin-echo pulse sequence provides a higher resolution and signal-to-noise ratio than conventional 2-dimensional, fast spin-echo imaging. Head position was standardized in the subjects with the neck in neutral position. The MRI scans were evaluated midsagittally at each spinal level from C3 to C7. Sagittal diameters measurements of the vertebral bodies, spinal canal, and spinal cord were traced manually. All imaging were performed and evaluated by a diagnostic radiologist.

Statistical Analyses

A Pearson product moment correlation was calculated to determine if there was a significant relationship among the selected variables. The Statistical Package for the Social Sciences (version 13.0, SPSS Inc, Chicago, IL) was used for all statistical analyses.

Results

Average sagittal spinal canal diameter, spinal cord diameter, SAC and Torg ratio scores were reported by spinal level (C3 to C7) for each subject.

Average sagittal vertebral body diameter varied from 14,8 mm SD (1.47) at C3 to 15,05 mm SD (1.6) at C4, 14,7 mm SD (1.4) at C5, 15,4 mm SD (1.7) at C6 and 15,6 mm SD (1.4) at C7 (Fig.2). Comparison of our data with the literature reveals disparate measurements that vary up 2 to 3 mm from our mean values (Table 1).

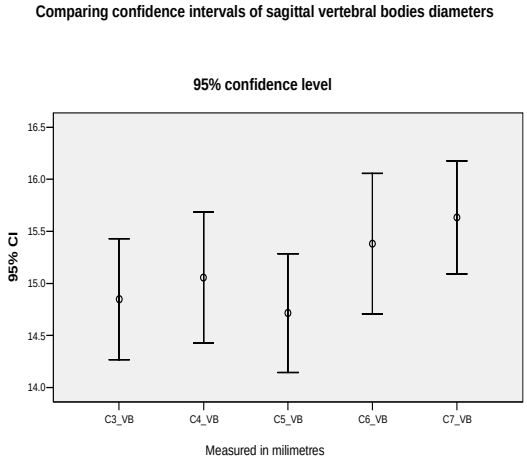

Fig. 2. Sagittal cervical vertebral bodies diameters (from C3 to C7)

Average spinal canal diameter varied from 15.4 mm SD (1.41) at C3 to 14,7mm SD (1.53) at C4, 14,5 mm SD (1.38) at C5, 14,7 mm SD (1.46) at C6 and 15,4mm SD (1.66) at C7 (Fig.3). Comparison of our data with the literature reveals disparate measurements that vary up 1 to 3 mm from our mean values (Table1).

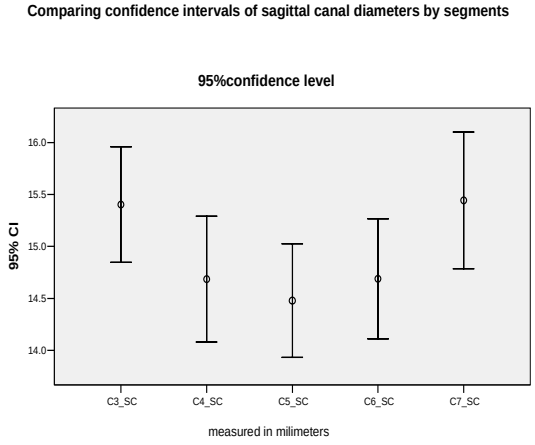

Fig. 3. Sagittal cervical spinal canal diameters by segments (from C3 to C7)

Table 1. Sagittal vertebral body diameters (means) and sagittal spinal canal diameters (means) by different authors

Authors	Instrumentation	N	Vertebral-Body Mean (SD)	Spinal-Canal Mean (SD)
Tierney et al (2002)†	Magnetic resonance imaging scans	14	17.70 (2.18)	13.28 (1.47)
Torg et al (1996)[5]‡	Radiographs	105	19.31 (1.86)	18.74 (1.84)
Herzog et al (1991)[9]†	Radiographs	80	17.70 (1.53)	15.14 (1.36)
Matsuura et al (1989)[15]†	Computed tomography scans	100	NR	14.09 (1.58)
Pavlov et al (1987)[7]‡	Radiographs	49	NR	18.89 (0.19)
Stanley et al (1986)[16]†	Computed tomography scans	52	NR	14.30 (0.34)
Hashimoto and Tak (1977)[3]†	Radiographs	48	NR	13.66 (1.09)

*N indicates number of subjects; SD, standard deviation; and NR, not reported.
†C3 to C7 measured.
‡C3 to C6 measured.

The cord varied in average anteroposterior diameters from 7.7 mm SD (0.74) at C3 and C4 to 7.5 mm SD (0.7) at C5 to 7.0 mm SD (0.67) at C6 and 6.7 mm SD(0.74) at C7. The cervical enlargement of the anteroposterior diameter of the cord was found from C3 to C6 (Fig.4).

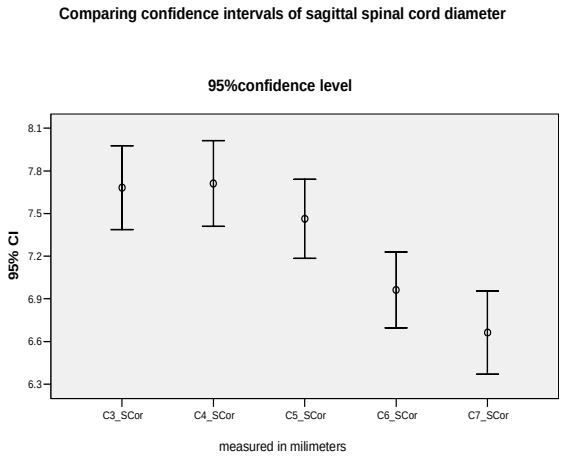

Fig. 4. Sagittal cervical spinal cord diameters by segments (from C3 to C7)

Torg ratio data ranged from 0.97 to 1,05 mm and average Torg ratio was greatest at C3, 1.05 SD (0.17).The average Torg ratio was the smallest at C6, 0,97 SD (0.16). Average Torq ratios at C4, C5 and C7 were 0.99. A Torg ratio less than .80 existed in at least one vertebral level in 6 from 30 subjects. Also, a Torg ratio less than .80 existed in 8 of 150 vertebral levels.

SAC data ranged from 4.8 to 12.5 mm and average SAC was greatest at C7, 8,78 mm SD (1.75). The average SAC was the smallest at C4, 6,97, SD (1.29). The data of the SAC values at C4 ranged from 4,80 to 9,40 mm.

A Pearson product moment correlation revealed a high level of correlation between the Torg ratio and SAC (r >0.5, P < .01) at each level from C3 to C7.

Discussion

Morphometric studies of the vertebral canal report racial and ethnic variation, apart from age and sex differences in the canal size [3, 4, 5, 6]. There is considerable variation in the transverse diameter of the spinal canal between different races . The canal size in Indians is much smaller than that in the other races [7, 8]. Also, many authors have reported level differences in the mean sagittal osseus spinal canal diameter, so our sagittal vertebral-body and spinal-canal diameters were, on average, 1 to 3 mm different than measurements reported in several studies. In some cases, the difference exceeded 3 mm. These differences due to the fact that we used MRI in determining measurements, and previous authors used radiographs or computed tomography scans. Compared with radiography, MRI avoids magnification error, allowing the direct measurement of the spinal cord.

Shape and morphometric aspects of the bony neural canals are particularly susceptible to changes with aging. Disc degeneration during the process of aging may alter or even threaten the functional anatomical relationships between successive adjacent “juncturae” of the vertebral column. At one level the intervertebral joint is made from three parts, the disc and the posterior facet joints. Changes affecting the discs also alter the posterior facet joint and vice versa. Evidence suggests that the sagittal diameter is more frequently involved in stenotic lesions. The factors that affect the sagittal diameter of the canal are alterations of anterior components of the canal: trabecular reorganization and spreading of vertebrae in aging and disc degeneration. These factors conjoined with thickening of the ligamentum flavum can contribute to diminishing the sagittal diameter of the vertebral canal. Osteophytic enlargement of the facet joints can also provoke narrowing of the spinal canal. Some authors have reported spinal canal dimensions as a risk factor for the development of symptoms of spinal stenosis.. In symptomatic patients spinal canal dimensions are significantly smaller, less then 12 mm than those in asymptomatic individuals [9].

We found a significant relationship (r > 0.5) between the Torg ratio and the SAC. The vertebral body is used in the Torg ratio as a way of controlling for magnification errors. Herzog et al explained that the Torg ratio relies on both the spinal canal size and vertebral-body size [10]. SAC measurements relie most heavily on the spinal canal and the spinal cord. These components are directly involved in a neurologic injury occurring at the cervical spine related to stenosis. Previous research studies revealed an increased risk of recurrence of a cervical-cord neurapraxia episodes with less SAC values [11].

In the published studies assessing the SAC, head position was not standardized. Torg et al. did not indicate a standard head position during the MRI, and Herzog et al. examined subjects with the neck in the neutral position. Our subjects’ head positions were standardized because head position affects spinal-cord size and spinal-cord size varies among individuals [12,13]. Using standardized head-positioning method is important to ensure reliable SAC measurements.

The limitation of our study is the small number of included subjects. Future research should examine the SAC value as an indicator of increased risk for neurologic injury and spinal stenosis. Critical SAC values may predict development of significant stenosis or may indicate an increased risk of neurologic injury which is especially important for sportists or people with occupations with increased risks for traumatic injury of the cervical spine.

References

1.Van Roy P, Barbaix E, Clarijs JP, Mense S. Anatomical background of low back pain: variability and degeneration of the lumbar spinal canal and intervertebral disc.Der Schmerz 2001;15:6.

2.Torg J S, Corcoran T A, Thibault L E, et al. Cervical cord neurapraxia: classification, pathomechanics, morbidity, and management guidelines. J Neurosurg. 1997;87:843–50.

3. Hinck VC, Clark WM, Hopkins CE. Normal interpediculate distances (minimum and maximum) in chil-dren and adults. Roentgen 1966; 97:141-53.

4. Amonoo-Kuofi HS. Maximum and minimum lumbar interpedicular distances in adult Nigerians. JAnat 1982; 135:225-33.

5. Amonoo-Kuofi HS. The sagittal diameter of the lumbar vertebral canal in normal adult Nigerians. J Anat 1985; 140:69-78.

6. Amonoo-Kuofi HS, Patel PJ, Fatani JA. Transverse di-ameter of the lumbar spinal canal in normal adult Saudis. Acta Anat 1990;137: 124-8.

7. Chhabra S, Gopinathan K, Chibber SR. Transverse di-ameter of the lumbar vertebral canal in north Indians. Anat 1991; 41 (1): 25-32.

8. Rema Devi, N Rajagopalan. Dimensions of the lumbar vertebral canal. Indian Journal of Orthopaedics 2003;37:13.

9.Torg J S, Naranja R J, Jr, Pavlov H, Talinat B J, Warren R, Stine R A. The relationship of developmental narrowing of the cervical spinal canal to reversible and irreversible injury of the cervical spinal cord in football players. J Bone Joint Surg Am. 1996;78:1308–14.

10. Herzog R J, Wiens J J, Dillingham M F, Sontag M J. Normal cervical spine morphometry and cervical spinal stenosis in asymptomatic professional football players: plain film radiography, multiplanar computed tomography, and magnetic resonance imaging. Spine.1991;16 (suppl):178–86.

11.Torg J S, Naranja R J, Jr, Pavlov H, Talinat B J, Warren R, Stine R A. The relationship of developmental narrowing of the cervical spinal canal to reversible and irreversible injury of the cervical spinal cord in football players. J Bone Joint Surg Am. 1996;78:1308–14.

12.Kameyama T, Hashizume Y, Ando T, Takahashi A. Morphometry of the normal cadaveric cervical spinal cord. Spine. 1994;19:2077–81.

13. Ros L, Mota J, Guedea A, Bidgood D. Quantitative measurements of the spinal cord and canal by MR imaging and myelography. Eur Radiol. 1998;8:966–70.

UDK: 611.728.3

MORPHOLOGICAL ANALYSIS OF THE FABELLA

Dodevski Ace[1], Lazarova-Tosovska D[1], Zhivadinovik J[1], Lazareska M[2], Stojkoski A[2]
[1] Institute of Anatomy, Medical Faculty, "Ss. Cyril and Methodius" University, Skopje, R. Macedonia
[2] University Clinic for Radiology, "Ss. Cyril and Methodius" University, Skopje, R. Macedonia

Abstract

There is variable number of sesamoid bones in the human body; one of them is fabella, located in the tendon of the gastrocnemius muscle. This study was conducted to examine the frequency of occurrence of fabella in the Macedonian population and to discuss the clinical implications of this bone. Over a time span of six months, 53 patients (38 males and 15 females, age range 19-60 years) were examined with computed tomography (CT) or magnetic resonance imaging (MRI). The reports were reviewed for the presence of fabella. In five (9.43%) patients of 53 analyzed reports, fabella was found in the lateral tendon of gastrocnemius muscle. Fabella is present in the Macedonian population and we should think of this sesamoid bone while performing diagnostic and surgical procedures.

Key words: fabella, sesamoid bone, anatomy, surgery.

Introduction

Galen is reputed to have first used the term "sesamoid" because of the resemblance of these bones to sesame seeds. Most sesamoid bones are only a few millimetres in diameter and vary in shape. The location of some saesamoids is constant, but many other sesamoids exist with variable frequency and sites. They are more frequent in hands and feet fingers. Most sesamoid bones are structures inside the tendons or in periarticular areas in close proximity to joints; however, their precise role is not understood. It is believed that they alter the direction of muscle pull, decrease friction and modify pressure. Some sesamoids ossify, whereas others remain cartialaginous [1].

In humans we can find about 46 sesamoid bones; fabella is found on knee joint. Fabella is placed inside the tendon of the gastrocnemius lateral muscle in posterior part of the condylus lateralis femoris. It is usually located in the lateral head of the muscle, and occasionally may occur in the tendon of the medial head of the muscle [2].

The aim of this study was to investigate the frequency of occurrence of fabella in the Macedonian population and to emphasize the clinical importance of this in some cases forgotten bone.

Material and methods

We retrospectively examined radiographs of 53 patients who had knee exams undertaken for a variety of clinical reasons, performed as a part of their medical treatment at the University Clinic for Radiology in Skopje, R. Macedonia. For the purpose of this study 15 females and 38 males, ranging in age between 19 and 60 years, mean age of 36.7±12.3 years, were examined. The patients were examined using CT or MRI. We received high quality images, which met the requirements of our study. Anatomical analysis of the images realized for medically justified goal was done. Images for each of the 53 patients were retrospectively analyzed by two independent authors.

Results

The radiological reports were reviewed for the presence of fabella. In five (9.43%) patients of 53 analyzed reports fabella was found in the lateral head of the gastrocnemius muscle. We did not find a significant gender or side difference in the appearance of fabella.

Fig. 1. CT images of the knee showing the presence of fabella.

Discussion

The fabella, or "little bean," is a bony or cartilaginous structure in the posterolateral aspect of the knee. It is generally believed to reside in the tendon of the lateral head of the gastrocnemius; however, many structures merge at the fabella. The fabella ranges in size from approximately 5 mm to over 20 mm in diameter, with the majority being oval in shape [3]. There are a few reports on the fabella's histology. Histological the fabella is classified by the predominant tissue as bone tissue, fibrous tissue and fibrocartilaginous [1, 4].

Until now, several studies reporting the incidence of the fabella have been published in the literature. Fabella was found by Silva in 3.1% of cases, Weiner in 12% of the cases, Phukubye in 23.5% of the cases and by Sarin in 31% of the cases. The results obtained in our study (9.43%)

for the frequency of the fabella are consistent with the published literature. Data derived from our study suggest that gender has no role in the appearance of the fabella, and confirmed some earlier findings by Sarin and Phukubye.

The search for elucidation the mysteries of formation and frequency of the sesamoid bones has been promoting the activity of many researchers. There are two theoretical propositions for the development of these bones, a functional and a phylogenetic. The functional theory finds support in the biomechanical aspect, where these bones are described as pulleys, reducing the friction of the tendons and potentiating the muscular handspike. The phylogenetic theory suggests genetic intrinsic factors developed during the evolutionary process that can be the key for development of sesamoid bones. They appear in the womb period. Initially cartilaginous they can calcify or not after the birth depending on the kind of activity done by the individual, that is, a "biomechanics embryological" origin [6].

Although initial anatomic studies emphasized a lack of significance of the fabella, this sesamoid bone has been associated with a spectrum of pathology affecting the knee ranging from fabellar syndrome to peroneal nerve injury, fabellar impingement and fracture [7].

Fractures of the fabella are extremely rare but important clinical entity, which may be easily overlooked clinically and radiographically, with few cases reported in the literature. Clinical information can provide a high index of suspiction, and when coupled with radiographic and CT findings, may lead to correct diagnosis [7]. Fractures of the fabella cause a severe posterolateral knee pain associated with decreased range of motion, inability to bear weight, and limited knee extension. On exam, tenderness is elicited with either hyperextension or compression of the fabella over the lateral femoral condyle [8]. Fracture etiologies include direct trauma to the lateral or posterolateral knee, repetitive microtrauma, and altered biomechanics in patients after total knee arthroplasties [9]. Early recognition and conservative treatment with rest, immobilization, and physical therapy are believed to be effective at relieving symptoms. However, fabellectomy is recommended only after a failed trial of conservative therapy or if there is impingement of the common peroneal nerve [7, 8, 9].

Several researchers have reported fabellar impingement after total knee replacement on either the tibial polyethylene component or the femoral component [10, 11, 12, 13]. Fabellar impingement can cause postoperative pain, swelling, catching and clicking around the knee joint, and can significantly compromise the results of total knee arthroplasty [10]. Diagnosis was made using lateral radiographs, and the symptoms resolved after fabellectomy [10, 11, 12, 13]. The cause of fabellar impingement after total knee replacement is probably multifactorial. It could be related to the large size (> 1 cm) of the fabella or to anatomic variation in the location of the fabella in the lateral head of the gastrocnemius muscle that may affect the relationship of the fabella to the prosthetic components. Other causes of postoperative fabellar impingement include incorrect positioning of the prosthetic components, a mismatch in sizes of the prosthetic and native femoral condyles, or ligament instability [11]. To avoid painful fabellar impingement after total knee arthroplasty, the preoperative radiograph should be carefully scrutinized. If there is a fabella that is larger than normal, thought should be given to its excision during replacement of the knee [12].

The common peroneal nerve is the most frequently damaged nerve in the lower limb. Until now, several studies reporting a peroneal nerve injury resulting from a fabella have been published in the literature. According to these studies we can conclude that the fabella should be considered as one of the possible reasons for peroneal nerve palsy. Therefore, whenever a patient complains of pain, palsy, or sensory changes in the distribution of the common peroneal nerve, and whenever a mass is found posterolateral to the head of the fibula or posterior femoral condyle, the presence of a fabella must be considered [14, 15].

The most common pathologic condition is fabellar syndrome characterized by posterolateral sharp knee pain, usually exacerbated in extension, and local tenderness over the region of the fabella, due to chondromalacia fabellae [2, 4, 5, 11, 14, 15, 16, 17]. The condition usually occurs during adolescence and is not related to previous knee surgery. Conservative treatment includes steroid injections, immobilization, rest from activity, and analgesics for up to 6 months. Indication for surgical treatment is failed conservative therapy after 6 month trial. Surgical intervention for recurrent knee dysfunction associated with this accessory bone has been reported as successful. A simple manual therapy intervention and subsequent education for effective self management strategies could significantly reduce the incidence of surgical excision of the fabella. Physical therapists need to be aware of fabella syndrome as a possible diagnosis for patients with posterior knee pain and need to include appropriate examination procedures to rule out or correctly diagnose this syndrome [16].

Conclusion

In conclusion, fabella in the Macedonian population was dominantly present in the tendon of the lateral head of the gastrocnemius muscle. Based on the presented information we highlighted the clinical significance of this bone. The authors believe that this article will add important contribution to the anatomical and clinical knowledge of the fabella and will refresh our knowledge for fabella.

References

1. Mark S Davies. Foot and ankle. In: Gray's H. Anatomy. The Anatomical Basis of Clinical Practice. 39 ed. New York: Elsevier; 2005. pp. 1507-45.

2. Silva JG, Chagas CAA, Torres DFM, et al. Morphological analysis of the fabella in Brazilians. Int J Morphol 2010; 28 (1): 105-10.

3. Noyes F. Knee disorders: surgery, rehabilitation, clinical outcomes.1th ed. Philadelphia; Saunders; 2009.

4. Phukubye P, Oyedele O. The incidence and structure of the fabella in a South African cadaver sample. Clin Anat 2011; 24: 84-90.

5. Weiner D, Macnab I, Turner M. The fabella syndrome. Clin Orthop 1977; 126: 213-5.

6. Sarin VK, Erickson GM, Giori NJ, et al. Coincident development of sesamoid bones and clues to their evolution. Anat. Rec. 1999; 257 (5): 174-80.

7. Heideman GM, Baynes KE, Mautz AP, et al. Fabella Fracture with CT imaging: a case report. Emerg Radiol. 2011; 18: 357-61.

8. Tang JY, Mulcahy H, Chew F. High-energy fracture of the fabella. Radiology Case Reports 2010; 5 (4): 454.

9. Theodorou SJ, Theodorou DJ, Resnick D. Painful stress fractures of the fabella in patients with total knee arthroplasty. AJR. 2005; 185 (5): 1141-4.

10. Larson JE, Becker DA. Fabellar impingement in total knee arthroplasty: a case report. J Arthroplasty 1993; 8 (1): 95-7.

11. Segal A, Miller TT, Krauss ES. Fabellar snapping as a cause of knee pain after total knee replacement: Assessment using dynamic sonography. AJR. 2004; 183: 352-4.

12. Jaffe FF, Kuschner S, Klein M. Fabellar impingement: a cause of pain after total knee replacement. J Bone Joint Surg (Am) 1988; 70 (4): 613-6.

13. Erichsen H. Bilateral fabellar impingement after knee replacement-a case report. Acta Orthop Scand 1997; 68 (4): 403.

14. Mangieri JV. Peroneal-nerve injury from enlarged fabella. J Bone Joint Surg 1973; 55: 395-7.

15. Kubota Y, Toyoda Y, Kubota H, et al. Common peroneal nerve palsy associated with the fabella syndrome. Anesthesiology 1986; 65: 552-3.

16. Zipple TJ, Hammer RL, Loubert PV. Treatment of fabella syndrome with manual therapy: a case report. J Orthop Sports Phys Ther. 2003; 33: 33-9.

17. Zenteno CB, Morales CIF, De la Tore IG. Fabella syndrome in a high preformance runner. Case presentation and literature review. Acta Ortop Mex 2010; 24 (4): 262-4.

UDK: 616.711.1-073.763.5

MRI FINDINGS IN ADULTS WITH CERVICOBRACHIAL SYNDROME

Chabukovska Radulovska J[1], Matveeva N[2], Poposka A[3]
[1]University Clinic of surgery "St.Naum Ohridski", Skopje
[2]Institute of Anatomy, Faculty of Medicine, University "Ss. Cyril and Methodius", Skopje
[3] PHI for Traumatology, Orthopedics, Anestesiology, Reanimation and Intensive Care, Emergency Center, Skopje

Abstract

Study Design. A cross sectional study of magnetic resonance imaging changes (MRI) in symptomatic individuals of different age.

Objective. To examine the prevalence of cervical spine MRI changes in symptomatic individuals and their relationship with age and gender.

Background. Previous studies of MRI changes have used population of asymptomatic individuals or patients with neck pain. Thus the influence of age and gender on the prevalence and pattern of the degenerative changes of the cervical spine evaluated within the symptomatic population can provide general insight into the etiopathogenesis of spinal degenerative pathologic process.

Methods. Cervical spine MRIs were obtained from 60 individuals with cervicobrachial syndrome between 25 and 65 years of age. MRI changes such as uncovertebral osteophytosis, disc degenerative changes and disc herniations (protrusions, extrusions) were assessed by two radiologists. Degenerative disc changes and herniations were evaluated and graded using the morphologic criteria accepted by the Nomenclature Committee of the North American Spine Society. In each subject, five disc levels from C2-C3 to C6-C7 were investigated.The severity of degenerative disc changes was calculated by the summation of the degenerative scores for each cervical level, Total Disc Degeneration score (TDS). The extent of the disc degeneration was determined by the summation of degenerated disc levels, (NDD) as a Number of Degenerated Discs.

Results. Disc degenerative changes were evaluated in all symptomatic adults aged 40 years and older. The severity of the disc degenerative process did not differ significantly between the adult symptomatic individuals of different age, but the number of degenerated disc levels increased with aging. Disc herniations were not associated with aging, but disc herniations evaluated at 3 or more levels were more frequent finding in individuals aged 45 and older. Disc herniations, with evident compression of the spinal cord, were observed in 45% of subjects, mostly over 45 years of age. Uncovertebral osteophytosis was evaluated in 63% of the individuals, over 45 years of age.

Key words: magnetic resonance imaging, cervical disc degeneration, cervicobrachial syndrome

Introduction

Disc degenerative process includes any or all of the following morphologic changes: real or apparent desiccation, fibrosis, narrowing of the disk space, extensive fissuring (ie, numerous annular tears) and mucinous degeneration of the annulus, defects and sclerosis of the endplates, osteophytes at the vertebral apophyses. At magnetic resonance (MR) imaging, degenerative disc changes are manifested by disk space narrowing, T2-weighted signal intensity loss from the intervertebral disk, presence of annular fissures, calcifications within the intervertebral disk, vertebral marrow signal changes and osteophytosis.

The term degenerative includes all previous mentioned changes [1-3]. Previous studies of MRI changes have used population of asymptomatic individuals or symptomatic patients. Boden et al. consider that abnormal MRI findings in asymptomatic subjects are common findings, since it is difficult to distinguish between aging discs and pathologically degenerated discs which cause symptoms [4]. Disc abnormalities in asymptomatic population have been reported in several studies [5, 6]. It is therefore important to know the frequency of degenerative changes on MRI in an asymptomatic and symptomatic population. Thus the influence of age and gender on the prevalence and pattern of the degenerative changes of the spine within the symptomatic adult population can provide general insight into the etiopathogenesis of pathologic spinal degenerative process. In order to examine the prevalence of cervical spine MRI changes in symptomatic individuals and their relationship with age and gender, we have made a cross sectional study and investigated degenerative cervical spine disorders on MRIs of symptomatic adult individuals.

Patients and Methods

A total of 60 patients (26 males and 34 females), aged 25 to 64 years (mean age 43.6), divided in two age groups, 25 to 44 (36 patients) and 45 to 64 years (24 patients) old subjects were investigated. All of the patients had current symptoms related to the cervical spine, known as cervico brachial syndrome within the last four weeks. Subjects with major neurologic symptoms indicative for cervical myelopathy (extremely reduced muscle strength, arm muscle atrophy, abnormal reflexes, difficulty walking and controlling bladder and/or bowel functions) or previous history of disease or trauma related to the cervical spine which had needed medical care were excluded from the study. These criteria were confirmed by a questionnaire before MRI. In the questionnaire more than three positive answers were considered to be inclusion criteria for the study. Neck pain was defined as a pain in the neck or shoulders of more than two weeks duration, severe enough to interfere with completion of activities of daily living, not relieved with changes in body position, radiating pain from the cervical spine to the upper limb, restricted mobility, tension in neck and shoulders muscles, tension and swelling in the hands, sensory disturbances (numbness or pareshesia), motor disturbances like stiffness or clumsiness in the arms and hands.

Imaging**.** MR imaging examination was preformed with 1,5 T MR unit (Signa HDi) with a spinal surface coil. The imaging protocol consisted of a sagittal T1-weighted fast spin-echo sequence (FSE) (repetition time msec/echo time msec, 800/14; section thickness, 4 mm; field of view, 360x360 mm; matrix, 448 x 224), sagittal T2-weighted turbo spin-echo sequence (3520/102; section thickness, 4 mm; intersection gap, 10 mm; echo train length of 24), and a transverse T2-weighted fast recovery fast spin-echo (FRFSE) sequence at one or multiple levels (4660/120; section thickness, 4 mm; intersection gap, 0.6 mm; echo train length of 27; field of view, 200x200 mm; matrix 320 x 256). The obtained MR images were assessed in consensus by two radiologists.

Before any of the MRI images were studied, a grading system was developed to evaluate disc degeneration. Using a well defined morphologic nomenclature disc abnormalities were evaluated and classified based on the morphologic criteria accepted by the Nomenclature Committee of the North American Spine Society [7]. Cervical intervertebral disc degeneration was evaluated on the basis of signal intensity changes and disc height. Disc degenerative changes were graded employing 3 point graded system. Grade 1 represented a slight decrease in signal intensity from the disc, grade 2 represented a generalized hypontense disc signal and grade 3 represented a generalized hypontense disc signal with narrowing of the disc height, DDS (Disc Degeneration Score). Two additional scores were developed to indicate the severity of degenerative disc disease and the extent of the degenerative disease. TDS (Total Disc Degeneration Score) was derived by summing the scores of 5 cervical intervertebral disc levels. A minimum TDS of 0 would mean that all 5 levels were not degenerated, and a maximum TDS of 15 would mean that 5 levels were severely degenerated (grade 3). TDS < 4 was considered as a mild degeneration, TDS ranging from 4 to 7 was considered moderate, while TDS > 7 was considered as a severe degeneration. The extent of the degenerative disc disease was represented by NDD (Number of Degenerated Discs), which was determined as the number of levels with disc degeneration scores (DDS) that were grade 2 or 3. Disc herniatons were evaluated as disc protrusions, or extrusions. Uncovertebral osteophytes that exceed 2 mm were also evaluated. We evaluated positive MRI findings from C2-C3 to C6-C7.

Statistical analysis. MannWhitney test was used to study the relationship between the frequency of MRI findings and subjects age and gender using the statistical package, SPSS 13.0 (SPSS Inc,Chicago, Illinois). Differences for a p value less than 0.05 were considered significant.

Results

Positive MRI findings like disc degeneration were evaluated in most of the symptomatic individuals. Grade 2 or grade 3 disc degeneration was not found only in 17% of young adults 25 to 34 years of age, while in adults 45 years and older disc degeneration was found at least at one level in all examinees. The number of degenerated discs was rising in individuals over 45 years of age. There were significant differences in spreading of the degenerative process (Number of Degenerated Discs) between individuals of different age (p=0.01) (Fig. 1). In 25% of the adults aged 45 years and older were observed 5 degenereted disc levels. There were no significant differences in the severity of disc degenerative process (Total Degenerative Score) between adults of different age. Total disc degenerative score (TDS >7) as an indicator of a severe disc degeneration was found in 47% of young adults and in 71% of adults aged 45 years and older (Fig. 2). Disc degenerative changes were seen most frequently at C5/6 level. Of 185 degenerated disc levels, 53 (29%) were at C5/6, while 47 (25%) were at C4/5 (Fig. 3). Disc degenerative changes were distributed more homogenously in the cervical spine in adults 45 years and older. There was not a significant difference between males and females in the severity of the degenerative

process (Total Degenerative Score), but this process involved more intervertebral levels (Number of Degenerated Discs) in females than in males ($p<0.04$).

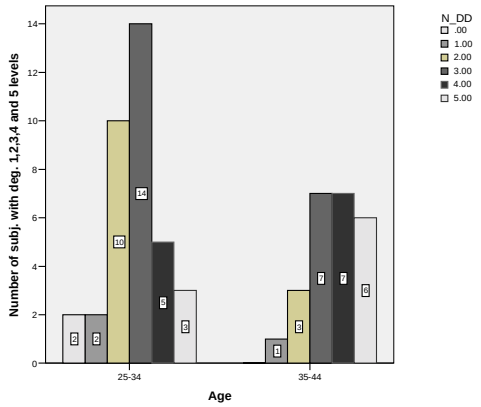

Fig. 1. Number of subjects with degenerated (1, 2, 3, 4, 5) disc levels stratified by age

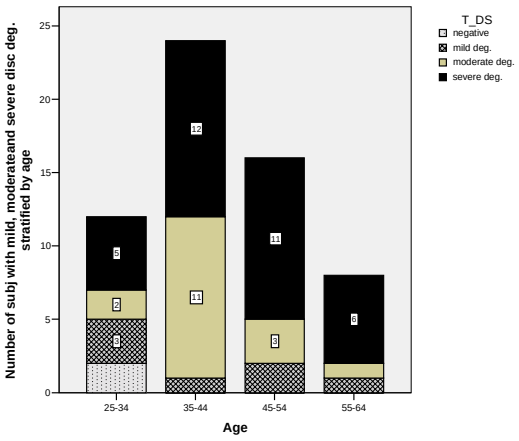

Fig. 2. Number of subjects with mild, moderate and severe disc degeneration stratified by age

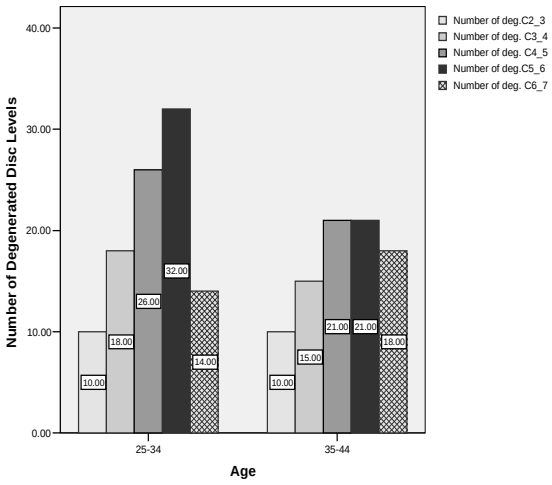

Fig. 3. Number of degenerated disc levels stratified by age

Disc herniations were seen in 63.3% of individuals. Posterior disc protrusions were most common at C5/6 level, (in 38.7%) and at C4/5 level, (in 28% individuals). The number of evaluated disc herniations did not differ significantly between individuals of different age (Fig. 4). There was a significant increase in the number of adults aged 45 years and over with herniated 2 or 3 disc levels. There was no significant difference between males and females in the number of evaluated disc herniations. Posterior disc protrusion, with spinal cord compression was found in 17 (45%) of 38 evaluated disc herniations, most of them in adults over 40 years of age (Fig. 5). Disc extrusions were observed only in 6 individuals. Dorsomedial protrusions were the most common (67%) types of protrusions on axial images. Posterior and anterior disc protrusions were evaluated at the same level in 4 individuals. Uncovertebral osteophytosis was evaluated in 63% of adults aged 45 years and older.

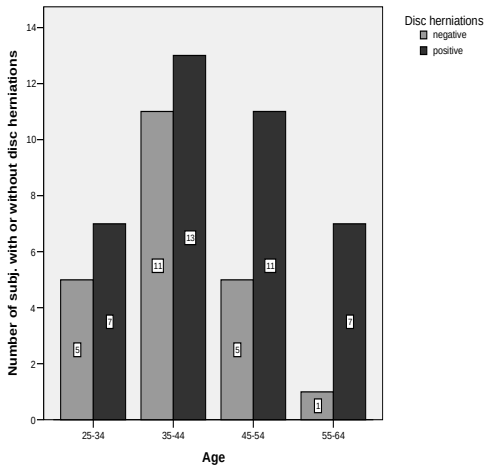

Fig. 4. Number of subjects with or without disc herniations stratified by age

Boden et al. reported major abnormalities on MRI in 19% of 63 asymptomatic individuals, with disc degeneration increasing with age, except for herniation of the nucleus pulposus and disc bulging. Disc degeneration is an aging phenomenon with increased prevalence with aging. Although disc degenerative process affected all individuals with symptoms aged 45 and older, there is also relative high prevalence of disc degeneration in young adults under 35 years of age. This would suggest that factors other than age are involved in the etiopathogenesis of disc degeneration, such as genetics, nutrition, trauma, etc. [8-13]. In addition to the changes in the severity of disc degenerative process with aging, the number of levels affected by the degenerative process increases with age.

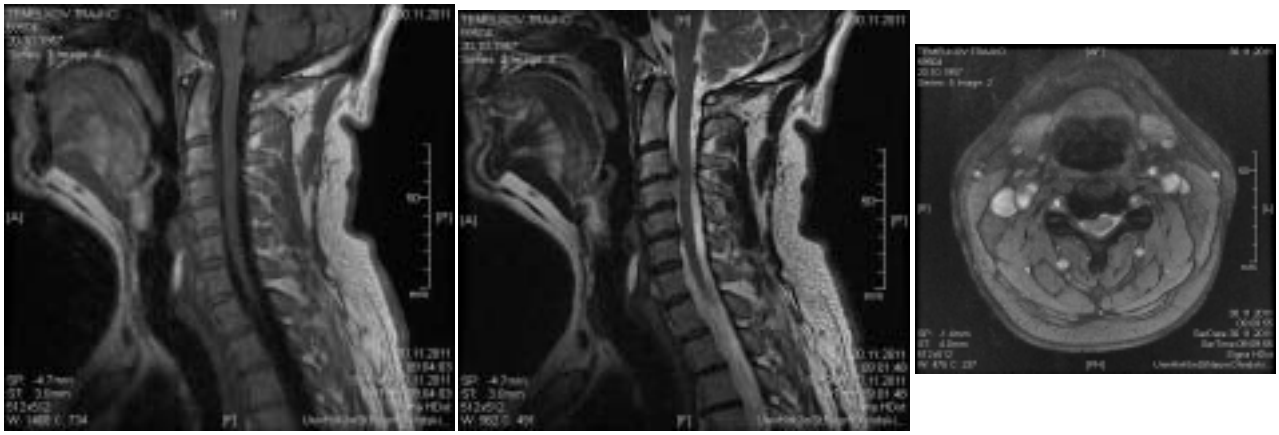

Fig. 5. Sagittal T1 (a) and T2-weighted (b) image and axial image (c) of a 45-year-old man. Posterior disc protrusions at C3/4 (with spinal cord flattening) and C5-6. Anterior disc protrusion with small spurs at C4/5.

Discussion

Nevertheless, our findings suggest that aging changes need to be taken into account in considering the clinical importance of MRI findings. Aging as a factor play a major role in spreading the disc degenerative process in adult symptomatic individuals than in progression of the severety of the disc degeneration of the affected levels. In this study a quantitative "Total Disc Degenerative Score" was used to describe disc degeneration. Utilization of this score provides an easy and reproducible quantitative score for comparison. A score of 6 could mean 4 levels of grade 2 degeneration (moderate generalized degeneration) or 1 level of grade 3 and 1 level of grade 3 degeneration (severe localized degeneration). These 2 patterns represent very different clinical conditions and the latter is more likely to be associated with symptoms. Despite this limitation, we used this method of semiquantitative assessment of disc degeneration in order to investigate the influence of age on the severity and the extent of the disc degenerative process.When only the "Number of Degenerated Disc Levels" was used we were able to demonstrate a significant influence of age on increasing number of affected levels providing justification for the use of this score. This method of semiquantitative assessment of disc degeneration has also been successfully used by many authors to identify predisposing genes for disc degeneration. Previous genetic studies would support significant ethnic differences in predisposing genes for disc degeneration [14, 15]. Ethnic differences might also result in differences in degenerative disease clinical presentation.

The prevalence of disc herniations does not increase with aging. Factors other than age are more likely to be involved in the etiopathogenesis of disc herniations, like trauma, occupation, physical activity, genes etc. Aging is moreover associated with increasing number of herniated disc levels. Posterior disc protrusions are clinically important as a cause of radiculopathy and myelopathy. We found that posterior protrusion conjoined with compression of the spinal cord was a frequent finding in symptomatic adults. A mild cord compression does not necessarily cause major neurologic symtoms like muscle weakness, abnormal reflexes, difficulty walking and controlling bladder and/or bowel functions, but long-term follow-up of these symptomatic individuals (with cervicobrachial syndrome) may provide useful information about the natural course of cervical myelopathy.

Key points

- The severity of disc degenerative process did not differ significantly between the adult symptomatic individuals of different age, but the number of degenerated disc levels increased with aging.
- Disc herniations were not associated with aging, but disc herniations evaluated at 2. 3 or more levels were more frequent finding in adults aged 45 and older.
- Almost 50% of the evaluated disc herniations in symptomatic individuals were conjoined with an evident compression of the spinal cord.

References

1. Czervionke LF. Lumbar intervertebral disc disease. Neuroimaging Clin N Am 1993; 3: 465–85.

2. Modic MT, Herfkens RJ. Intervertebral disk: normal age-related changes in MR signal intensity. Radiology 1990; 177: 332–3.

3. Sether LA, Yu S, Haughton VM, Fischer ME. Intervertebral disk: normal age-related changes in MR signal intensity. Radiology 1990; 177: 385–8.

4. Boden SD, McCowin PR, Davis DO, et al. Abnormal magnetic resonancescans of the cervical spine in asymptomatic subjects. J Bone Joint Surg [Am] 1990; 72-A: 1178-84.

5. Stadnik T, Lee R, Coen H, et al. Annular tears and disc herniation: preva-lence and contrast enhancement on MR images in the absence of low back pain or sciatica. Radiology 1998; 206: 49-55.

6. Carragee E, Paragioudakis S, Khurana S. 2000 Volvo award winner in clin-ical studies: lumbar high intensity zone and discography in subjects without low back problems. Spine 2000; 25: 2987-92.

7. Fardon DF, Milette PC. Nomenclature and classification of lumbar disc pathology. Spine 2001; 26 (5): E 93-E 113.

8. Simmons E, Guntupalli M, Kowalski J, et al. Familial predisposition for degenerative disc disease: a case control study. Spine 1996; 21:1527-9.

9. Kelsey J, Golden A, Mundt D. Low back pain/prolapsed lumbar interverte-bral disc. Rheum Dis Clin North Am 1990; 16: 699-716.

10. Sambrook P, MacGregor A, Spector T. Genetic influences on cervical and lumbar disc degeneration. Arthritis Rheum 1999; 42: 366-72.

11. Adams MA, Roughley PJ. What is intervertebral disc degeneration, and what causes it? Spine 2006; 31: 2151-61.

12. Kjaer PP, Leboeuf-Yde DC, Sorensen JS, et al. An epidemiological study of MRI and low back pain in 13-year-old children. Spine 2005; 30: 798-806.

13. Battie MC, Videman T, Parent E. Lumbar disc degeneration: epidemiology and genetic influences. Spine 2004; 29: 2679-90.

14. Jim JJ, Noponen-Hietala N, Cheung KMC, et al. The TRP2 allele of COL9A2 is an age-dependent risk factor for the development and severity of intervertebral disc degeneration. Spine 2005; 30: 2735-42.

15. Cheung KM, Chan D, Karppinen J, et al. Association of the Taq I allele in vitamin D receptor with degenerative disc disease and disc bulge in a Chinese population. Spine 2006; 13: 1143-8.

UDK: 612.65.087.1-053.4

ANTHROPOMETRIC PARAMETERERS OF GROWTH IN CHILDREN AGED 5

Zafirova Biljana, Lazarova D, Trpkovska B, Matveeva N, Cadikovska E
Institute of Anatomy, Medical faculty, Skopje, Macedonia

Abstract

Aim: Evaluation of sex-specific differences of anthropometric parameters that were used as indicators for growth in children aged 5.

Examinees and methods: The study included 260 healthy children aged 5 from Macedonian nationality. Fourteen anthropometric parameters were measured which define longitudinal, circular and transversal measures of skeleton using standard equipment and measurement technique. The following indicators were calculated: weight-for-age (BW), height-for-age (BH), weight-for-height and BMI.

Results: The majority of anthropometric parameters have shown significant sex-specific differences in favour of boys, with exception of leg length and circumferences of upper-arm, forearm, thigh and calf that were no significant differences. Values of the 50th percentile in boys were as follows:21 kg for BW,114.5 cm for BH and 15.95 kg/m^2 for BMI. The values of these parameters in girls were: 20 kg for BW,114 cm for BH and 15.42 kg/m^2 for BMI.

Conclusions: These results can be used as criteria for the assessment of the morphological characteristics and detection of deviations in the growth and nutritional status in children aged 5.

Kye words: anthropometry, growth, child population

Introduction

One of the most important characteristics of childhood is the continuous process of growth and development. Childhood is one of the most vulnerable periods in human growth, during which there are unique changes in the organism (1). On the other hand, nutrition is also an important ecological phenomenon which influences all phases of growth and development. That is why we should constantly monitor and evaluate how nutrition reflects on growth, since growth is particularly sensitive to nutritional deficit or surplus (2). The increased presence of the risk factors which affect the occurrence of non-infectious diseases such as obesity has imposed the need for evaluation and monitoring of growth and nutritional status (3). The anthropometric examinations are non-invasive, simple and especially adapted for children. They provide the opportunity to monitor a child's physical growth and its dynamics, as well as to point to all the problems related to growth and nutritional status in that period (4). This is all done by measuring certain dimensions which define longitudinal, transversal, circular dimensionality of the skeleton, the mass and the volume of the body.

Aim

Evaluation of sex-specific differences of the anthropometric parameters used as growth indicators in children at the age of 5.

Examinees and methods

The study included healthy children at the age of 5, of both sexes, of Macedonian nationality and from different urban areas of Macedonia, chosen randomly. The total number of examinees (n=260) according to the sex criterion was divided into two groups: (n=130 male and n=130 female).

Anthropometry

14 anthropometric variables were chosen in accordance with the aim of the study and they were measured according to the International Biological Program (IBP). For evaluation of the longitudinal dimensionality of the skeleton we measured: body height, arm length, leg length; for evaluation of the transversal dimensionality of the skeleton: elbow diameter, wrist diameter, knee diameter, ankle diameter; for evaluation of the mass and circular dimensionality, i.e. body volume: body weight, chest circumference, head circumference, mid upper arm, forearm, thigh, calf circumferences. The following standard anthropometric equipment was used: anthropometer by Martin with 1 mm accuracy; caliper-square which can detect values of 1mm, and elastic plasticized band which also detects values of 1 mm.

The following anthropometric indexes were calculated and derived: BMI (as a square of the ratio between body weight and height), weight-for-age (BW), height-for-age (BH) and weight-for height.

Definition

To define the values of these anthropometric indicators, most authors recommend the following percentile ranks with cut off points: (4-8)

- Normal distribution (average values) mostly corresponds to the percentile rank from the 15th - 85th percentile.
- Percentile rank from the 5th to the 15th percentile points to under average values
- Values under the 5th percentile point to underweight, as well as to retarded growth, if we analyze the parameter height-for-age.
- Children who have values between the 85th and 95th percentile for the indexes weight-for-age, height-for-age and BMI are defined as above average, i.e. children with above average growth who run the risk of becoming overweight.

· Values over the 95th percentile point to the category of children with extremely high growth, i.e. overweight/obese children.

Statistics

The gathered information is analyzed with descriptive statistics represented by: measures of central tendency and its deviation (arithmetic mean value ± standard deviation) and ranges (percentiles). Testing the significance of the differences between two arithmetic series was done by analysis of variance -ANOVA, and the differences with $p < 0.05$ level of significance were taken as significant differences.

Results

The mean values and the standard deviations of the examined anthropometric parameters in children at the age of 5, as well as their sex-specific differences, are presented in tables 1 and 2.

Table 1 shows the mean values and the standard deviations of weight, height, BMI, upper and lower limb length as well as the diameters of the elbow, the wrist, the knee and the ankle.

5-year-old male children have body mass with a value of 21.89 kg ± 3.58, height 115.5 cm ± 4.51 and BMI with a value of 16.36 kg/m^2±2.29. Girls at the same age have the following values for the same parameters: 20.51 kg ± 3.14 for weight, height 114.0 cm ± 4.43 and 15.72 kg/m^2 ± 2.57 for BMI. The results from the comparative examinations of these parameters show sex-specific differences in favor of boys.

There were sex-specific differences detected in the transversal parameters i.e. in all diameters, also in favor of the boys. When it comes to the longitudinal parameters, there were sex-specific differences in arm length, but no significant differences in leg length, although there were slightly higher values detected in boys.

Table 2 shows mean values and standard deviations of circumferences (head, chest, mid upper arm, forearm, thigh, calf circumferences).

Of the circular parameters, only head and chest circumferences showed sex-specific differences in favor of boys. The average values of the other circular parameters (forearm, thigh, calf circumferences circumference) were slightly higher in boys, but the sex-specific difference was no significant. Only the average/mean value of upper arm circumference of 17.35 cm ± 2.29 in girls was slightly higher than the value of 17.09 cm ± 2.18 found in boys, but the sex-specific difference for this parameter was also insignificant.

Sex-specific percentiles of the indexes weight-for-age, height-for-age and BMI for 5-year-old children are shown in table 3.

Table1. Body weight, body height, BMI, lengths and diameters of the extremities in 5 year-old -children from R Macedonia (mean and standard deviation).

Sex	n	Body weight (kg)	Body height (cm)	BMI (kg/m^2)	Lengths (cm)		Diameters (cm)			
					Arm	Leg	Elbow	Wrist	Knee	Ankle
Male	130	21.89±3.58[a]	115.5±4.51[a]	16.36±2.29[a]	49.76±3.21[a]	63.36±3.08	5.23±0.52[a]	3.79±0.35[a]	7.49±0.60[a]	5.39±0.43[a]
Female	130	20.51±3.14	114.0±4.43	15.72±2.57	47.92±3.08	62.46±5.19	4.95 ±0.49	3.67±0.30	7.18±0.75	5.10±0.5

[a]$p<0.05$ vs female children (ANOVA)

Table 2. Circumferences 5 year-old children from R. Macedonia (mean and standard deviation).

Sex	n	Circumferences (cm)					
		Head	Chest	Mid upper	Forearm	Thigh	Calf
Male	130	50.65±1.21[a]	57.47±4.72[a]	17.09±2.18	15.4±1.63	32.26±3.74	22.952.43
Female	130	50.15±1.19	56.12±5.63	17.35±2.29	15.08±1.86	31.98±4.10	22.59±2.93

[a]$p<0.05$ vs female children (ANOVA)

Table 3. Sex-specific percentiles of the indexes: weight-for-age, height-for-age and Body Mass Index in 5 year-old-children from R Macedonia

	PERCENTILES								
MALE	**5**	**10**	**15**	**25**	**50**	**75**	**85**	**90**	**95**
Weight-for-age	17.68	18	18.67	19.28	21	24	25.65	27	29
Height-for-age	108.03	110.08	111.01	112.53	115.45	118	119.76	121.51	123.38
BMI	13.35	13.93	14.22	14.92	15.95	17.62	18.42	19.71	21.16
FEMALE									
Weight-for-age	15.6	17	17	18	20	22	24.75	25	26
Height-for-age	107.05	109	109.6	110.55	114	117.5	119.25	120	121
BMI	13.13	13.74	14.08	14.47	15.42	16.94	17.66	18.08	19.14

Table 4. Means (x), st.deviation (Sd) and Medians (Me) for the index weight-for-height for 5-year-old-children by sex.

Height (cm)	***Weight (kg)***		
	X	**Sd**	**Med**
Male			
103-109	15.94	0.487	16
109.1-115	19.7	0.96	20
115.1.-121	23.42	1.15	22
121.1-127	28.1	0.75	27.5
Female			
103-109	15.9	0.64	15.8
109.1-115	19.12	0.72	19
115.1.-121	23.1	1.37	22
121.1-127	26.1	1.32	25

The values on the 5th and 85th percentile in 5-year-old boys were from 108.03 cm (5th percentile), and 119.76 cm on the 85th percentile for height-for-age, 17.68 and 25.65 kg for weight-for-age, 13.35 and 18.42 kg/m^2 for BMI. The corresponding values for girls were: 107.05 and 119.25 cm for height-for-age, 15.6 and 24.75 kg for weight-for-age, and 13.13 and 17.66 kg/m^2 for BMI.

Table 4 shows the mean values, standard deviation and median of the index weight-for-height, which puts weight in relation with height.

Discussion

Our study included examination of several anthropometric parameters which define the longitudinal, circular, transversal dimensionality of the skeleton, body mass and volume, and which are used for evaluation of the growth and the level of nutrition in children. As a result of that, we can conclude that the mean values of almost all examined parameters (with the exception of upper arm circumference) are higher in boys. There were also sex-specific differences of certain parameters in favor of boys. The results were statistically no significant only in terms of limb circumference and leg length. Percentile ranks of the anthropometric indexes in 5-years-old children were also derived and calculated.

The obtained values allow comparison of our values with the corresponding anthropometric examinations of children from other areas and populations.

Longitudinal parameters are considered to be one of the most stable indicators of physical growth. Transversal parameters are good indicators of bone maturity, circular parameters together with body weight show the volume of the body, i.e. its mass. The body mass and height as basic somatic characteristics are used as indexes for more accurate interpretation of growth and nutritional status during childhood. The index height-for-age depicts the reached linear growth and the deviation in its value which is detected with the bordering 5th percentile. This is used in discovering children with problems in reaching the potential for linear growth as a result of a long-term, cumulatively impaired nutrition or health (9). The values of the indexes body weight and body height on the 50th percentile in our 5-year-old male examinees was 21 kg and 115.5 cm, i.e. 20 kg and 114 cm for female examinees. These values are insignificantly higher than the values of NCHS referent population (8). Values over the 95th percentile detect children who run the risk of endocrine illnesses, tumors which produce growth hormones and other similar states. The children in our study are insignificantly heavier and taller than children in Belarus and India, and lighter and shorter than the children in Arlene and Lindgren's study (10-13). The index of body mass, known as BMI, as well as the index weight-for-age, is a parameter for monitoring the level of nutrition during childhood. The values of BMI on the 50th percentile in children from our country (MKD) are lower than the ones published about 5-year-old children from Canada (Can), Verona-Italy (I), Saragossa-Spain (E), Australia (A), Germany (D), America (USA) and the referential NCHS (8, 14-19).

From the cut-off points for BMI on the 85th and 95th percentile in male and female examinees and the corresponding values obtained from Cole's representative international referential sample which identify individuals with the risk of overweight and obese we can see that the cut-off points obtained from the examinations of our male examinees are slightly higher than the international sample

published by Cole. The values of BMI on the cut-off points for our female examinees are similar to the ones published by Cole et.al (20).

The differences between the children from this study and the children from other studies and in relation to the standard values, are another confirmation for the existence of population differences in anthropometric characteristics which depends on a series of internal (genetic) and external exogenous factors (9). The results of our studies confirm the recommendation of WHO that every country needs to have its own anthropometric standards which are necessary for precise classification and detection of the deviation from the growth and the nutritional status in children of every age.

Conclusion

Based on the results of this study, we can derive the following conclusions:

- 5-year-old boys of Macedonian nationality and from an urban area have higher values of longitudinal, transversal and circular parameters than girls.

- There were statistically significant sex-specific differences in terms of weight, height, BMI, arm length, all 4 diameters and 2 circumferences (head and chest circumference) in favor of boys. No statistically significant sex-specific differences were registered for the rest of the examined parameters (leg length and 4 circumferences: mid upper arm, forearm, thigh, calf circumferences).

- There were sex-specific percentile ranks determined from the 5^{th} to the 95^{th} percentile, i.e. cut-off points for the anthropometric indexes in 5-year-old children.

It is recommended to use the obtained results in everyday routine as anthropometric criteria for evaluation of the growth and the nutritional status. They can also point to certain misbalances as criteria for selecting individuals for further clinical examinations. By defining border values - cut-off points, we can identify children who need intervention. Undoubtedly, this has big practical importance in planning certain activities and measures of precaution in the field of child nutrition.

References

1. Nader PR et al. Identifying risk for obesity in early childhood. Pediatrics 2006;118 (3): 594- 601.

2. Ben-Seffer E et al.Childhood obesity:current literature,policy and implications for practise.Int Nurs Rev 2009;56 (2)166-73.

3. Dimitrovska Z, et al. editors. Nutritivna antropometrija. Skopje: Republicki zavod za zdravstvena zastita; 2006.

4. WHO Multicentre Growth Reference Stady Group.WHO Child Growth Standars:height-for-age,weight-for-age,weight-for-length,weight-for-height and body mass index,methods and development. Geneva: WHO; 2006.

5. WHO Child Growth Standards Geneva: WHO; 2007. Available from: http://www.who.int/childgrowth/en/

6. De Onis M, Garza C et al. Comparasion of the WHO Child Growth Standards and the CDC 2000 Growth Charts. J of Nutrition 2007; 137:144-8.

7. CDC table for calculated BMI values for selected heights and weights for ages 2–20years. National Health and Nutrition Examination Survey 2000. Available from: http:www.cdc.gov

8. Mc Dowell AM, Fryar DC, et al. Anthropometric references data for children and adults: US Population, 1999-2002. Vital Health Stat Ser 2005; (361): 1-31.

9. Zafirova B et al.Anthropometric parameters of growth and nutritional status in children aged 6 to 7 years in R. Macedonia.Advances in Medical Sciences,2009;(54): 289-295.

10. Tegako IL. Fizi~eskoe razvitie detei Belarus. Glasnik ADJ 2003; 38:115-120.

11. Kaushik B, et al. Age trends in anthropometric characteristics among 5-9 years old Bengalee Hindu school girls of Kolkata, India. Anthrop Anz 2005; 63(4): 439-48.

12. Arlene MM, et al. Anthropometric measurements of 3-4-5- and 6 year old girls and boys. Growth, 1999; 44:253-67.

13. Lindgren G, Strandell A, Cole T, Heavy M, Tanner J. Swedish population reference standards for height, weight and body mass index at 5 to 16 years (girls) or 19 (boys). Acta Paediatr 1995; 84:1019-28.

14. Tremblay MS, Katzmarzyk PT and Williams JD. Temporal trends in overweight and obesity in Canada, 1981-1996. Int J Obesity 2002; 26: 538 - 543.

15. Luciano A, Bressan F, Zoppi G. Body mass index reference curves for children aged 3-19 years from Verona, Italy. Europ J Clin Nutr 1997; 51: 6-10.

16. Lynch J, Wang XL, Wilcken ELD. Body mass index in Australian children: recent changes and relevance of ethnicity. Arch Dis Child 2000; 82:16-20.

17. Moreno LA, Fleta J, Sarría A, Rodríguez G, Gil C, Bueno M. Secular changes in body fat patterning in children and adolescents of Zaragoza (Spain),

1980-1995. Int J Obes Relat Metab Disord 2001; 25(11):1656-60.

18. Rosner B, Prineau R, Loggie J, Daniels S. Percentiles for body mass index in U.S.children 5 to 17 years of age. J Pediatr 1998; 132: 211 - 22.

19. Schaefer F, Georgi M, ScharerWuhl and Karen. Body mass index and percentage fat mass in healthy German schoolchildren and adolescents. International Journal of Obesity 1998; 22: 461-69.

20. Cole TJ, Bellizzi CM, Flegal MK, Dietz HW. Establishing a standard definition for child overweight and obesity worldwide: international survey. BMJ 2000; 320 :1240 – 6.

UDK: 611.92.087.1:618.29

FACIAL ANTHROPOMETRIC PARAMETERS IN FETAL BIOMETRY

Trpkovska Biljana, Nakeva N, Zafirova B, Chadikovska E
Institute of Anatomy, Medical faculty, Skopje, Macedonia

Abstract

The aim of this study is to show correlation between some anthropometrical parameters of fetal face and their role in early determination of fetal abnormalities.

The total number of fetuses (n=180) ex utero, according to gestational age was divided in three groups .Anthropological measurements were done using the methodology of the International Biological Programme with standard technique of the measurements.

Some anthropometrical parameters were analyzed: body weight, body length, biparietal diameter, head circumference, crown-rump length, fetal nasal bone lenght, fetal nasal spread, morphological face lenght, face spread.

Results showed that was not a difference between measurements, they are in correlation with gestational age. These anthropometrical measurements are useful in identification of some fetal anomaly and fetal intrauterine retardation in fetal growth, like trisomy 21, Down syndrome e.t.c. In the future those parameters were measurements in routine practice to determine the fetal chromosome abnormality in early gestational age in first trimester of intrauterine growth.

Key words: fetus, gestational age, anthropometrical parameters of the fetal face, biparietal diameter.

Introduction

The information about the research on some of the characteristics of the intrauterine growth of the fetus show that most studies on this topic agree that changes in the fetal period are relatively slow and prolonged and can be actively determined with quantitative methods.

During the last few years, some authors (1) emphasize the measurements of the parameters of the face, especially the width and height of the nose, parameters dependent upon gestational age. There is a significant correlation between the facial parameters and BPD, HC and crown-rump length. This information can be useful in antenatal prediction of chromosome abnormalities (2). Viora E, Masturzo B et al. confirm the same in their paper by measuring the height of the fetal nasal bone. They believe that we can diagnose prenatal abnormalities with the length of the bones in the face during the first trimester of the intrauterine growth of the fetus (3).

The indexes of the fetal growth by gestational weeks, determined based on previously measured fetal parameters, can most adequately be used for a fetus that develops normally or a fetus with growth retardation. Determining face and nose indexes can prove them to be independent from gestational age. With statistical data processing, the correlation of facial anthropometric parameters, gestational age and crown-rump length provides standard values of the corresponding parameters for each gestational week. Fetal biometry is a fast, easy and noninvasive applicative method which is used in obstetrics.

Aim: Correlation among some facial anthropometric parameters and their role in discovering early fetal anomalies.

Materials and methods

The material includes 180 fetuses measured ex utero and divided into 3 age groups: first group (11-13 g.w.); second group (14-16 g.w.); and third group (17-19 g.w.). Fetuses that didn't have visible malformations served as criterion.

The following anthropometric parameters were measured: body weight, body height, crown-rump length, biparietal diameter, head circumference, fetal nasal bone lenght, fetal nasal bone spread, face lenght and face spread. The measurements were conducted based on the Methodology of the International Biological Program (IBP), with standard equipment and measurement techniques.

Measures of central tendency and variability, SD, X, MED, MIN, MAX were used from the descriptive statistics. The correlation between certain anthropometric parameters was determined with regressive analysis and correlating coefficients.

Results

Results show that measurements of the facial anthropometric parameters which were in correlation with crown-rump length and biparietal diameter, as basic indicators of the physical growth and development of the fetus, are of great practical value because they tell us whether the fetus develops normally for its gestational

week or whether there are any deviations which lead to abnormal development.

Based on the information we got, we can see that the following anthropometric parameters showed highest level of positive correlation with crown-rump length in all of the examined groups: head circumference (r=0.53); biparietal diameter (r=0.89); as well as the facial anthropometric parameters: face spread (r=0.82); face lenght (r=0.87); nose spread (r=0.68) ; nose lenght (r=0.71); body weight (r=0.95); body length (r=0.99). Table 1.

The values of descriptive statistics in the tables for the measured facial anthropometric parameters of the total number of fetuses show that all given values are dependent upon gestational age. The values of the biparietal diameter in the first group are 3.28 ± 0.48, 3.73± 0.50 in the second group, and 3.98 ± 0.71 in the third group. The values of the other measured parameters are given in Table 2 (a, b, c,).

Table 1. Correlation of some anthropometrical parameters with gestational age and crown-rump lengh (r)

	gestational age	crown-rump lenght
body weight	0.89	0.95
body lenght	0.90	0.99
head circumference	0.52	0.53
morfol face lenght	0.81	0.87
face spread	0.77	0.82
biparietal diameter	0.85	0.89
fetal nasal bone lenght	0.55	0.71
fetal nasal bone spread	0.53	0.68

Table 2. a. Values of some anthropometrical parameters

n = 60 (11-13 g.w.)	Body weight(gr)	Body lenght(cm)	HC(cm)	BPD(cm)	Nasal bone lenght(cm)	Nasal bone spread (cm)	Morfolog face lenght (cm)	Face spread (cm)
X	126.33	17.83	12.05	3.28	0.90	0.73	1.98	2.43
SD	38.42	1.99	1.40	0.48	0.26	0.17	0.39	0.40
MED	130	18.4	11.8	3.35	0.9	0.7	1.9	2.4
MIN	55	14.1	9.7	1.5	0.3	0.4	1.2	1.6
MAX	210	22	15	4.1	1.7	1.2	2.8	3.2

Table 2. b. Values of some anthropometrical parameters

n = 60 (14-16 g.w.)	Body weight(gr)	Body lenght(cm)	HC(cm)	BPD(cm)	Nasal bone lenght(cm)	Nasal bone spread (cm)	Morfolog face lenght (cm)	Face spread (cm)
X	161.75	19.51	14.72	3.73	1.03	0.91	2.29	2.77
SD	52.31	2.39	1.58	0.50	0.27	0.29	0.44	0.47
MED	147.5	19.5	13.2	3.8	1	0.8	2.3	2.8
MIN	70	15	9.7	2.6	0.5	0.6	1.2	1.9
MAX	290	25	10.2	5	2	1.9	3.3	3.6

Table 2. c. Values of some anthropometrical parameters

n = 60 (17-19 g.w.)	Body weight(gr)	Body lenght(cm)	HC(cm)	BPD(cm)	Nasal bone lenght(cm)	Nasal bone spread (cm)	Morfolog face lenght (cm)	Face spread (cm)
X	221.67	21.49	16.64	3.98	1.13	1.01	2.54	2.91
SD	96.16	2.91	2.11	0.71	0.31	0.51	0.43	0.55
MED	190	20.6	14.6	3.85	1.1	1	2.5	3
MIN	100	16.2	10.5	2.6	0.5	0.4	1.6	1
MAX	520	28	20	6.9	2.3	3.6	3.5	4.1

Discussion

Considering the fact that there are differences in the factors that influence the weight and the length of the fetus (such as the economic and social composition of the population, geographical factors etc), the growth curve changes in different environments. Because of those reasons, and recommended by WHO, other, more stable parameters are introduced in the classification: length of gestation, biparietal diameter, crown-rump length, head circumference, limbs circumference (4). According to Cicero S, Bindra R, (5) measuring the length of the nasal bone in the first trimester of intrauterine growth of the fetus can also be a useful parameter for discovering early chromosome abnormalities (11-14 gestational week). In their studies they noticed that in normal chromosomal groups of fetuses there is significant correlation between the length of the nasal bone and the crown-rump length as a standard for evaluation of gestational age. Absence of the nasal bone or abnormal fetal karyotypes is often connected with the occurrence of Trisomy 21 (6). Many authors compare the length of the fetal nasal bone (which increases linearly with gestational age) with biparietal diameter in evaluation of gestational age between 15th and 19th gestational week, especially in diagnosing fetal abnormalities that are most common during the second trimester (7-8). Examinations of facial parameters are good indicators for detecting some chromosomal abnormalities like Trisomy 21, some risk groups, hypoplasias, etc. The values of the length of the nasal bone (length of the nose) in our study were 1.08cm and they were 0.27cm higher compared to the measurements in a study in Israel, and 0.9cm lower than the ones in Korean fetuses. During development, the physical proportions of the fetus are significantly different from those of an adult. The head is relatively big and comprises 1/4 of body length, the face is small and round, and the limbs are short. Knowing these proportions is important for early detection of intrauterine growth restriction which is still one of the major causes of morbidity and mortality in many countries. These indexes can point to proportional decrease in the values of anthropometric parameters and, along with that, to decrease in body weight inadequate for the gestational age, as well as to proportional decrease of the value of the index. The big number of chromosomopaties, osteochondroplasias, and hypoplasias is usually the cause of the so-called disharmonic asymmetric growth. Longitudinal dimensions are one of the most reliable indicators of the intrauterine growth of the fetus that show whether the growth is adequate for the corresponding gestational week (9). Every deviation from the linear dimensions requires a larger observation in order to respond to the type, level and etiology of the changed growth. This anthropometrically diagnostic information should further be used together with other clinical and laboratorial data (10). The recommendations of WHO opened up new phases when considering the use of other fetal parameters that correlate highly with gestation and crown-rump length, parameters whose use increases the accuracy in the determination of the proper development of the fetus.

Conclusion

Measuring fetuses can serve as an additional method that can give us information about fetal growth and the changes that can occur during fetal growth and development. Body weight, body length, crown-rump length, head circumference and gestational age as certain fetal parameters which are routinely measured during the entire intrauterine growth of the fetus are considered to have a big role in evaluating fetal growth and development as well as in diagnosing early fetal abnormalities in the first trimester of intrauterine growth. Measuring facial parameters has proved to be simple and reliable and it can be used as an additional method in determining chromosomal abnormalities, hypoplasias, aneuploidy, Trisomy 21 during the first trimester of intrauterine growth of the fetus.

References

1. Senat MV, Bernard JP, Bouivain M. Intra-and interoperator variability in fetal nasal bone assessment at 11-14weeks of gestation. Ultrasound Obstet Gynaec 2003; 22(2): 138-41.

2. Shin JS, Yang JH, Chung JH at all. The relation between fetal nasal bone length and biparietal diameter in the Korean population. Prenatal Diagnosis 2006; 26(4):321-3.

3. Viora E, Masturzo B at all. Ultrasound evaluation of fetal nasal bone at 11 to 14 weeks in a consecutive series of 1906 fetuses. Prenatal Diagnosis 2003;23(10):784-7.

4. Garg A, Pathak N, Gorea RK. Ultrasonographical Age Estimation from Fetal Biparietal Diameter. Ultrasound Obstet Gynecol 2002;20:564-574.

5. Cicero S, Bindra R at all. Fetal nasal bone length in chromosomally normal and abnormal fetuses at 11-14 weeks of gestation. J Matern Fetal Neonatal Med 2002; 11 (6): 400-2.

6. Chen M, Lee CP, Tang R, Chan B. First trimester examination of fetal nasal bone in the Chinese population. Prenat Diagn 2006; 26(8):703-6.

7. Yanik FF, Eroglu D at all. Second trimester fetal nasal bone lenght in a low-risk Turkish population. Prenatal Diagnosis 2011; 31(10):962-6.

8. Ozer A, Ozaksit G at all. First trimester examination in fetal nasal bone in the Turkish population. J Obstet Gynaec 2010; 36(4): 739-44.

9. Akinola, R.A. Akinola, O.I. Sonography in fetal birth weight estimation. Educational Research and Review 2009; 4(1):16-20.

10. Pam Loughna, Lyn Chitty, Tony Evans at all. Fetal size and dating: charts recommended for clinical obstetric practice. British Medical Ultrasound Society 2009; 17(3):161-7.

UDK: 616-006.81

PREDICTIVE FACTORS IN MALIGNANT MELANOMA

Noveski Lazo, Dzhokik G, Pejkova S, Dzhonov B, Peneva M
University Clinic of Plastic and Reconstructive Surgery, Skopje, R. Macedonia

Abstract

The vertical melanoma thickness according to Breslow, the anatomical level of the tumor skin invasion according to Clark, mitotic activity in the tumor cells, the type and the phase of growth of the tumor, the localization, the local inflammatory response to the tumor cell and the presence of the tumor infiltrating lymphocytes as well as the age and the sex of the patient are considered as factors which could influence the prognosis of the melanoma.

The aim of this study was to define the correlation between the predicting factors of malignant melanoma (vertical melanoma thickness according to Breslow, the presence of the ulceration and the presence of tumor infiltrating lymphocytes), and the presence of metastases in the sentinel nodes, and, to determine the predicting value of these factors in patients with malignant melanoma of the skin.

Thirty patients with malignant melanoma, who had undergone surgery at the University Clinic of Plastic and Reconstructive Surgery in Skopje in the period from 2005 until 2009, were retrospectively evaluated. The following parameters were analyzed: primary tumor thickness according to Breslow, presence of ulcerations, lymphocytic infiltration and their relation with onset of metastases in the sentinel lymph node.

The results showed that there was a statistically significant correlation of the vertical thickness of the tumor according to Breslow and the presence of the lymphocytic infiltration with the sentinel node positivity for metastasis. Higher value of Breslow indicates higher possibility for metastasis in the sentinel nodes. A more intense tumor lymphocytic infiltration is related to the lower possibility for metastasis in the sentinel nodes. The correlation between the ulceration of the melanoma lesion and the positivity for metastasis of the sentinel node was statistically insignificant.

Key words: malignant melanoma, lymph node, metastasis

Introduction

The prognosis of malignant melanoma greatly depends on its stage at the time of establishing the diagnosis. There are a numerous studies analyzing the clinical and pathological factors that could predict the outcome of the disease in patients with malignant melanoma (1, 2, 3, 4). The vertical melanoma thickness according to Breslow, the anatomical level of the tumor skin invasion according to Clark, mitotic activity in the tumor cells, the type and the phase of growth of the tumor (radial and vertical), the localization, the local inflammatory response to the tumor cell and the presence of the tumor infiltrating lymphocytes as well as the age and the sex of the patient are considered as factors which could influence the prognosis of the melanoma (5, 6, 7, 8, 9, 10).

The most important, independent prognostic factor, which has been statistically proved to predict the prognosis in patients with malignant melanoma, is the vertical melanoma thickness (11). The Breslow classification can be used to determine the tumor thickness. It categorizes the tumor tissue depth from 1 to 2 mm, from 2 to 4 mm and more than 4 mm.

The ulceration is determined according to the macroscopic appearance of the lesion. It is proportional to the enlargement of the tumor thickness, but statistical analyses have shown that it is an independent predicting factor of the patient survival (7, 8).

The presence of tumor infiltrating lymphocytes (TIL) represents the body immune response to the melanoma cells or some other tumor cells. The immune response is most commonly measured by the intensity of the lymphocyte infiltration at the base of the vertical phase of growth, and it is categorized as severe, milde and negative. TIL population mostly consists of T lymphocytes, and some other subpopulation such as dendritic cells, macrophages, natural killer (NK) cells and B lymphocytes. The results of many studies have shown that the presence of TIL is related to better prognosis (12, 13, 14).

The aim of this study was to define the correlation between the predicting factors of malignant melanoma (vertical melanoma thickness according to Breslow, the presence of the ulceration and the presence of tumor infiltrating lymphocytes), and the presence of metastases in the sentinel nodes, and, to determine the predicting value of these factors in patients with malignant melanoma of the skin.

Material and methods

Thirty patients with malignant melanoma, who had undergone surgery at the University Clinic of Plastic and Reconstructive Surgery in Skopje in the period from 2005 until 2009, were retrospectively evaluated.

All patients, according to the established surgical protocol, underwent radical excision of the primary malignant melanoma lesion and biopsy of the sentinel node. The operative material was sent to patohistological analysis.

The primary lesions of malignant melanoma were grouped according to the localization.

The following parameters were analyzed: primary tumor thickness according to Breslow, presence of ulcerations, lymphocytic infiltration and their relation with onset of metastases in the sentinel lymph node.

The results were statistically analyzed using multivariate tests, and the correlation between the

examined factors (primary tumor thickness according to Breslow, presence of ulcerations, lymphocytic infiltration) and the onset of metastases in the sentinel lymph node was determined.

Results

The primary malignant melanoma lesion was on the upper extremity in 6 patients (20%), it was on the trunk in 3 patients (10%) and on the lower extremity in 21 patients (70%).

The examination of the localization of the tumor lesion related to the type of the malignant melanoma showed that all of the patients with melanoma on the upper extremity (6 patients) and on the trunk (3 patients), had a nodular type of malignant melanoma. The lesions on the lower extremity were of nodular type in 16 patients, acral type in 3 patients, amelanotic type in one patient and a lesion with superficial spreading in one patient. Therefore, 24% of all nodular malignant melanoma were found on the upper extremity, 12% on the trunk and 64% on the lower extremity. All (100%) of the acral and amelanotic tumor lesions, and lesions with superficial spreading were located on the lower extremity (Table 1).

The results of this study showed that there was a statistically significant correlation of the vertical thickness of the tumor according to Breslow and the presence of the lymphocytic infiltration with the sentinel node positivity for metastasis. Higher value of Breslow indicates higher possibility for metastasis in the sentinel nodes. A more intense tumor lymphocytic infiltration is related to the lower possibility for metastasis in the sentinel nodes (Table 2).

The correlation between the ulceration of the melanoma lesion and the positivity for metastasis of the sentinel node was statistically insignificant.

Discussion

Primary skin melanoma can be classified according to the TNM classification of American Joint Committee on Cancer (AJCC). This classification defines the tumor, lymph nodes and metastasis (15).

The main factors that influence on T stage are the thickness of the tumor tissue measured in mm according to Breslow and the ulceration of the tumor. The stage of the lymph nodes (N) is determined by the spreading of the melanoma cells in the regional lymph nodes. The identification of the first drainage lymph node (sentinel node) is performed using radioactive colloid. The status of the sentinel node, confirmed by biopsy, is the most significant independent clinical pathologic factor which determinates the survival of the patients with primary malignant melanoma (16, 17, 18, 19, 20, 21).

Table 1. Distribution of the tumor lesions according to the type of the malignant melanoma and its localization

Localization	Type of malignant melanoma				
	nodular	acral	amelanotic	supp.spread	Total
Upper extremity	6 (24.0%)	0 (.0%)	0 (.0%)	0 (.0%)	6 (20.0%)
Trunk	3 (12%)	0 (.0%)	0 (.0%)	0 (,0%)	3 (10.0%)
Lower extremity	16 (64.0%)	3 (100.0%)	1(100.0%)	1 (100.0%)	21(70.0%)
Total	25 (100.0%)	3 (100.0%)	1(100.0%)	1 (100.0%)	30 (100.0%)

Table 2. Correlation between the presence of ulceration, tumor thickness according to Breslow and lymphocytic infiltration and the onset of metastasis in sentinel lymph node.

		Sentinel lymph node			
		negative	positive	Total	
Ulceration	negative	9 (30.0 %)	5 (16.7 %)	14 (46.7%)	p=.293
	positive	9 (30.0 %)	7 (23.3 %)	16 (53.3%)	
Total		18 (60.0 %)	12 (40.0 %)	30 (100.0%)	
Breslow	1-2mm	9 (30.0 %)	1(3.3 %)	10 (33.3%)	p<.001
	2-4 mm	9 (30.0 %)	4 (13v4 %)	13 (43.4%)	
	> 4 mm	0 (.0%)	7 (23v3 %)	7 (23.3%)	
Total		18 (60. 0%)	12 (40.0 %)	30 (100.0%)	
TIL	TIL +	12 (40. 0%)	1 (3.3 %)	13 (43.3%)	p<.001
	TIL + -	6 (20 v 0%)	5 (16. 7 %)	11(36.7%)	
	TIL -	0 (.0%)	6 (20. 0 %)	6 (20. 0%)	
Total		18 (60.0%)	12 (40.0%)	30 (100.0%)	

*TIL + severe lymphocytic infiltration
TIL +- milde lymphocytic infiltration
TIL – no lymphocytic infiltration

Today the widely spread and generally accepted is the classification of the melanoma staging according to the recommendations of the American Joint Committee of Cancer and Union International Contra le Cancer, which has being revised and updated in line with the latest knowledge since 1988 (4, 11). Thus, the newest revised edition is that from 2010. This classification is being supplemented with classifications according to the Breslow vertical melanoma thickness. Microstaging of malignant melanoma is determined by Breslow according to the vertical melanoma thickness in millimeters: up to 1 mm or less, from 1.0 to 2.0 mm, from 2.0 to 4.0 mm and from 4.0 mm and larger.

The results of this study showed that there was a statistically significant correlation of the vertical thickness of the tumor according to Breslow with the sentinel node positivity for metastasis. Higher value of Breslow indicates higher possibility for metastasis in the sentinel nodes.

According to the literature ulceration has a statistically significant value for the prognosis and staging of malignant melanoma (7, 8). Our finding was not in agreement with the results in the other studies comprising a larger number of subjects, which might be due to the small number of patients and to the fact that there were no patients in the early stage of the disease in relation to the overall analysis of our material.

Tumor infiltrating lymphocytes have the main role in the antitumor immune response of the host, by increasing the cytotoxicity of T lymphocytes and by inducing apoptosis of tumor cells.

T lymphocyte population is mainly consists of different CD4+ helper and/or CD8+ cytotoxic T lymphocyte (CTL) (22). Tumor infiltrating lymphocytes have tumor specific characteristics. CD8+ T lymphocytes recognize tumor antigens and tumor associated antigens presented by molecules of MHC class I. After the recognizing and activation, the cytotoxic T lymphocytes directly kill the tumor cells by releasing litic granules, which contain preforin and granines, into the target cells. Also, they transmit Fas ligands in tumor cells, which are mediators of signals of apoptosis. Cytotoxic T lymphocytes secrete cytokines which destroy or help destroying the target cells.

T helper lymphocytes are capable of recognizing tumor antigens and tumor associated antigens of MHC class II molecules. After their activation, CD4+ T helper cells release cytokines which participate in regulation of the immune response (22, 23).

Another group of tumor infiltrating lymphocytes is CD4+ and CD25+ lymphocytes, which have an important role in immunosuppression (22, 23).

Tumor infiltrating lymphocytes also produce soluble cytokines, like interferon –ã which is essential for the cell immune response (23, 24, 25, 26).

The results of our study indicate that the presence of more intense tumor lymphocytic infiltration in the primary melanoma lesion is related to the smaller possibility for metastasis in the regional lymph nodes.

The knowledge of the tumor biology and the role of the tumor infiltrating lymphocytes in the immune response are particularly important for introducing new modalities of immunotherapy in the therapy of malignant melanoma

References

1. Balch CM, Soong SJ, Gershenwald JE, et al. Prognostic factors analysis of 17600 melanoma patients: validation of the American Joint Committee on Cancer melanoma staging system. J Clin Oncol 2001; 19:3622–34.

2. Manola J, Atkins M,Ibrahim J, et al. Prognostic factors in metastatic melanoma: A pooled analysis of Eastern Cooperative Oncology Group trials. J Clin Oncol 2000; 18:3782 - 93.

3. Goldstein BG, Goldstein AO. Diagnosis and management of malignant melanoma Am Fam Physician 2001; 63(7):1359-74.

4. Melanoma Study Group, British Association of Dermatologists. UK guidelines for the management of cutaneous melanoma. Br J Plast Surg 2002; 55(1):46-54.

5. Clark WH, Fromm L, Bernardino EA et al. The histogenesis and biologic behavior of primary human malignant melanomas of the skin. Cancer Res. 1969; 29:705-26.

6. Eggermont AM, Keilholz U, Autier P, Ruiter DJ, Lehmann F, Lienard D. The EORTC melanoma Group: a comprehensive melanoma research programme by clinicians and scientist. European Organisation for Research and Treatment of Cancer. Eur J Cancer 2002; 38(4):114-9.

7. Dabrowska DM, Elashoff RM, Ho W, Morton DL. Identifying predictive factor in melanoma progression. Oncol Rep 1998; 5:569-75.

8.Vollmer RT. Malignant melanoma: a multivariate analysis of prognostic factor Pathol Annu 1989; 24:383-407.

9. Kretchmer L, Preusser KP, Marsch WC, Neuman C. Prognostic factors of overall survival in patient with delayed lymph node dissection for cutaneous malignant melanoma. Melanoma Res 2000;10(5): 483-9.

10. Clark WH, Elder DE, Guerry DT et al. Model predicting survival in stage I melanoma based on tumor progression. J Natl Cancer Inst 1989; 81:1893-904.

11. Breslow A. Thickness, cross-sectional areas and depth of invasion in the prognosis of cutaneous melanoma. Ann Surg 1970; 902-8.

12. Mansfield AS, Holtan SG, Grotz TE, Allred JB, Jakub JW, Erickson LA, Markovic SN. Regional immunity in melanoma: immunosuppressive changes precede nodal metastasis. Mod Pathol 2011; 4:487–494.

13. Yamaguchi T, Sakaguchi S. Regulatory T cells in immune surveillance and treatment of cancer. Semin Cancer Biol 2006; 16:115–23.

14. Hoon DS, Bowker RJ, Cochran AJ. Suppressor cell activity in melanoma draining lymph nodes. Cancer Res 1987; 47:1529–33.

15. Balch CM, Gershenwald JE, Soong SJ et all. Final version of 2009 AJCC melanoma staging et classification. J Clin Oncol 2009; 27(36):6199-206.

16.Morton DL, Wen DR, Wong JH et al. Technical details of intraoperative lymphatic mapping for early stage melanoma. Arch Surg 1992; 127:392-9.

17. Reintgen D. Lymphatic mapping and sentinel node harvest for malignant melanoma. J Surg Oncol 1997; 66:277-81.

18. Bruns SD, McGee JM, Phillips JW. Current treatment of cutaneous melanoma and the sentinel lymph node. J Okla State Med Assos 2002; 95(5);332-5.

19. Morton DL, Thompson JF, Essner R et al. Validation of the accuracy of the intraoperative limphatyc mapping and sentinel lymphadenectomy for early-stage melanoma: a multicenter trial.Multicenter Selective Lymphadenectomy Trial Group. Ann Surg 1999; 230:453-65.

20. Cochran AJ, Huang RR, Lee J, Itakura E, Leong SP, Essner R.Tumour-induced immune modulation of sentinel lymph nodes. Nat Rev Immunol 2006; 6:659–70.

21. Negin B, Panka D, Wang W, Siddiqui M, Tawa N, Mullen J, et al. Effect of melanoma on immune function in the regional lymph node basin. Clin Cancer Res 2008; 14:654–9.

22. Hanson EM, Clements VK, Sinha P, Ilkovitch D, Ostrand-Rosenberg S.Myeloid-derived suppressor cells down-regulate L-selectin expression on CD4 + and CD8 + T cells. J Immunol 2009; 183:937–944.

23. Shimizu J, Yamazaki S, Sakaguchi S. Induction of tumor immunity by removing CD25 +CD4 + T cells: a common basis between tumor immunity and autoimmunity. J Immunol 1999; 163:5211–8.

24. Porter GA, Abdalla J, Lu M, Smith S, Montgomery D, Grimm E, et al. Significance of plasma cytokine levels in melanoma patients with histologically negative sentinel lymph nodes. Ann Surg Oncol 2001; 8:116–22.

25. Lee JH, Torisu-Itakara H, Cochran AJ, Kadison A, Huynh Y, Morton DL, Essner R. Quantitative analysis of melanoma-induced cytokine-mediated immunosuppression in melanoma sentinel nodes. Clin Cancer Res 2005; 11:107–12

26. Massi D, Puig S, Franchi A, Malvehy J, Vidal-Sicart S, Gonzalez-Cao M, et al. Tumour lymphangiogenesis is a possible predictor of sentinel lymph node status in cutaneous melanoma: a case-control study. J Clin Pathol 2006; 59:166–73.

UDK: 616.314-089.23

DENTAL ENAMEL AROUND FIXED ORTHODONTIC APPLIANCES AFTER FLUORIDE VARNISH APPLICATION

Zabokova - Bilbilova E, Bajraktarova B, Sotirovska - Ivkovska A, Georgiev Z

Department of Pedodontic Dentistry, University Dental Clinical Centre "St. Pantelejmon", Faculty of Dentistry, Skopje, Macedonia

Abstract

The aim of this study was to evaluate the effects of a topical fluoride varnish application on enamel around orthodontic brackets bonded with a composite resin.

The study involved 60 premolars extracted for orthodontic reasons. The patients were evaluated during a 30-day period and did not use any kind of fluoride supplement during the experimental period, except fluoridated toothpastes. The adhesive used in this study for bonding brackets was Con Tec LC (Dentaurum, Germany). After bracket bonding, the left premolars (test specimens) were kept dried by careful tooth isolation and the enamel received a single topical application of a fluoride varnish (Duraphat®, Germany) with the aid of a brush applicator. The right premolars were used as controls (i.e., did not receive any varnish application) and brackets were fixed using identical procedures. After 30 days, teeth were extracted carefully to avoid accidental brackets removal and stored in artificial saliva (20 mmol/l $NaHCO_3$, 3 mmol/l NaH_2PO_4 and 1 mmol/l $CaCl_2$, neutral pH) until analysis. After that, the samples (20 premolars) were prepared for scanning electron microscopy, SEM (JEOL JSM 5300). Determination of the fluoride in enamel (60 premolars) was done by spectrophotometer.

Analysis of the level of fluoride in enamel before and after bonding the brackets with composite resin (Dentaurum, Germany), and application of a fluoride varnish clearly showed that after its application the content of fluoride in enamel was significantly increased. Examination of enamel surfaces adjacent to orthodontic brackets revealed calcium fluoride-like material (CaF_2) deposition as a reaction product of topical fluoride varnish application. An adhered thin layer of varnish was also seen in some teeth of the test group, which was in close contact with the enamel around the orthodontic brackets.

Fluoride varnish could indeed be considered an efficient preventive method to enhance enamel resistance against the cariogenic challenges during orthodontic therapy. Thus, topical application of fluoride varnish on enamel adjacent to orthodontic accessories, incorporated as a routine clinical preventive procedure, is a simple measure of great significance. It is strongly recommended for decreasing the risk of enamel demineralization during orthodontic treatment.

Key words: enamel, brackets, demineralization, fluoride varnish

Introduction

Poor oral hygiene has been considered to be one of the main problems routinely faced in the orthodontic treatment. Orthodontic appliance creates an environment that provides mineral loss from the dental enamel [1]. Such condition is clinically seen as white spot lesions and cavitations in the most severe cases.

Very effective agents for local application, providing a high level of fluor in the oral environment, are fluoride varnishes. Fluoride varnishes are used in order to help for fluorides to remain on the enamel surface as long as possible, and to be incorporated in the enamel crystal lattices as much as possible. The use of fluoride varnishes before cementing of orthodontic bands with a glass ionomer, suppresses the occurrence of the initial carious lesion - the white spot [2]. Materials for brackets bonding and for cementing the bands are used in orthodontic practice. The interface between the teeth and bonding material is a sensitive area. The basis of adhesion in orthodontic therapy with fixed devices is contained in the pre-treatment of the tooth enamel surface with acid, thus creating the microcracks i.e. the retention surfaces for subsequent application of a bond – an adhesive material [3].

The application of fluoride varnish is a preventive protocol that does not require patient compliance and permits the orthodontist to benefit from the bond strength of composite resins [4, 5]. Prolonged contact time with fluoride varnish permits significantly more incorporation of fluoride than other cooperation - based fluoride

applications, e.g. acid phosphate fluoride gel, monofluoride phosphate dentifrices, home fluoride rinses [6, 7]. Peterson et al. observed that a tri-monthly application of fluoride varnish resulted in a dramatic reduction in caries incidence and the application of a fluoride varnish can be easily adapted to current orthodontic bonding techniques [8].

The manufacturers of a new system of self etching basic coat believe that an adequate bonding strength can be achieved by way of bonding orthodontic brackets to the wet tooth enamel surface [9]. Some of the most extensively studied adhesives are glass - ionomer cements (GJCs), with some well described advantages. They are bonded directly to the tooth enamel surface, without previous etching, with an interaction of polyacrylate ions with hydroxyapatite calcium. Glass - ionomer cements exert, in addition, a cariostatic effect by way of releasing the ions of fluor [10]. Using the glass-ionomer cement as an adhesive for orthodontic brackets bonding, Fricker has studied the process of demineralization (white spots) occurring in the pre-treatment period and process of remineralization as the result of fluoride action from the adhesive material [11]. After the observation period of 12 months, the results demonstrated a significant reduction of demineralized enamel in the group of studied samples with glass-ionomer cement after brackets debonding.

Scanning electron microscopic (SEM) study of the fluoride retention in sound demineralized enamel demonstrated that bacteria accumulation around modified orthodontic bands led to a marked and localized direct etching of the tooth under the plaque at the junction of the tooth visible after only one week. Another study showed that fluoride was more effective in inhibiting demineralization of lesions, supporting the vitro observation that low levels of fluoride in acidic buffer solutions decrease considerably the solubility of the mineral [12].

The aim of this study was to evaluate the effects of a topical fluoride varnish application on enamel around orthodontic brackets bonded with a composite resin.

Material and methods

The study involved 60 premolars extracted for orthodontic reasons. The patients were evaluated during a 30-day period and did not use any kind of fluoride supplement during the experimental period, except fluoridated toothpastes. Brackets were bonded with one type of adhesive according to manufacturers‘ bonding instructions. The adhesive used in this study for bonding brackets was Con Tec LC (Dentaurum, Germany). After bracket bonding, the left premolars (test specimens) were kept dried by careful tooth isolation and the enamel received a single topical application of a fluoride varnish (Duraphat®, Germany) with the aid of a brush applicator. The right premolars were used as controls (i.e., did not receive any varnish application) and brackets were fixed using identical procedures. After 30 days, teeth were extracted carefully to avoid accidental bracket removal and stored in artificial saliva (20 mmol/l $NaHCO_3$, 3 mmol/l NaH_2PO_4 and 1 mmol/l $CaCl_2$, neutral pH) until analysis. Before laboratorial analysis, teeth were rinsed with ethanol for 60 s to remove organic substances and debris from enamel without fluoride dissolution.

Determination of the fluoride in enamel (60 premolars) was done by spectrophotometer. First of all, distillation was initiated, and then 50 ml of the distillate was mixed with 10 ml SPADNS and acidic circonyl. The absorbance was read on the spectrophotometer. The results were calculated by the formula: *F ppm= 50A/V,* where A is ppm of fluoride measured by the spectrophotometer, and V ml of the sample.

After that, the samples (20 premolars) were prepared for scanning electron microscopy, SEM (JEOL JSM 5300), using the technique of sputtering in a vacuum evaporator. By SEM analysis we monitored micromorphologic changes in the enamel structure on the places where brackets had been previously fixated.

Results

Table 1 shows the value of F in enamel in the first group of teeth brackets bonded with Con Tec Duo (Dentaurum, Germany), 30 days after topical application of a fluoride varnish. The average value of F in the examined group of teeth was 831,763 ppm, and 625,240 ppm in the control group of teeth. For this time period a statistically significant difference was found between values of F in the enamel in both examined groups of teeth.

Table1. The value of F in enamel 30 days after topical application of a fluoride varnish

Group	*N*	*Mean*	*SD*	*t - value*	*p*
test	30	831,763	324,130		
				3,480	0,00065*
control	30	625,240	167,149		

The initial demineralization of enamel prisms was observed in the control group (Figure 1a, b).

Examination of enamel surfaces adjacent to orthodontic brackets revealed calcium fluoride-like material (CaF_2) deposition as a reaction product of topical fluoride varnish application. An adhered thin layer of fluoride varnish was also seen in some teeth of the test group,

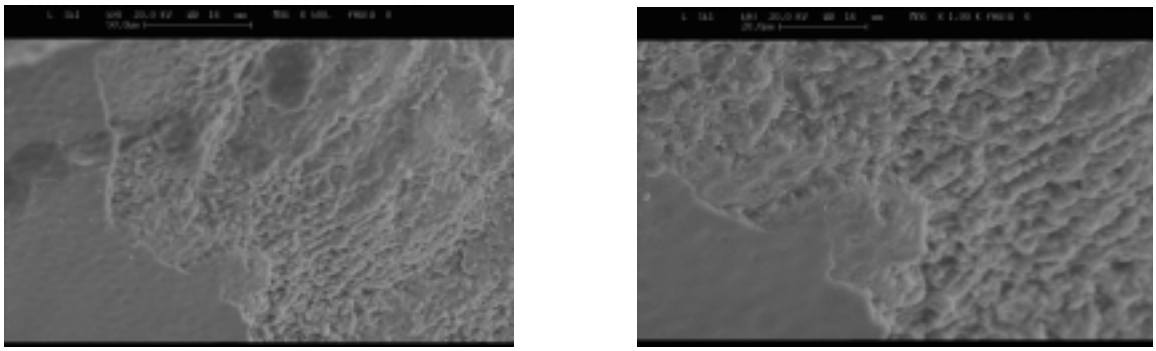

a) *b)*

Fig. 1. SEM micrographs of initial demineralization of enamel prisms (a - magnification x 500; b - magnification x1000)

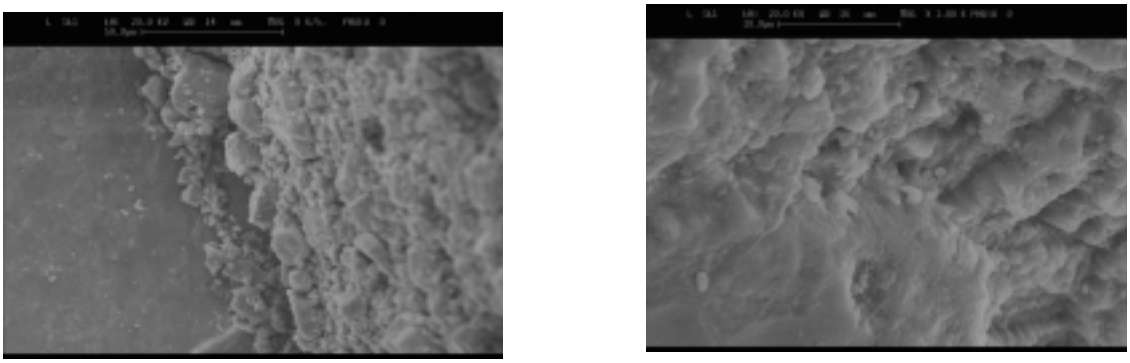

a) *b)*

Fig. 2. (a, b) - Deposits of CaF_2 on enamel adjacent to the orthodontic brackets

which was in close contact with the enamel around the orthodontic brackets (Figure 2a, b).

Discussion

During treatment with fixed orthodontic appliances certain problems may occur, such as: fractures or even loss of enamel, which may be related to the pretreatment of the enamel surface during prophylaxis and/ or during phosphoric acid etching; additional loss of enamel during brackets debonding, removal of debris from the tooth and decalcification of the enamel around the brackets, which is considered the most common problem in patients undergoing orthodontic treatment with fixed appliances [13].

Given the fact that it is difficult to secure patient compliance in plaque control and use of fluoride and due to the inconvenient effects caused by the unsightly white spots, researchers started to develop adhesives with the addition of fluoride to prevent enamel demineralization around the brackets [14]. These materials were investigated for their fluoride releasing efficacy, which has been confirmed by several studies [15, 16].

The mechanisms of action of fluorides have been investigated for many years. In many ways, fluorides represent an ideal agent as a public health measure against dental caries (a disease of microbial etiology); since: a) it stabilizes the tissues at risk (enamel and dentin), b) it reduces the advantage of aciduric organisms within the plaque and c) it does not change the normal oral flora (as would an antibiotic), but reduces the acidogenity of cariogenic bacteria. There is also substantial evidence that fluorides influence metabolism of plaque microbiota, possibly their adhesion to the enamel surface, inhibition of microbial enzyme system, reduction of growth rates of bacteria and possible bactericidal effect [17]. One of the factors that are also considered to be important is the release of F - ions when CaF_2 is dissolved, producing an antimicrobial effect [18, 19]. This study investigated whether fluoride varnish application could improve the local condition of dental enamel areas with a high risk of demineralization.

Nelson [20] suggested that the particle size of CaF_2 deposits in the surface coating produced by topical fluoride agent may be an important factor in determining the effectiveness of topical fluoride agents. As the

solubility of crystals decrease with their increasing sizes, CaF_2 particles occurring as a result of APF application will dissolve slower than those of NaF.

The results obtained in this study about on the level of fluoride in enamel before and after bonding the brackets with composite resin (Dentaurum, Germany), and application of a fluoride varnish clearly showed that after its application the content of fluoride in enamel was significantly increased. Thus, the amount of fluoride in enamel before fixing the brackets was 614,230 ppm. After 30 days of fluoride varnish application the amount of fluoride in enamel was 844.044 ppm, which was statistically significantly higher than the initial coverage of fluoride in enamel. Our results confirmed that fluoride varnish application is a simple and fast technique that could be useful in preventing enamel demineralization associated with orthodontic treatment.

Topical treatments with fluoride varnish result in formation of calcium fluoride-like material on the surface of the teeth. Scanning electron microscopy (SEM) shows it as small globules on the surface of fluoridated teeth. According to Ögaard, calcium fluoride is the largest and the most important reaction product formed on enamel after topical application of any fluoride-containing material [21]. Calcium fluoride has also been considered a fluoride ions reservoir, which can be used for enamel protection during higher cariogenic challenges in the oral cavity.

Conclusions

Fluoride varnish could indeed be considered as an efficient preventive method which enhances the enamel resistance against the cariogenic challenges during orthodontic therapy.

Thus, topical application of fluoride varnish on enamel adjacent to orthodontic accessories, incorporated as a routine clinical preventive procedure, is a simple measure of great significance. It is strongly recommended for decreasing the risk of enamel demineralization during orthodontic treatment.

References

1. Ögaard B, Rolla G, Arends J. Orthodontic appliances and enamel demineralization: Part 1. Lesion development. Am J Orthod Dentofacial Orthop 1988; 94: 68-73.

2. Todd M, Staley R, Kanellis M, Donly K, Wefel J. Effect of a fluoride varnish on demineralization adjacent to orthodontic brackets. Am J Orthod Dentofacial Orthop 1999; 116: 159-67.

3. Schmit JL, Staley RN, Wefel JS, Kanellis M, Jakobsen JR, Keenan PJ. Effect of fluoride varnish on demineralization adjacent to brackets bonded with RMGI cement. Am J Orthod Dentofacial Orthop 2002; 122:125-34.

4. Bowman SJ. Use of a fluoride varnish to reduce decalcification. J Clin Orthod 2000; 34: 377-9.

5. Gorton J, Featherstone JD. In vivo inhibition of demineralization around orthodontic brackets. Am J Orthod Dentofacial Orthop 2003; 123: 10-4.

6. Demito CF, Vivaldi-Rodriguez G, Ramos AL, Bowman SJ. The efficacy of a fluoride varnish in reducing enamel demineralization adjacent to orthodontic brackets: An in vitro study, Orthod Craniofac Res 2004; 7: 205-10.

7. Vivaldi-Rodrigues G, Demito CF, Bowman SJ, Ramos AL. The effectiveness of a fluoride varnish in preventing the development of white spot lesions. World J Orthod 2006; 7: 138-44.

8. Petersson L, Magnusson K, Andersson H, Almquist B, Twetman S. Effect of quarterly treatments with a chlorhexidine and a fluoride varnish on approximal caries in caries-susceptible teenagers: A 3-year clinical study. Caries Res 2000; 34: 140-4.

9. Vorhies AB, Donly KJ, Staley RN, Wefel JS. Enamel demineralization adjacent to orthodontic brackets bonded with hybrid glass ionomer cements: an in vitro study. Am J Orthod Dentofacial Orthop 1998 December; 114 (6): 668-74.

10. Voss A, Hickel F, Holkner S. In vivo bonding of orthodontic brackets with glass ionomer cements. Angle Orthod 1993; 63: 149-53.

11. Fricker JP. A 12 month clinical evaluation of a light activated glass ionomer cement for the direct bonding of orthodontic brackets. Am J of Orthod Dentofacial Orthop 1994; 105: 502-5.

12. Ögaard B. CaF_2 formation: cariostatic properties and factors of enhancing the effect. Caries Res 2001; 35: 40-4.

13. Arends J, Lodding A, Petersson LG. Fluoride uptake in enamel: in vitro comparison of topical agents. Caries Res 1980; 14: 403-13.

14. Corry A, Millett DT, Creanor SL, Foye RH, Gilmour WH. Effect of fluoride exposure on cariostatic potential of orthodontic bonding agents: an in vitro evaluation. J Orthod 2003; 30 (4): 323-9.

15. Basdra EK, Huber H, Komposch G. Fluoride released from orthodontic bonding agents alters the enamel surface and inhibits enamel demineralization in vitro. Am J of Orthod Dentofacial Orthop 1996; 109: 466-72.

16. Gaworski M, Weinstein M, Borislow A, Braitman L. Decalcification and bond failure: A comparison of a glass ionomer and a composite resin bonding system in vivo. Am J Orthod Dentofacial Orthop 1999; 116: 518-21.

17. Geiger AM, Gorelick L, Gwinnett AJ, Griswold PG. The effect of a fluoride program on white spot formation during orthodontic treatment. Am J Orthod 1998; 93: 929-38.

18. Gillgrass T, Creanor S, Foye R, Millett D. Varnish or polymeric coating for the prevention of demineralization? An ex vivo study. J Orthod 2001; 28: 291-5.

19. Glasspoole E, Erickson R, Davidson C. Demineralization of enamel in relation to the fluoride release of materials. Am J Dent 2001; 14: 8-12.

20. Nelson DGA and Arends WLJ. Morphology of Enamel surfaces Treated with Topical Fluoride Agents. J Dent Res 1983; 62:1201-8.

21. Ögaard B, Duschner H, Ruben J, Arends J. Microradiography and confocal laser scanning microscopy applied to enamel lesions formed in vivo with and without fluoride varnish treatment. Eur J Oral Sci 1996; 104: 378-83.

UDK: 616.314.18

NERVE FIBERS IN HUMAN DECIDUOUS DENTAL PULP

Georgiev Zlatko[1], Kovacevska I[3], Zabokova-Bilbilova E[1], Petruševska G[2], Sotirovska-Ivkovska A[1]
[1] Faculty of Dentistry, University "Ss. Cyril and Methodius" - Skopje; Republic of Macedonia
[2] Faculty of Medicine, University "Ss. Cyril and Methodius" - Skopje; Republic of Macedonia
[3] Faculty of Medicine, University "Goce Delèev" - Štip; Republic of Macedonia

Abstract

Deciduous teeth contrary to permanent ones have relatively short lifetime and functional duration; they are formed in a much shorter period of time, and are subordinated to an early physiological resorption of the roots, in order to make free space for lining of the permanent teeth. Dental pulp is a unique tissue, which is responsible for maintaining of the tooth vitality. In order to examine the reparatory pulp ability of deciduous teeth we investigated histological changes of the nerve fibers in the pulp. Histological findings were performed on a light microscope and on a Transmission Electron Microscope. Nerve fibers in deciduous dental pulp showed some disturbances when physiological resorption had been started.

Under light microscopy, nerve fibers showed unclear pathological changes – they begain to loose the myelin coat because of increased edema. Using TEM, non-myelin nerve fibers showed disorder in the homogeneousness of the axoplasmal structure, less density of mucopolysaccharide matrix in some places, which suggested edematous vacuolar changes and probably under its pressure an atrophy of the axons occurred gradually. The myelin nerve fibers showed deformations and division of the myelin coat; type lamellar osmiophillic bodies in shape of sphinx's myelin figures, with irregular thickness, developed from formation of vacuoles, filled with shapeless and low granulated material. The Schwann´s cells were degenerated, with relatively preserved nucleus, contrary to the cytoplasm where collagen fibers are inserted directly and the increased collagenisation became apparent endoneurally. The myelin nerve fibers are plased longitudinally, their diameters is enlarged; they has interlamellar fissures, and they atrophy with resorption progress.

Key words: deciduous teeth, dental pulp, root resorption, ultrastructure.

Introduction

Deciduous teeth contrary to permanent ones have relatively short lifetime and functional duration; they are formed in a much shorter period of time, and are subordinated to an early physiological resorption of the roots, in order to make free space for lining of the permanent teeth.

Dental pulp is a unique tissue, which is responsible for maintaining of the tooth vitality. When this tissue is damaged by disease, it reacts in an attempt to defend by production of protective - tertiary dentine. The survival of the tissue in some pathological conditions depends from its non-specific and specific defensive mechanisms.

The pulp is also a sensory organ. But, the innervations of human primary teeth has received little attention compared to similar research of permanent teeth, because they are smaller and short - lived, and it was thought that the pulps were similar. Another area which lack of information involves changes in the neural tissue of the deciduous teeth during the period of root resorption [1]. Immunohistochemical investigation performed by Egan et al. had shown that deciduous dentine was innervated, similar to permanent [2]. The structure and relationships of the nerve fibers in the dental pulp are of interest because of their involvement in the genesis of the pain. The apical region was observed to have 72% unmyelinated nerves – C fiber range 0.79 µm and conduit pain sensation and postganglionic autonomic innervations. Only 28% were myelinated nerves in the A delta fiber range 3.36 µm and conduct pain sensation [3]. Nerve fibres give neurological control of the dental pulp.

Aim: In order to examine the reparatory pulp ability of deciduous teeth we investigated histological changes of the nerve fibers in the pulp; that had neurological control of the dental pulp, because the dental pulp is necessarily active member in the life of tooth, when it's not infected.

Methods

The pulps used for this research had originated from intact teeth of healthy children, aged 5 to 9 years (5 deciduous teeth without signs of physiological resorption, and the second group – consisted of 5 deciduous teeth with progressive physiological resorption). Immediately after the extraction (performed due to orthodontic reasons, under local anesthesia), each tooth was cut perpendicularly to its long axis with rotating carborundum disc under a water jet. The halves were separated with plastic instrument, and the tooth pulp was excavated completely. Histological findings were performed on a light microscope Orthoplan Leitz-Wetzlar (haematoxyllin-eosin HE, toluidine blue TB) and on a Transmission Electron Microscope (TEM) Tesla BS 500 (60 KV).

Results

The innervations of deciduous dental pulp were studied in human deciduous teeth using a light microscope and TEM (Fig. 1, 2, 3).

Fig. 1. Nonmyelinated nerve fibers with Schwann cells (TEM, 8500 x)

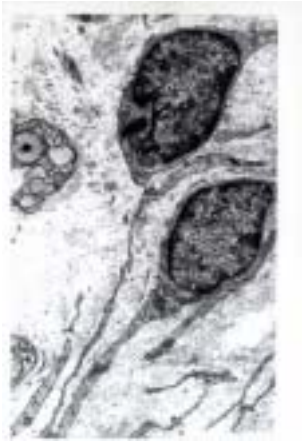

Fig. 2. Nonmyelinated nerve fibers with Schwann cells (TEM, 17000 x)

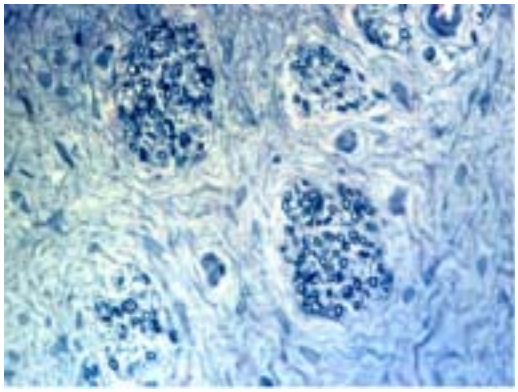

Fig. 3. Nerve fibers with myelin coat (TB, 400 x)

Nerve fibers in deciduous dental pulp in the second group - when the physiological resorption had been started showed some disturbances.

Under light microscopy, the nerve fibers showed unclear pathological changes – they began to loose the myelin coat due to increased edema (Fig. 4, 5).

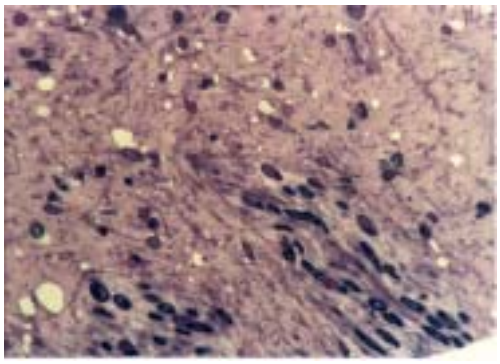

Fig. 4. Myelinated nerve fibers (HE, 400x)

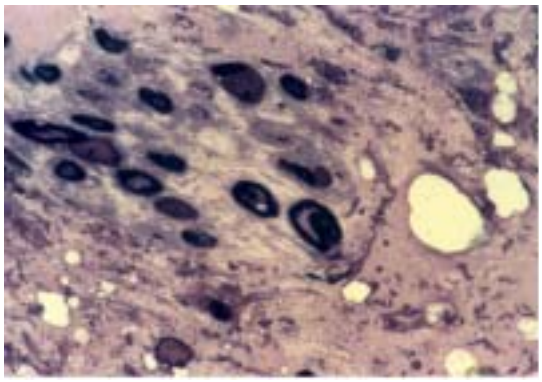

Fig. 5. Nerve fibers with myelin coat (HE, 1000 x)

Using TEM, non-myelin nerve fibers showed disorder in the homogeneousness of the axoplasmal structure, less density of mucopolysaccharide matrix is less in some places, which suggested edematous-vacuolar changes resulting in atrophy of the axons.

The myelin nerve fibers showed deformations and division of the myelin covert; type lamellar osmiophillic bodies in shape of sphinx´s myelin figures (Fig. 6), with irregular thickness, developed from formation of vacuoles, filled with shapeless and low granulated material. The Schwann´s cells were degeneratied, with relatively preserved nucleus (Fig. 7); contrary to the cytoplasm where collagen fibers were inserted directly and the increased collagenisation became apparent endoneurally. The myelin fibers were turned longitudinally, while its diameter was enlarged and had interlamellar fissures. Progress of resorption resulted in they atrophy.

Fig. 6. Axonal degeneration, disturbance in the myelin coat (TEM, 10000 x)

Fig. 7. Axonal degeneration (vacuoles), lamellar osmiophillic

Discussion

Pashley et al. have demonstrated that numbers and concentrations of nerves in dental pulp vary with the stage of tooth development and also with location [4]. Prior to tooth eruption only a very few nerves appear in the human pulp, with is contrary to the process after eruption. In addition, the largest number of nerves is found in the pulp horn, and about 40% of the dentin tubules are innervated, despite in the cervical region with only 1% innervations and an occasional in radicular dentin. However, Egan et al. have show that despite the similarities with the permanent dentition, deciduous dental pulp has high density of dentinal innervations in the cervical region [2].

Sympathetic nerves - unmyelinated are usually found in contact with blood vessels and appropriately function in vasoconstriction. The myelinated nerves trunks appear in the pulp organ at about the time of the clinical appear the oral cavity [5].

Our results were in agreement with Rapp et al. confirming that root resorption degenerative changes, such as thickening varicosities and fragmentation, appear in the nerve [6]. The quantity of neural tissue in dental pulp also decreases.

In our opinion, physiological resorption of the root produces consequences to deciduous dental pulp similar to aging - with age, nerve and blood supply to the pulp tend to decrease, and the pulp becomes more fibrous and less cellular [1, 7].

Conclusions

Physiological resorption of the root produces consequences to deciduous dental pulp similar to aging - with age, nerve and blood supply to the pulp tend to decrease, and the pulp becomes more fibrous and less cellular.

References

1. Fried K, Erdelyi G. Changes with age in canine tooth pulp-nerve fibres of the cat. Arch Oral Biol 1984; 29 (8): 581-5.

2. Egan CA, Bishop MA, Hector MP. An immunohistochemical study of the pulpal nerve supply in primary human teeth: evidence for the innervation of deciduous dentine. J Anat 1996; 188 (3): 623-31.

3. Reader A, Foreman DW. An ultrastructural quantitative investigation of human intradental innervation. J Endodon1981; 7 (11): 493-9.

4. Pashley D, Walton R, Slavkin H. Histology and physiology of the dental pulp. In: Endodontics 5th ed. Ingle JI, Bakland LK. BC Decker Inc, Hamilton. 2002. 25-60.

5. Avery J. Repair potential of the pulp. J Endodon 1981; 7 (5): 205-12.

6. Rapp R, Avery J, Strachan D. The distribution of nerves in human primary teeth. Anat Rec 1967; 159: 89-104.

7. Yu C, Abbott PV. An overview of the dental pulp: its functions and responces to injury. Australian Dental Journal Endodontic Supplement 2007; 52 (1): S4-S16.

Acta morphol. 2012; Vol.9(1):53-55

UDK: 616.314-097

IMMUNOHISTOCHEMICAL STUDY OF HLA-DR-POSITIVE CELLS IN UNERUPTED AND ERUPTED NORMAL AND CARIOUS HUMAN TEETH

Sotirovska-Ivkovska Ana,[1] Zabokova-Bilbilova E,[1] Georgiev Z, [1] Ivkovski Lj[2]

[1]Department of Pedodontic Dentistry. University Dental Clinical Centre "St. Pantelejmon", Faculty of Dentistry, Skopje, Macedonia

[2]Department of Histopathology and Clinical Cytology, Institute for Radiotherapy and Oncology, Faculty of Medicine, Skopje, Macedonia

Abstract

Antigen-presenting cells are capable of participating in the stimulation of T cells by antigen presentation. One of their essential characteristics is to express MHC class II antigen in the lymphoid tissue. Antigen-presenting cells are essential for the induction and expansion of the immune reaction, because their interaction with antigen is the first step in immune induction.

We have studied the distribution of class II-expressing cells in developing, normal, and carious human teeth to clarify when human pulp acquires an immunologic defense potential and how this reacts to dental caries. Antigen-expressing cells were identified immunohistochemically with monoclonal antibody to human HLA-DR.

In the pulp of unerupted developing teeth, HLA-DR-positive cells were distributed mainly in and around the odontoblast layer. In erupted teeth, HLA-DR-positive cells were located, for the most part just beneath the odontoblast layer. Superficial and moderate caries lesions caused an aggregation of HLA-DR-positive cells in the dental pulp corresponding to the lesion.

The results obtained have shown that:

1. Human teeth are already equipped with an immunological defense potential prior to eruption.
2. In the initial stage of caries infection, an immunoresponse mediated by class-II-expressing cells is initiated in human dental pulp.

Key words: human dental pulp, developing tooth, dental caries, HLA-DR monoclonal antibody, immunohistochemistry

Introduction

Various types of immunocompetent cells are known to be present in normal dental pulp [1, 2, 3, 4, 5]. Antigen-presenting cells are considered to play crucial role in induction and expansion of the immune reaction, because their interaction with antigen is the first step in immune induction. One of their main characteristics is to express MHC class II antigen in the lymphoid tissue. They can absorb and process complex antigens and present them to T lymphocytes, a function essential to the initiation of immune responses [6].

Changes of the distribution of class II-expressing cells have been shown in rat incisors during tooth development [7], as well as in molar pulp [8] and the responses of class II-expressing cells to experimentally induced pulpitis [9] have also been reported.

Izumi [10] have shown that human dental pulp contains two kinds of class II MHC antigen-expressing cells: dendritic cells and macrophages. Both dendritic cells and macrophages are believed to participate in the immune defense system in the dental pulp. In general, the dendritic cells have little or no phagocytotic activity, in contrast to the macrophages, which possess a high phagocytotic activity [11, 12].

In intact teeth, enamel and cementum protect dentinal pulp from external stimuli transmitted through dentinal tubules. In carious conditions, however, the pulp tissue is subject to constant exposure. These differences in environment might affect the distribution of class II-expressing cells in dental pulp.

The aim of this study was to elucidate the distribution of class II-expressing cells in developing, normal, and carious human teeth, to clarify when human pulp acquires an immunologic defense potential and how this reacts to dental caries.

Material and method

Four partially developed unerupted teeth were surgically extracted, four erupted developing intact premolars, and four premolars with closed apices were extracted. Ten premolars with various stages of decay were obtained from patients presenting no clinical symptoms. Teeth were obtained from patients who needed orthodontic therapy and who were from 11 to 18 years old.

Immediately after extraction, the teeth were cut longitudinally; the pulp was extirpated and fixed in 10% buffered paraformaldehyde, embedded in paraffin and sliced into 4-5mm sections. After deparaffinization, immunoperoxidase staining was done using monoclonal antibodies. The commercially available primary antibody was anti-HLA-DR monoclonal antibody (CR3/43; DAKO Co. Ltd, Denmark). The sections were further incubated with pre-formed ABC (*Elite*® ABC, VECTOR Laboratories, and Burlingame, USA) for 30 min. at room temperature. Finally the localization of peroxidase activity was made visible by incubation of the sections with 3'.3'-Diaminobezidin (DAB) in PBS buffer for five to seven minutes and counterstained with hematoxylin. The depth

of each caries lesion was determined by the pigmentation on the sections.

Results

Unerupted developing teeth

During the stage of root formation, HLA-DR-positive cells appeared in the coronal pulp. Distribution of HLA-DR-positive cells was especially dense in and around the odontoblast layer. Only a few HLA-DR-positive cells were scattered in the dental papila.

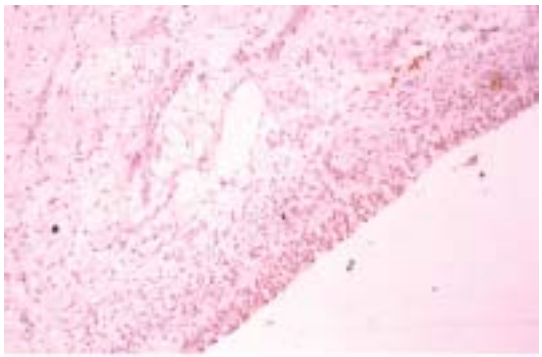

Fig. 1. Immunohistochemical localization of HLA-DR positive cells in unerupted developing teeth

Erupted, intact teeth

Immunoperoxidase-labeled HLA-DR-positive cells were located, for the most part just beneath the odontoblast layer. In the connective tissue of the coronal and radicular pulp they were distributed mainly around blood vessels.

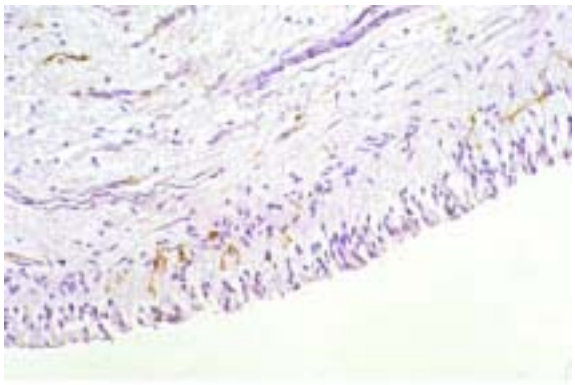

Fig. 2. Immunohistochemical localization of HLA-DR positive cells in erupted, intact teeth

Carious teeth

In teeth where caries lesions extended from the enamel into the dentin, an aggregation of HLA-DR-positive cells was found in the subodontoblastic region. No distributive changes were noted in other areas.

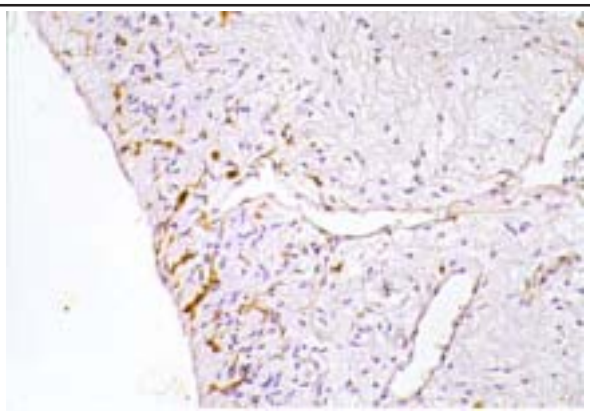

Fig. 3. Immunohistochemical localization of HLA-DR positive cells in the pulp affected by initial caries

As the caries lesion advanced, the aggregated cells expanded along the odontoblast layer, and in the most severely affected lesion, they advanced toward the center of the pulp.

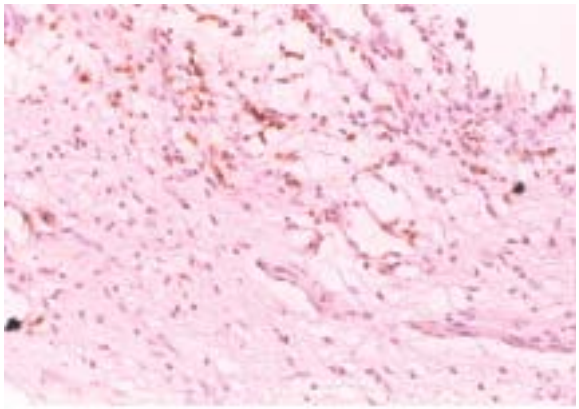

Fig. 4. Immunohistochemical localization of HLA-DR positive cells in the pulp affected by moderate caries

Discussion

The existence of two types of class II antigen-expressing cells (dendritic cells, characterized by poor phagocytic activity, and macrophages) has been reported in the dental pulp of both rat and human teeth [2, 3, 5, 13]. Dendritic cells are localized to the periphery of the pulp, while macrophages tend to be more centrally located [2, 3].

The HLA-DR-positive cells observed throughout the odontoblast layer are dendritic cells, and their location is ideal for capturing antigens invading the dental tubules. Previous studies of Jontell [7] and Kosaka [8] on rat dental pulp have shown that the majority of class II- expressing cells occur only after eruption, suggesting that there is a post-eruptive increase due to the invasion of bacterial antigens. Contrary to the findings obtained in rats, numerous HLA-DR-positive cells were found in the pulps of unerupted human teeth concentrated

within the odontoblast layer. Thus, the results of our study indicate that human teeth are already equipped with an immmunological defence potential before they erupt.

We also observed distributive changes in class II-expressing cells in the pulps of carious teeth. Changes were evident in teeth with early caries and the aggregation of HLA-DR-positive cells was observed in the restricted area corresponding to caries lesion, which suggested that antigenic materials had already spread into the pulp tissue through dentinal tubules. Similar lymphocyte infiltration was reported during enamel caries [14]. The relationship between these data on carious teeth has been demonstrated by in vitro experiments [11], which show that dendritic cells in dental pulp have the capacity to co-stimulate T-lymphocytes, an important relationship during the early stages of pulpal immunoresponse.

More advanced caries induced more expanded aggregations of HLA-DR-positive cells along the odontoblast layer and subodontoblastic area of the pulp. This subodontoblastic zone is composed of a rich network of nerve fibers, capillaries and a collagen matrix. The exact role of this zone remains unknown, but the present findings suggest its importance for accommodating immunoresponsive cells. HLA-DR-positive cells were observed along the dentin pulp border corresponding to the caries lesion.

Conclusions

Our findings indicate that human teeth are already equipped with an immunological defense potential prior to eruption, even before they are submitted to antigenic challenges in the mouth. The mode of immunological reaction of the dental pulp seems to be strongly influenced by hard tissue encasement. Class-II-expressing cells are able to respond to trans dentinal antigen provocation and the kinetics of these cells are strongly influenced by changes in dentin permeability. Upon antigenic challenge, these cells may interact locally with T-lymphocytes and induce an immunological response to mount defense and repair of the dentin pulp complex.

References

1. Jontell M, Gunray MN, Bergenholtz G. Immunocompetent cells in the normal dental pulp. J Dent Res 1987; 66:1149-53.

2. Jontell M, Bergenholtz G, Scheynius A, Ambrose W. Dendritic cells and macrophages expressing class II antigens in the normal rat incisor pulp. J Dent Res 1988; 67:1263-6.

3. Jontell M, Bergenholtz G. Accessory cells in the immune defense of the dental pulp. Proc Finn Dent Soc 1992; 88: 344-55.

4. Okiji T, Kawashima N, Kosaka T, Matsumoto A, Kobayashi C, Suda H. An immunohistochemical study of the distribution of imunocompetent cells, especially macrophages and Ia antigen-expressing cells of heterogenous populations, in normal rat molar pulp. J Dent Res 1992; 71 (5): 1196-202.

5. Ohshima H, Kawahara I, Maeda T, Takano Y. The relationship between odontoblasts and immunocompetent cells during dentinogenesis in rat incisors:an immunohistochemical study using OX6-monoclonal antibody. Arch Histol Cytol 1994; 57: 435-47.

6. Steinman PM. The dendritic cell system and its role in immunogenicity. Ann Rev Immunol 1991; 9: 271-96.

7. Jontell M, Jiang WH, Bergenholtz G. Ontogeny of class II antigen expressing cells in rat incisor pulp. Scand J Dent Res 1991; 99: 384-9.

8. Kosaka T, Okiji T, Kawashima N, Kobayashi C, Suda H. Changes in the distribution of various immunocompetent cells in rat molar pulp during tooth development. Jpn J Conserv.Dent 1992; 35: 1474-80.

9. Bergenholtz G, Nagaoka S, Jontell M. Class II antigen expressing cells in experimentally induced pulpitis. Int Endod J 1991; 24: 8-14.

10. Izumi T, Kobayashi I, Okamura K, Matsuo K, Kiyoshima T, Ishibashi Y, Inoue H, Sakai H. An immunohistochemical study of HLA-DR and a_1-antichimotrypsin-positive cells in the pulp of human non-carious and carious teeth. Arch Oral Biol 1996; 41 (7): 627-30.

11. Jontell M, Eklog C, Dahlgren UI, Bergenholtz G. Difference in capacity between macrophages and dendritic cells from rat incisor pulp to provide accesory signals to concavalin-A-stimulated T-lymphocytes. J Dent Res 1994; 73 (5): 1056-60.

12. Kamal AMM, Okiji T, Kawashima N, Suda N. Defence responses of dentin/pulp complex experimentally induced caries in rat molars: An immunohistochemical study on kinetics of pulpal Ia antigen-expressing cells and macrophages. J Endod 1997; 23 (2): 115-20.

13. Ohshima H, Sato O, Kawahara I, Maeda T, Takano Y. Responses of immunocompetent cells to cavity preparation in rat molars: An immunohistochemical study using OX6-monoclonal antibody. Connect Tissue Res 1995; 32: 303-11.

14. Izumi T, Kobayashi I, Okamura K, Sakai H. Immunohistochemical study on the immunocompetent cells of the pulp in human non-carious and carious teeth. Arch Oral Biol 1995; 40 (7): 609-14.

UDK: 159.932:618.282.1-76

FUNDAMENTAL DIFFERENCES AND BENEFITS OF HEARING BEHIND THE EARS AMPLIFICATION AND COCHLEAR IMPLANT WITH HEARING SENSOR NEURAL IMPAIRMENTS

LazarovskaVesna[1], Topuzovska G[2], Jovanovska M[1], Gjorgeska B[1], Delevski B[1]
Center for rehabilitation for hearing, speech and voise – Skopje[1], Medical Faculty – Skopje[2]

Abstract

The aim of the hearing amplification in a person with impaired hearing is to use the remaining auditory potentials. One of the most important factors affecting the success of the auditory and speech perception in a person with impaired hearing is the time and the quality of the amplification. The main purpose of the hearing aids is to make the sound signal available for the damaged ear, to transfer the sound information as accurately as it can, and to adjust the transmission and the quality of the sound information to the receptive capacity of the ear to the highest degree. The purpose of this paper is to show the difference in the transmission of the sound signal with the hearing amplifications and the cochlear implants, as well as their benefits. 31 patients were tested for the purpose of this paper, and their aural condition was measured three times: without a hearing amplification, with a hearing amplification and finally with cochlear implant. The obtained results show that the benefit of the cochlear implants is much larger than the one of the hearing amplifications.

Key words: hearing amplification, cochlear implant, sensorineural damage, speech

Introduction

Individual hearing aids, hearing or amplificatory cochlear implant should provide social contact by auditory pathway. There are various definitions of hearing amplification.

1. Aid that provides an opportunity for persons with hearing loss to hear better,

2. Under auditory prosthesis we mean a means of aiding or restoring the function of hearing in people with reduced hearing.

In the group of individual hearing amplificationwe have more models: cloven, amplification in the form of glasses, canal, behind ears, vibrators, and most recently as a revolutionary discovery cochlear implant.In the most severe sensor neural damage the primate is hold by hearing amplification behind ears and certainly cochlear implant. Hearing amplification (behind ears) has a dozen models with different output power (the strongest one for those with the most severe damage with gein and up to 81 dB). Today most are made in three sizes, and those with the smallest enclosures are used for babies and children up to three years.

Regardless of the size of enclosures the modern technology allows incorporation of the most powerful amplifiers and multichannel filters. This type of device allows different possibilities of adjustment of the output power in relation to the frequency range over which there is no audiogram which is an issue of adjustment. (Figure 1).

Fig. 1. Hearing (behind ear) amplification

The basis for this is the system of conversion, amplification and filtering the sound signal. Converting the sound signal into amplificatory system is performed twice: a) in the microphone, when the sound signal is converted into electric and b) when the electrical signal is converted back into sound by the speaker (headphones). (Figure 2).

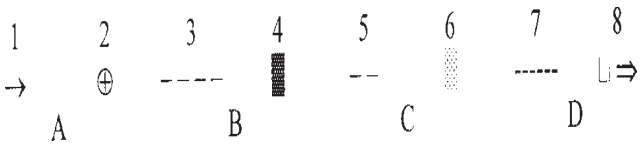

Fig. 2. System conversion, filtering and amplification of the sound signal
1 - Sound signal, 2 - microphone, 3 - converted acoustic signal into an electric, 4 - amplifier, 5 - filters, 6 - amplifiedsound signal 7 - Speaker, 8 - amplified sound signal.
A - Converter B - Amplifier C - Filter D – Converter

The cochlear implant is a custom hearing aid of the last generation. It's different fromthe other hearing aids because it is built in the inner ear. The appearance of the cochlear implant is considered revolutionary in terms of solving problems with hearing. It is recommended for people who have no significant amplification of sound through the individual hearing amplifier, and have little benefit to people whose disability is over 90dB at 500, 1000, 2000 and 4000 Hz. Restrictions apply only to the site of damage, only in a cochlear damage. The cochlear implant has internal and external parts.

Fig. 3.

The external part is composed of the microphone (5, 6, 7), speech processor, which can be worn behind the ear or neck (8, 9) and transmitter with a thin cord is attached to the microphone and speech processor. External parts are placed three to six weeks after recovery from the surgical intervention, when it will be ready to be activated.Activation is performed by using a software program that is located inside the voice processor.
The internal part is consisted of a receiver (stimulator), electrodes whose number varies by type of implant (10, 11). External and internal parts are joined by a magnet that is embedded in the transmitter.

Material and method

The survey was conducted in 31 subjects with different gender and age. The diagnostic process is made in the Clinic for Ear, Nose and Throat in Skopje and is diagnosed with severe bilateral partial deafness and deafness. In the program of this rehabilitation treatment are involved the Institute for Rehabilitation of hearing, speech and voice, in Skopje.Evaluation of hearing and verbal perception among all respondents and measurement of aural stimulus was conducted in three stages, namely: without hearing amplifier, with hearing amplifier and with installation of cochlear implant at the same respondents. The results are shown graphically

Results

In Figure 4, the lower curve represents the hearing status of all respondents without hearing amplifier (CA). The upper curve represents the hearing condition of the same subjects that is made with hearing amplification device. Clearly we can easy recognize the little difference where the level of hearing threshold is elevated approximately 10dB. This increased threshold still gives us a sound image because of the absence of most of the frequencies in the voice area (up to 1000 Hz - 100 dB). This increase derived by application of the hearing apparatus is not sufficient for successful speech therapy treatment.

In Figure 5we can observe the hearing condition of the same subjects in the left ear, the lower curve without hearing amplifier and the upper curve with hearing amplifier also a small increase in the sound threshold around 10 dB.

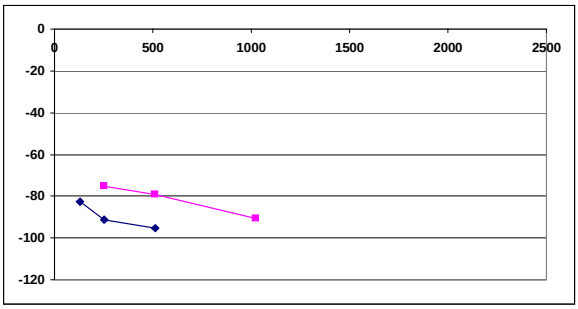

Fig. 5. Left ear (lower curve without SA, upper curve with CA).

Acoustic effect of these hearing aids is partial and therefore these patients are subjected under operating cochlear surgery (cochlear implantation). In Figure 6 is shown the hearing condition of the same respondents with a cochlear implantation. Clearly is showed that the hearing threshold was significantly raised throughout the speech frequency range. It suggests that people will be able to develop acoustic image of all votes of speech area, or you can develop speech without reading lips depending only on the function, listening.

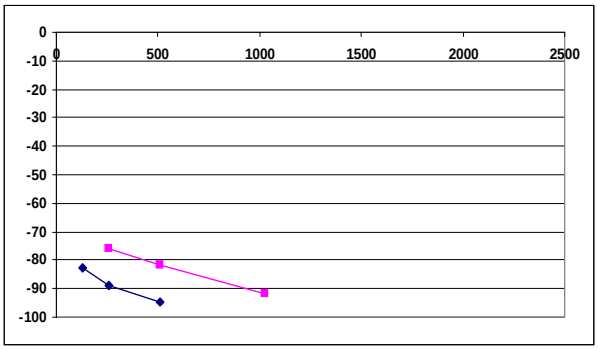

Fig. 4. Right ear (lower curve without SA, upper curve with CA)

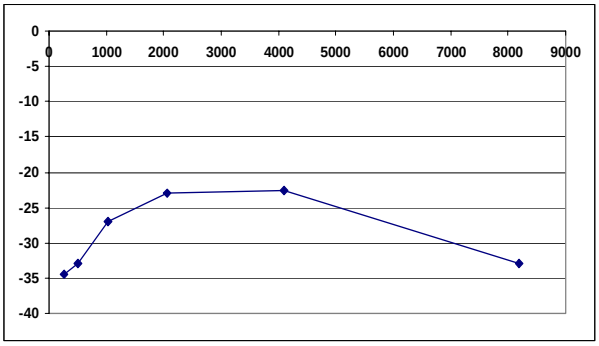

Fig. 6. The cochlear implant

Table 1. Test for development of aural perception (RSP)

Behavior	without SA	With SA	With KI	p McNemar
Response to sounds from the environment				
No	29(93,5%)	14(45,2%)	6(19,3%)	*0,0003
Yes	2(6,5%)	17(54,8%)	25(80,7%)	**0,00001
				***0,043
Identification of sounds from the environment				
No	31(100%)	31(100%)	26(83,9%)	
Yes	/	/	5(16,1%)	
Response to the sound of drum / extracted				
No	31(100%)	31(100%)	31(100%)	
Yes	/	/ /		
Response to a second musical instrument / extracted				
No	7(22,6%)	/	/	
Yes	24(77,4)	31(100%)	31(100%)	
Response to voice / extracted				
No	23(79,3%)	19(76%)	4(16%)	*0,47
Yes	6(20,7%)	6 (26%)	21(84%)	**0,00006
				***0,0003
Response to voice / spontaneous				
No	31(100%)	31(100%)	3(10%)	
Yes	/	/	27(90%)	
Distinction between two musical instruments				
No	31(100%)	31(100%)	1(3,6%)	
Yes	/	/	27(96,4%)	
Distinction between loud / quiet drum				
No	31(100%)	31(100%)	7(25%)	
Yes	/	/	21(75%)	
Discrimination between single / recurrent				
No	31(100%)	31(100%)	31(100%)	
Yes	/	/	/	

*p tested differences between groups with SA / without SA
** p tested differences between groups with without SA/ with KI
*** p tested differences between groups with SA/ with KI

From the performed test (Table 1) of the respondents without SA, the SA and the cochlear implant, in terms of their ability to react to sound and speech sounds, to distinguish the two sounds (drum and whistle), and the ability to distinguish sounds with different strength and repetitive votes received as follows:

Discussion

The condition of hearing participants is defined as hearing damage from the most difficult stage: Dg Surdomutitas. This practically means that a person with such a hearing impairment is unable to record acoustic sounds and sound signals and stimuli placed with the largest, most intense volume. Some of these persons there is a possibility of a sound stimulus response below 200 Hz and intensity of 100 dB –low frequency area. This gives us the right to access audio prosthetic thus performs application hearing amplification for the air control with pronounced dynamics in the low frequency range. The negative side is that here is emphasized sound stimulus only in the low frequency region, thus there is no sound stimulus in the higher frequency region. It is not enough to form acoustic picture of all votes, and thus unable to develop verbal communication solely on function, listening.

In such a state hearing people rely on speech reading from the mouth. (Figure 4 and Figure 5)Acoustic effect of these hearing aids is partial and therefore patients must care the fashion of undergoing in cochlear surgery where cochlear implantation is performed. Measurements of hearing after surgery (Figure 6) clearly show how the sound stimulus is distributed throughout the frequency hearing area.Voice rehabilitation treatment of this benefit should necessarily lead to development of acoustic image of the votes from speaking areas, and further treatment to the development of speech as a means of verbal communication. It should be emphasized that by implanting cochlear implant is by no means reduced the need for intensive and long rehabilitation. The basic

principles of rehabilitation process applicable in all other cases also apply in this type of hearing aid.

From the performed test (Table 1) of the respondents without SA, the SA and the cochlear implant, in terms of their ability to react to sound and speech sounds, to distinguish the two sounds (drum and whistle), and the ability to distinguish sounds with different strength, length and repetitive votes received as follows:

From 31 subjects, patients with pre lingual sensor neural hearing impairment, only 2 (6.5%) reacted to sounds from the environment, there were no respondents who could identify the sounds from the environment and react to sound drum, 24 (77%) of them had reaction from the second musical instrument. There are no respondents with a positive test response for spontaneous voice, while 6 (20.7%) of them had positive test for the derived voice. The test was negative in all subjects in terms of ability to distinguish the two musical instruments, to distinguish loud and quiet and a single and repeatable.

After placing the hearing amplifier, more than half of respondents, or 54.8% had a positive test response to sounds from the environment. Also they had significantly improved ability to respond to a second musical instrument, thus all participants after placing the SA had a positive response to a second musical instrument. After cochlear implantation, participants responded significantly better to sounds from the environment in relation to the period when they did not have SA, but insignificant in terms of ability they had with the SA. Positive reaction to sounds from the environment only had 25 (80.7%) respondents with KI. Cochlear implant significantly improved the ability to identify sounds from the environment (16.1%), ability to respond to spontaneous (90%) and extracted voice (84%) and distinction between two musical instruments (96.4%) and between loud and quiet drum (75%).

Conclusion

Benefit of cochlear implantation in terms of hearing amplifikatori in people with severe senzoneuralno damage is as follows:

- People with cochlear implants have the opportunity to hear and understand sounds from the surrounding environment. People with hearing amplifierare not able to hear sounds from low frequency region.

- Listen to and understand speech without reading lips. Persons with hearing amplifier can understand speech only by reading the lips.

- Improvementof the speech capabilities is only possible with cochlear implant. Persons with hearing amplifier can improve only with speech therapist to read a speech from the mouth.

- Listening in noisy environment it is impossible for people with hearing amplifier.

- Possibility of the implant patient to use the phone (impossible for people with hearing amplifier).

References

1. Simonovic M. Mogucnosti audioloske rehabilitacije osoba sa ostecenjem sluha. Beograd; Univerzitetska klinika za ORL, 1979.
2. Keramitcievski S. Audiologija. Beograd; Savez gluvih Jugoslavije, 1971.
3. Ostojic S. Adaptacija na slusni aparat kod dece ostecenog sluha. Casopis Rehabilitacija hendikepiranih,1998: 27.
4. Ostojic S. Auditivni trening i razvoj govora nagluve dece. Beograd: 2004.
5. Wilson B.S. Engineering Design of Cochlear Implants. In Zeng FG, Popeer AN, Fay RR, Eds. Cochlear Implants: Auditory Prostheses and Electric Hesring. New York: Springer; 2004. pp.14-5.
6. Clark. Cochlear implants. In GreenbergS, Ainsworth WA, Popper An, fay RR,eds Speech Processsing in the Auditory System. New York: Springer; 2004. p. 422-62.
7. Wikipedia contributors. Microphone. Available from: http//www.en.wikipedia/ org/wiki/ Microphone/. Accessed April 2006.
8. Wright El Anomalous Dispersion, not faster than Lignt. UCLA Astronomy. Available from: http// www.astro. ucla.edu/wright/wave-packet.gif/. Accessed April 26 th 2000.
9. Rubenstein JT. How Cochlear Implants EncodeSpeech. Current Opinions in Otolaryngology and Head and Neck Surgery 2004; 12: 444-8.
10. Moy PL. Simulting Bilateral Cochlear Implant Processing In Normal- Hearing Listeners. Available from: http//www.bu.edu./dbin/binaural/pubs/. Accessed May 4 th. 2002.
11. Frijns, JHM, Briare, JJ. The importance of human cochlear anatomy for the results of modiolus-hugging multichanel cochlear implants. Otology&Neurology 2001; 22 (3):340-9.

Acta morphol. 2012; Vol.9(1):60-68

UDK: 611.81:618.29

DEVELOPMENT AND CONGENITAL CHARACTERISTICS OF EMBRYONIC AND FETAL CNS IN CORRELATION WITH PRODUCTION OF S100B PROTEIN AS A BIOLOGICAL MARKER FOR BRAIN INJURY

Sofijanova Aspasija[1], Piperkova K[2], Jordanova O[1]

Department of Neonatal and Pediatric Intensive Care[1], Department of Neonatology[2] University Children's Hospital, Medical Faculty Skopje, Republic of Macedonia

Abstract

Perinatal brain development is one of the most fascinating stages.Fetal brain cells are generated at about 250,000 per minute. It is most likely that infants will have all the neurons they are going to ever have in their life at the time of birth..The next stage of neuron development is cell migration. In this stage neurons move from near the center of the brain, which is where they are produced, to their appropriate locations. The process of cell migration is completed seven months after conception.The third stage of neuron development is concerned with cell elaboration. During this stage axons and dendrites grow and form connections with other cells. Cell elaboration continues for many years after birth .Another process that begins prenatally and continues after birth, is myelination. This is a process in which nerve cells are covered and insulated with a layer of fat cells. Myelination increases the speed of information which travels through the nervous system.The nervous system starts to form as a hollow tube on the embryo back. The brain forms into a large mass of neurons and loses the tubular appearance. Three major divisions in the brain form. These are:hindbrain - located at the lowest portion of the brain; controls motor development midbrain - located between the hind and forebrain; relaying information to eyes and ears; forebrain – a large part of the brain; it plays the most critical role in the process of thinking and speaking. Most neurons are produced between 10 and 26 weeks after conception. S100B and S100A6 (calcylin) are two members of the S100 Ca^{2+}-binding protein family and have been localized in the mammalian nervous system. From week 15 onwards, an increase with advancing gestation at age in both the number and staining intensity of S100B positive, astrocyte-like cells are found in the pyramidal layer of the hippocampus, while both the molecular and polymorphic layers show similar S100B immunoreactivities at all stages examined. A decrease in the immunoreactivities is found in the molecular layer of the aged adult hippocampus while other layers exhibited immunoreactivities similar to those of the late fetus. At week 15, the molecular, pyramidal and ganglionic/multiform layers of the entorhinal cortex also showed positive S100B immunoreactivities which were maintained throughout the rest of the gestation and in adult specimens. In the occipital cortex, the numbers of positive cells for all layers were about twofold higher than those found in the hippocampus and entorhinal cortex, and immunoreactivities detected in the granular layer increased from week 21, reaching a plateau at around week 27. S100B positive fibers were also found week 30 but were not observed in aged adult specimens.The differential spatio-temporal expression of S100B and S100A6 proteins suggests that the proteins play different roles in different brain regions during development and in adulthood.

Key words: brain development, S100Bprotein, brain injury,

Prenatal Development

Characteristics of brain development.The first signs of pregnancy are subtle. While a women wonders what's happening, the developing fetus is about a month old, and the basic components of its brain have already been formed.

Many people do not realize just how early a child's brain begins to develop—and how long it continues to mature after birth. The process starts between the second and third week of fetal development, and it continues well into early adulthood (fig.1). No other organ in the human body takes so long to develop as the brain

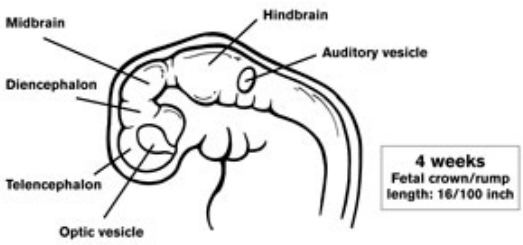

Fig. 1

does or goes through as many changes[1]. This unique growth process explains the brain's complexity and amazing activities, as well as its vulnerability to injury.

*Nature of the human brain.*The debate in brain development is not one of nature versus nurture, but of how these factors interact and which is more important in the development of particular traits, behaviors, and disorders. Brain is malleable because it develops partly as a result of the preprogrammed instructions encoded in genes, and partly as a result of exposure to the outside environment. Genes govern the type of brain cell produced, its location and function, and what type of neurotransmitters it will respond to. But whether a particular neuron will develop further and realize its full potential, or go unused and wither away, depends on external stimulation—everything from sight to sound to stress.

In the beginning the developing child follows a standard and predictable course of development. But while a baby's nine-month gestation includes many clearly defined stages, at the cellular level these processes tend to overlap. Some are repeated several times. This development is guided by the genes built into every cell of the embryo. It is by following those genes' complex instructions that the human brain is able to develop from a group of primordial cells into one of the most powerful organs in the universe[1, 2].

Building Blocks of the Brain.The changes the developing embryo undergoes are enormous. At birth the child's brain will consist of 100 billion neurons, organized into groups that perform such particular functions as interpreting sounds, storing memories, and learning new skills. Yet this complex organ, like every other part of the human body, must grow from a single fertilized egg. The brain develops at a phenomenal rate in the nine months from conception to delivery. At the height of this process, a quarter of a million new brain cells are born every minute. In the first week, the fertilized egg goes through a series of divisions, giving birth to a hundred or so progenitor cells, all exactly alike. The cells are clustered in a small ball known as a blastocyst. During the second week, the original generation of cells give birth to others, which begin to differentiate, or take on unique characteristics that distinguish them from their cousins and forebears. As the cells differentiate, the developing embryo evolves from a small round cluster of cells into an elongated disk that consists of three layers of tissue. The upper layer of the disk, or ectoderm, will eventually give rise to the outer covering of a person (skin, fingernails, and hair) and—with help from the middle layer, or mesoderm—to the brain and central nervous system. The bottom layer, or endoderm, gives rise to internal organs, such as the lungs and stomach[1,2,3].Brain development begins with a process known as induction, which takes place in the third week of embryonic growth. Cells multiply rapidly along the lines of the ectoderm so that a structure called the neural plate forms. This process is not completely understood, but it seems to be sparked by contact between the ectoderm and mesoderm (fig.2). Chemical factors produced in the mesoderm create a reaction in the neighboring ectoderm, pushing some cells along the developmental pathway that leads to skin and hair, and others on a different developmental pathway that leads to brain and spinal cord.

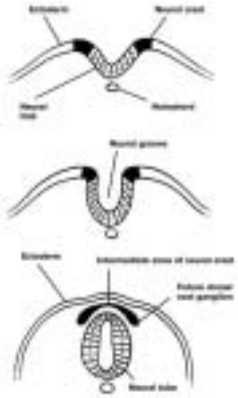

Fig. 2. At about the third or fourth week after conception, the neural tube begins to form and to show bulges that will become parts of the brain and spinal cord. (image credit: Kathryn Born)

By the fourth week, part of the neural plate has folded in on itself to form a neural tube. At this point, primitive brain cells called neuroepithelial cells begin to divide rapidly, or proliferate. At first the wall of the neural tube is composed of only a single layer of such cells. Yet this initial layer grows, forming additional layers. Cells proliferate at a furious pace, in part because the neuroepithelial cells begin to divide into three new cells rather than two. Three bulges emerge from the top of the neural tube, eventually giving rise to the forebrain, midbrain, and hindbrain. The rest of the neural plate becomes the neural crest, which will become the spinal cord. As cells proliferate in the three primitive brain structures, the brain begins to grow and fluid-filled spaces known as ventricles form in the middle [3, 4, 5]. Even at this early stage, primitive brain cells are organized into distinct groupings known as neuromeres, visible as tiny grooves on the ventricles. Although the neuromeres disappear in another two weeks, they are precursors of

the large-scale differences between parts of the brain . Development of the fetal brain: The presented five drawings chart the development of the fetal brain. They are not to scale—at 4 weeks, the fetal brain is not much bigger than a grain of salt; at 7 weeks, it measures barely a quarter inch. As the brain grows, it begins to develop the characteristic folds as it expands to fill the cranium. (images credit: Kathryn Born)

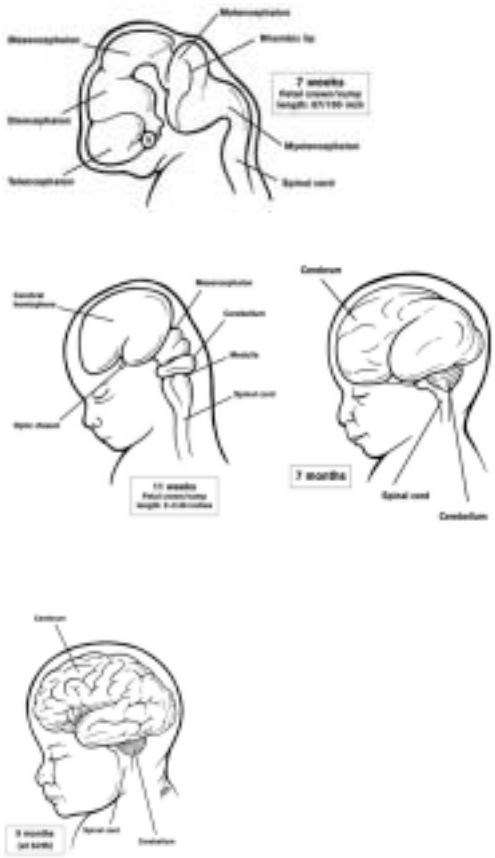

Fig. 3.

Milestones in development. Scientists have studied prenatal brain growth in two main ways. By examining fetuses that did not survive until birth, they learned about the anatomical changes that take place at different stages of human development. Researchers have also conducted experiments in animals, particularly in monkeys (whose brains most resemble those of people), to learn more about normal development and what can disrupt it (fig.3). Today it is also possible to use imaging technology, while a child is still a fetus in the womb, to examine the developing brain. With these methods, we have a good picture of how a fetus normally develops. It takes about 38 weeks for a single fertilized egg to grow into a baby. Pinpointing the exact date of conception is often difficult, however, so pregnancy is most often said to last for 40 weeks [6,7].

MONTH 1

Brain: A preliminary structure known as the neural tube forms. Part of this eventually becomes the spinal cord, and the other part the brain.

Other milestones: All major organs are forming by the third week of development, and the heart begins to beat.

MONTH 2

Brain: The major structures of the brain begin to form, including the cerebral cortex. As the brain grows, the embryo's head begins to look more human.

Other milestones: All major organs have now developed. The eyes, ears, nose, and mouth begin to take shape.

MONTH 3

Brain: The brain continues to grow new cells and make connections between those already in place. The fetus develops physical reflexes.

Other milestones: The eyes are in place, and eyelids are beginning to form. The fetus cannot control its movements, but it can react to stimuli by moving its arms and kicking.

MONTH 4

Brain: Parts of the brain begin to receive signals from the developing ears and eyes. The fetus can detect bright lights and hear sounds like its mother's voice, although it will not yet know how to interpret them. As facial muscles develop along with the brain, the fetus can squint and frown.

Other milestones: The lungs begin to function, although the fetus still receives its oxygen through the placenta. Taste buds form on the tongue. Eyebrows and eyelashes grow.

MONTH 5

Brain: As the brain makes more and more connections, the fetus begins to control its movements, turning and stretching, perhaps even somersaulting. The fetus also begins to react to sounds outside the mother, such as music.

Other milestones: The sex organs become visible on an ultrasound. The beginning of an immune system emerges.

MONTH 6

Brain: The cerebral cortex is now the largest part of the brain and has started to separate into lobes. As this part of the brain develops, a primitive type of memory and conscious behavior emerge. You may notice the fetus reacts more to some noises and music than others. Some experts believe the fetus will remember music and voices "heard" at this stage and unconsciously react with comfort to them after birth.

Other milestones: The facial features are so developed that the fetus looks almost like a newborn. All muscles are in place, and the bones begin to harden.

MONTH 7

Brain: The once-smooth fetal brain has begun to form the grooves and indentations typical of a more mature brain. An electroencephalogram (EEG) can detect fetal brain waves. Myelin begins to form a protective sheath around nerves from the brain, like insulation keeping wires from crossing; this sheath enhances communication among nerve cells.

Other milestones: The fetus gains weight as it builds up fat stores that will later help to maintain temperature. Eyelids open, the fetus begins to "see" inside the womb. It may swallow or suck its thumb.

MONTH 8

Brain: The auditory cortex, the visual cortex, and Broca's area have begun to function. The fetus is thus developing a primitive ability to interpret sights and sounds and distinguish language.

Other milestones: All organs except the lungs have now matured. As the eyes develop further, the fetus can begin to focus. The fetus has grown so large that it can no longer easily move about.

MONTH 9

Brain: The brain continues to grow, and by this time most of the neurons your child will ever have are in place. Just before birth, the brain is one fourth the size and weight of an adult brain.

Other milestones: The fetus gets into position for birth, usually with its head facing downward toward the mother's cervix. The lungs mature. The immune system continues to develop.

*Growing by Leaps and Bounds.*During this second month of fetal development, the brain grows by leaps and bounds. Construction begins on all its major components. What happens in this month will lay the foundation for the child's ability to see, hear, speak.

During the second and third months of fetal development, the growing brain begins to take shape. The hindbrain gives rise to the medulla oblongata and the pons (part of the brain stem), which are involved in many functions essential to life, such as breathing and heartbeat. The cerebellum, the part of the brain involved in maintaining balance and coordinating movement, emerges partly from the hindbrain and partly from the midbrain. But it is the forebrain that undergoes the most complicated changes. The forebrain divides into two distinct structures: the diencephalon and telencephalon [8,9,10]. The diencephalon develops into the thalamus and hypothalamus, which will affect everything from emotions to sensory perception. The telencephalon gives rise to several parts. First come the hippocampus, which eventually will be involved in short-term memory, and other structures involved in the olfactory pathways, which will enable the human being to smell. Next, the telencephalon produces the basal ganglia, which will eventually contain structures that control movement, sensory information, and some types of learning. The amygdala will eventually help the brain attach emotional significance to signals it relays elsewhere.The last structure to evolve out of the telencephalon is the cerebral cortex, one of the most complex parts of the brain and the site of what are considered "higher functions": learning, language, and abstract thought. The cerebral cortex begins to develop in the eighth week of embryonic growth but will continue to form during much of the prenatal period. The connections between neurons in the cerebral cortex continue to mature into early adulthood, and some experts say they never stop maturing.This tremendous growth is possible because the neurons are still proliferating [11]. Although cells have been dividing since the moment of conception, this activity builds to a fevered pace about day 40 (or in the sixth week) of embryonic development. This process, known as neurogenesis, continues until day 125 (around the seventeenth week). Even then, it does not completely stop but only slows down.In these early months of prenatal development, cells not only proliferate—they begin to take on particular identities. This process starts when some of the cells in the ventricular zone stop dividing and begin to do a microscopic dance. Precursor cells divide on the innermost surface of the neural tube, which borders the ventricles, then move to the outermost surface to synthesize DNA, the blueprint of life. Then the precursor cells return to the ventricular surface to divide again. The cells repeat these steps a set number of times, depending on their types. According to this model, columns of cells form on the surface of the ventricles with genetic instructions on how many particular cells the brain needs, where they will eventually be located, and what they will do. The result is both a prototype of the brain and a map of it—hence the term protomap. Some neuroscientists have challenged this theory as too simplistic, but it offers a helpful way to picture how the parts of the brain develop.The primordial cells in the neural tube eventually become either neurons or long, thin glial cells [12].The neurons are the brain cells that do the actual work of thinking and controlling movement. The glial cells have been compared to scaffolding that helps guide the building of the brain, especially the cerebellum. These glial cells sprout from the ventricular zone, extending upward to the outer surface of the developing brain. Neurons begin to migrate in different directions, depending on their preprogrammed roles.Guiding all this movement are genes, which we can compare to blueprints. Each contains instructions for creating a protein, which in turn might induce cells to divide or perform particular functions. Early embryonic cells divide and give rise to progenitor cells, which then give birth over several generations of divisions to more specialized cells. No one gene contains a master plan. Rather, one set of genes controls the initial phase of development, other genes then kick in and take it to the next level, and so on. At the end of the third month, the

fetus is still very small—about 3.5 inches (9 cm) from head to rump, and weighing only (48 g) [13,14].

Moving, Thinking, Being

*The Cerebral Cortex***.**The middle part of pregnancy is a significant time in fetal development, when the brain evolves from a primitive structure into a much more complex form. Cells continue to proliferate and differentiate during this phase, but they do much more besides. They have begun to travel (migration), form communities (aggregation), and make connections that facilitate the communication necessary to brain function (synaptic formation). All of this lays the foundation for what makes us human: movement, learning, conscious thought, and memory. Although all of brain development involves some combination of cell growth, migration, aggregation, and synaptic formation, this process is most dramatic in the cerebral cortex [14, 15]. This is the largest part of the human brain and the site of the so-called higher functions. The cerebral cortex builds itself from the inside out, with the neurons of the deeper layers being made before those of the outer layers. But all the neurons are born deep inside the brain, in the ventricles, so some must travel to the outermost reaches of the organ. At about the eighth week of embryonic development, primitive brain cells begin to migrate outward from the innermost part of the brain and start to build the first layer of the cerebral cortex. Succeeding groups of cells follow, slowly building all six layers of the cortex, a process that continues for most of gestation. Meanwhile, neurons continue to proliferate, creating new cells. The peak growth occurs in the fourth and fifth months of pregnancy, when the cortex (also known as the brain's gray matter) grows much more rapidly than the supporting structures underneath (known as white matter) [15, 16]. By the time the cortical growth spurt ends, in the sixth or seventh month of development, 70 percent of the brain's neurons are located in the cerebral cortex. At the same time, the fetal skull has begun to harden as cartilage turns to bone throughout the body. Both the rapid growth and the hardening skull help explain why the cortex acquires its characteristic folds, but that wrinkling is far from random (fig.4). The fully developed cortex has peaks and valleys that are generally the same from one person to the next, pointing to some underlying genetic blueprint. Even so, there are many small differences between individual brains, even the brains of identical twins, who share the same genes. The exact contours of the cortex are thus a product of both nature and nurture.

*Cells Settle In and Start to Talk.*Cells that have recently arrived at their proper destination seek out similar cells and begin to form their own versions of communities, so called aggregation. The cells recognize each other by their distinct biochemical properties and receptors. Cell adhesion molecules, sometimes called sticky molecules, help the cells bind.

Once settled, a neuron sprouts an axon for sending signals to other brain cells, and numerous dendrites for receiving signals from others. In forming connections, neurons do not simply reach out randomly

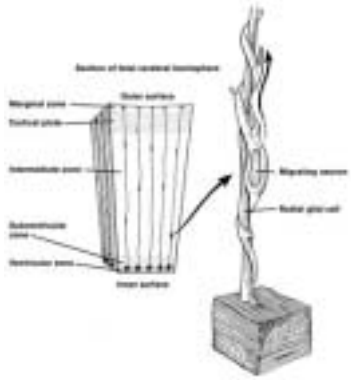

Fig. 4. Neuron climbing a glial cell: During development, neurons follow specific cues and migrate along glial cells (the support cells that act as the "road" on which the neurons travel) to their designated locations in the brain, spinal cord, and nervous system. Scientists say this journey, for some neurons, is like walking from New York to California. (image credit: Kathryn Born)

to the closest cells. They seem to be programmed to seek out specific targets. In some parts of the brain, such as the cerebral cortex, the cells even align themselves in the same way, axons pointing down and dendrites pointing up.The axons that send signals and the dendrites that receive them communicate for this purpose at specialized contact zones, where the sending axon physically connects to the dendrite. These specialized contact zones are called synapses. Although there is a thin gap between the axon and the dendrite at such connections, the chemical signals (neurotransmitters) from the axon can diffuse rapidly across it to deliver the signal to the dendrite. As the signal spreads from the cell body of the sending neuron, a wave of activity flows down the axon, caused by the movement of sodium ions from outside the cell into the axon. As the wave of activity reaches the nerve terminal at the synaptic contact point, calcium ions also enter the axon and trigger the release of the neurotransmitter. The neurotransmitters bond with receptors on the target cell, prompting a new electrical signal to surge through that neuron. In this fashion, brain cells can send many different messages to each other with varying degrees of urgency.Although most neurons connect to a limited number of other brain cells, some send signals to as many as 10,000. This web of communication helps explain the brain's vast computing power. Scientists are still trying to explain how so many connections are made, and so precisely, in the developing brain. In some cases, the distance an axon travels before reaching its target is astounding, as much as a thousand times the diameter of the cell itself. At other times, axons must twist and turn along their route. Some grow as long as a few santimeters. For starters, time determines, to a great degree, when a neuron will first sprout an axon and

begin making connections. We believe that neurons form the bulk of their connections during a particular period in their development, soon after they arrive at their destinations and sprout axons. At that time, they can make connections only with cells already in place. If other cells arrive later, the neuron will no longer be able to forge a link. Neurons that arrive early seem to connect to their neighbors. Later, when the communities grow in number, cells need additional help to find the right targets for their connections.

Typically, for instance, a fetus begins moving its arms and legs around the tenth week of development. At first these movements are uncoordinated and random. But gradually the fetus becomes more purposeful in its movements.The child's increasing ability to coordinate movements, which continues to grow after birth, is due to the gradual development and strengthening of the appropriate transmitters, receptors, and connections between all the cells involved.

Preparing for Birth. By month seven, electroencephalography (EEG) can detect fetal brain waves. The fetus can see and hear, although these senses are only in the earliest stages of development and will become much more refined outside the womb. During this last phase of development, the earlier processes of cell proliferation and migration continue to some degree, and synapses continue to form all over the brain. But two new processes begin in earnest: a pruning of unnecessary cells and connections, known as apoptosis, or programmed cell death, and the protection, known as myelination, of vulnerable neurons and connections.

Until this point, everything about brain growth has been about more: more cells, more axons and dendrites, more synaptic connections. And the result is more than the brain needs. The brain overproduces cells and synapses. Apoptosis provides balance. This large-scale elimination of neurons affects some parts of the brain more than others. Relatively few neurons in the spinal column die, as compared with five in ten motor neurons (which control muscle movement), and nine in ten cells in the cerebral cortex. How all this happens is still a matter of investigation and conjecture. We know that when a cell undergoes apoptosis, its DNA begins to fragment and it eventually dies. What is not as clear is what triggers apoptosis. One theory is that cells need growth factors in order to survive, much as people need nutritious meals on a regular basis. Once a neuron makes the right connections with other brain cells, it receives the growth factors it needs. Cells unable to make appropriate connections "starve" and die. Another theory is that neurons are preprogrammed to self-destruct but that exposure to growth factor inactivates the genes that contain these instructions [16].

In the final months of pregnancy, the brain also begins to protect itself. Around the eighth month of prenatal development, myelination begins; it will continue well into childhood. Myelin is a protective membrane produced by oligodendrocytes, which are types of glial cells. The membrane extends from the oligodendrocyte's body and wraps itself many times around an adjacent axon, forming layers. Myelin not only protects the brain cells; it helps them communicate by facilitating, and speeding, the transmission of their signals. Since electrical signals can enter and exit the axon only where it is exposed, the myelin covering ensures that those signals will pass quickly to the target brain cell. In multiple sclerosis, Guillain-Barré syndrome, and other conditions, the myelin covering is damaged; the axon is thus exposed to signals from neurons it normally does not communicate with, and the result is something like an electrical short circuit, causing loss of motor control and other problems [17].

Myelination occurs at different times in different parts of the brain. Generally, motor and sensory brain cells are protected first, before birth. The last area to be myelinated is the cerebral cortex, and that happens long after birth, in childhood. The process of myelination coincides with the development of more advanced and coordinated skills. Your child will become better able to control arm and leg movements, and will thus be better able to crawl and walk (fig.5) Over the same period the child's cerebral cortex becomes myelinated, he or she will start to form words, string them into sentences, and finally form abstract thoughts, one of the highest brain functions of all.

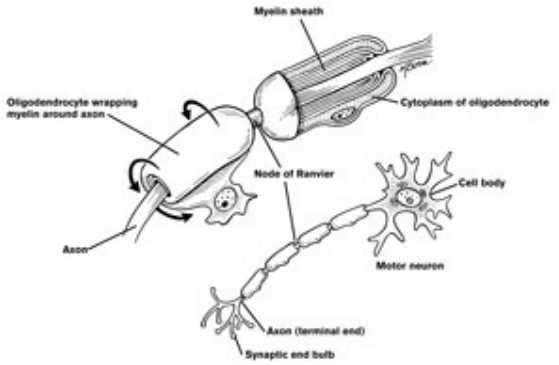

Fig. 5. Myelin—the white fatty insulation around axons—helps move the electrical impulses more efficiently. Myelin sheaths are formed by a type of glial (supporting) cell known as an oligodendrocyte. As the brain and nervous system develop in the embryo, the oligodendrocyte wraps around and around the axon in layers resembling an onion. Lengths of oligodendrocytes wrap around the entire length of the axon in a pattern much like links of sausage. (image credit: Kathryn Born)

S100 B protein and the developing brain in the fetus and early neonate. S100B and S100A6 (calcylin) are two members of the S100 Ca^{2+}-binding protein family and have been localized in the mammalian nervous system. However, information on their distribution in the human nervous system, especially in the developing human fetal brain, is scarce. In the present study, an

immunocytochemical method was used to examine the spatio-temporal protein expression patterns of S100B and S100A6 in normal human fetal hippocampus, entorhinal cortex and occipital cortex. Normal aged adult human brain specimens were also included for comparison. From week 15 onwards, an increase with advancing gestation age in both the number and staining intensity of S100B positive, astrocyte-like cells was found in the pyramidal layer of the hippocampus, while both the molecular and polymorphic layers showed similar S100B immunoreactivities all stages examined. A decrease in the immunoreactivities was found in the molecular layer of the aged adult hippocampus while other layers exhibited immunoreactivities similar to those of the late fetus. At week 15, the molecular, pyramidal and ganglionic/multiform layers of the entorhinal cortex also showed positive S100B immunoreactivities which were maintained throughout the rest of the gestation and in adult specimens. In the occipital cortex, the numbers of positive cells for all layers were about twofold higher than those found in the hippocampus and entorhinal cortex, and immunoreactivities detected in the granular layer increased from week 21, reaching a plateau at around week 27. S100B positive fibers were also found at week 30 but were not observed in aged adult specimens. S100A6 positive cells were on the whole fewer in number than those of S100B in the brain regions examined. The S100A6 immunoreactivities which were localized in some pyramidal neuron-like and some glial-like cells of the pyramidal and molecular layers of the hippocampus increased by midgestation and became weak in the late fetus and in aged adult specimens. Weakly stained S100A6 positive cells were also observed in the entorhinal cortex throughout the gestation and in aged adult cortex. S100A6 immunoreactivities were weak in the fetal occipital cortex [18].They were also localized in the glial-like cells of the aged adult occipital cortex. The differential spatio-temporal expression of S100B and S100A6 proteins suggests that the proteins play different roles in different brain regions during development and in adulthood.

Aim of the study: To determine whether S100â, an acidic calcium-binding protein previously demonstrated as a reliable indicator of a brain lesion, could be helpful in detection of brain distress in intrauterine growth-retarded (IUGR) fetuses, as well as in neonates born with neurological deficit.

Methods

A total of 119 neonates were recruited from the Neonatal Intensive Care Unit of the Pediatric Clinic divided into a control group (N=48) and an overall risk group (N=71). The risk neonates were categorized into subgroups according to their clinical presentation. A serum blood sample was obtained from each patient at 24h after admission: 4th and 7th S100B levels were measured using ECLIA (Electro-Chemi-Luminiscence Immuno Assay) method. The risk groups were actually the asphyxiated neoantes and premature infants(N=60) that were expected to have acute brain injury and neonates with IUGR and the one born with neurological deficit that are expected to have chronic brain affection.(N=11). We analysed neonates with chronic brain injyry due to intrapartum suffering of the brain according to S100B protein.

Table 1. Statistical descriptors for the S100B measurements in the group of term neonates with IUGR

Time Intervals	N	Mean	St Dev	Min	Max	Mean Rank
1st day	9	0,029	0,020	0,010	0,070	1,56
4th day	9	0,053	0,041	0,010	0,120	2,06
7th day	9	0,058	0,039	0,010	0,120	2,39

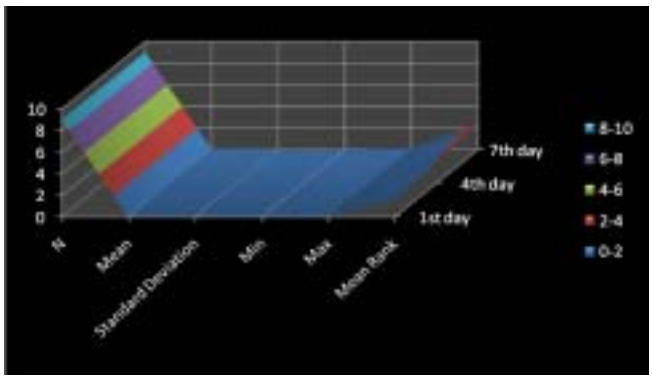

Results

The Friedman test value $\div^2$ (2;N= 9) is 3,46 (p>0,05) not statisticaly significant and therefore the within-subject differences in all measurment time-points are not significant.

Difference in the 3 measurment time-points within the neonates with ND.Because the data in the first two measurmnets time-points doesn't stand up to the parameters for repeated measures ANOVA we substitite with the Friedman test.

The Friedman test value $\div^2$ (2; N=3) is 0,67 (p>0,05) not statisticaly significant and therefore the within-subject differences in all measurment time-points are not significant.

Discussion

S100 B protein in a marker for acute brain injury. Elevated measures of S100 B protein in the neonates suffering intrapartum, even not significantly higher from the control group of the healthy neonates still shows that something was going wrong with the developing brain. The monitoring of the level of S100 B protein on the 3rd, and the 7th day and not elevating from the level measured the first day also represents that the damage was done prior to the delivery.

Conclusion

This study provides evidence that circulating S100â protein is increased in IUGR and the one with neurological defects fetuses and correlates with cerebral hemodynamics, suggesting that it may represent an index of cerebral cell damage in the perinatal period (although is not statistically significant as in asphyxtiated neonates where is a parameter odf early brain damage. In fact the score higher from the control group shows that even during the prenatal time if there is something going on with the brain S100B protein is rousen but in thios conditions it is because of the chronical discharge, while in asphyxtiated neonates it is due to acute insult.

Table 2. Statistical descriptors for the S100B measurements in the group of term neonates with ND(neurological deficit).

Time Intervals	N	Mean	St Dev	Min	Max	Mean Rank
1st day	3	1,733	1,086	0,990	2,980	1,67
4th day	3	1,620	1,504	0,220	3,210	2,00
7th day	3	1,890	1,904	0,300	4,000	2,33

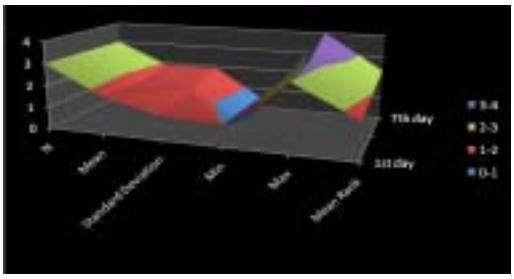

References

1. Tiu SC, Chan WY, Heizmann CW et all. Differential expression of S100 B protein and S100A in the human fetal and aged control cortex. Developmental Brain Research volume 119, issue 2, 2000, 159-68.

2. Freeman JM, Nelson KB. Intrapartum asphyxia and cerebral palsy. Pediatrics 1988; 82 : 240 - 9.

3. Hughes I, Newton R. Genetic aspects of cerebral palsy. Dev Med Child Neurol 1992; 34 : 80 - 6.

5. Hagberg B, Hagberg G, Olow I, van Wendt L. The changing panorama of cerebral palsy in Sweden. VII. Prevalence and origin in the birth year period 1987 - 1990. Acta Paediatr 1996; 85 : 954 - 60.

6. Hagberg B, Hagberg G, Beckung E, Uvebrandt P. Changing panorama of cerebral palsy in Sweden. VIII. Prevalence and origin in the birth year period 1991â•“1994. Acta Paediatr 2001; 90 : 271 - 7.

7. Volpe JJ. Intracranial hemorrhage: germinal matrix-intraventricular hemorrhage of premature infant. Volpe JJ eds. Neurology of the newborn 1995: 403 - 63.

8. Hypoxic-ischemic encephalopathy: clinical aspects. Volpe J eds. Neurology of the newborn 1995: 314 - 70.

9. Leviton A, Pagano M, Kuban KC, Krishnamoorthy KS, Sullivan KF, Allred EN. The epidemiology of

germinal matrix hemorrhage during the first half - day of life. Dev Med Child Neurol 1991; 33: 138 - 45.

10. Paneth N, Pinto-Martin J, Gardiner J, Wallenstein S, Katsikiotis V, Hegyi T, et al. Incidence and timing of germinal matrix/intraventricular hemorrhage in low birth weight infants. Am J Epidemiol 1993; 137: 1167 - 76.

11. Pezzani C, Radvanyi MF, Relier JP, Monod N. Neonatal electroencephalography of the newborn during the first twenty-four hours of life in full-term newborn infants. Neuropediatrics 1986; 17 : 11 - 1.

12. Rennie JM, South M, Morely CJ. Cerebral blood flow velocity variability in infants receiving assisted ventilation. Arch Dis Child 1987; 62: 1247 - 51.

13. Ilves P, Talvik R, Talvik T. Changes in Doppler ultrasonography in asphyxiated term infants with hypoxic-ischaemic encephalopathy. Acta Paediatr 1998; 87: 680 - 4.

14. Shortland DB, Gibson NA, Levene MI, Archer LN, Eveans DH, Shaw DE. Patent ductus arteriosus and cerebral circulation in preterm infants. Dev Med Child Neurol 1990; 32: 386 -93.

15. Palencia - Luaces R. Encefalopatia hipóxico-isquémica del recien nacido a término: recientes avances, marc a d o res de hipoxia y opciones terapêuticas. Rev Neurol 2000; 31: 617 - 23.

16. Volpe J. Neurology of the newborn, unit III, 4th edition, chapter 6 - 9, 2001.

17. Ferriero DM. Neonatal brain injury. N Eng J Med 2004; 351: 1985 - 95.

18. Macaia A. Muerte celular en la hipoxia-isquemia neonatal. Rev Neuro l 2000; 31: 784 -9.

UDK: 616.124.2-073.432.19

ECHOCARDIOGRAPHIC ASSESSMENT OF RIGHT VENTRICULAR FUNCTION

Grueva Lujza
University Clinic of Cardiology, Medical Faculty, Skopje, R.Macedonia

Abstract

This review will provide the practicing clinician with an understanding of the advantages and disadvantages of the available echocardiography techniques and aims to give some guidance on the most useful methods in specific clinical circumstances.

To allow optimal patient management an ideal measure of right ventricular performance should give an accurate objective assessment of function, be practicable in everyday clinical use and provide accurate prognostic information.

Key words: right ventricle, structural changes, echocardiography

Introduction

The demonstration of right ventricular dysfunction is important because it is often associated with different kind of diseases

Myocardial Infarction

Right ventricular dysfunction is present in at least one third of patients with inferior myocardial infarction and is associated with significant increase in mortality. Cardiogenic shock and the requirement for temporary transvenous cardiac pacing are more common in patients with right ventricular dilatation. Furthermore, by implying multivessel coronary artery disease, the presence of right ventricular dysfunction carries an adverse prognosis irrespective of infarct location. The demonstration of right ventricular dysfunction is important because it is often associated with a distinct clinical syndrome requiring specific management. In the presence of low cardiac output volume loading to restore left ventricular filling pressure is required. Inappropriate vasodilator and/or diuretic therapy may prove fatal. Information about right ventricular function can be applied in thrombolysis decision making when a relative contraindication is present. In fact, the findings of one study suggested that patients with inferior myocardial infarction derived no benefit form thrombolysis in the absence of right ventricular involvement. Cardiogenic shock commonly develops when ventricular septal rupture complicates myocardial infarction. In these circumstances shock appears to be more related to impairment of the right ventricular function than left ventricular function, territory of myocardial infarction or the extent of coronary disease.

Pulmonary Thrombo-embolic Disease

In the case of acute massive pulmonary embolism, right ventricular dilatation reflects the acute rise in pulmonary vascular resistance. Right ventricular failure causes a decrease in left ventricular pre-load which contributes to the fall of cardiac output. The increase in right ventricular after load leads to higher right ventricular oxygen demand and ischemia , which may even culminate in biochemically detectable infarction. There is a relationship between the degree of right ventricular overload and the proportion of the pulmonary vascular bed occluded as measured by the extent of perfusion defects and assessment of right ventricular function in patients with acute pulmonary embolism allows risk stratification with right ventricular dysfunction being a marker for both in-hospital and medium term mortality.

Diastolic dysfunction of right ventricle

Diastole is the period of ventricular relaxation incorporating periods of isovolumetric relaxation and early and late diastolic filing. Impaired diastolic function with relative preservation of systolic function is an early feature of right and left ventricular disease. The relevant echocardiographic methods will be described in the section on Doppler. Right ventricular diastolic dysfunction has been found to occur in patients with chronic pulmonary disease and pulmonary thromboemolism, systolic left ventricular failure and systemic sclerosis.

Right ventricular diastolic dysfunction has been shown to occur in patients with left ventricular dysfunction without other causes of right ventricular disease or concurrent pulmonary hypertension implicating ventricular interdependence as a mechanism. Conversely, it has long been recognized that when there is right-sided volume or pressure overload there may be a mechanical effect on the interventricular septum that can alter left ventricular systolic or diastolic function. This has been observed in chronic obstructive pulmonary disease, primary pulmonary hypertension and atrial septal defect and right ventricular infarction. The effect on LV function and clinical consequences may vary between individuals with similar degrees of right ventricular volume or pressure overload.

Discussion

Attempts to measure right ventricular dimensions echocardiographically were made soon after the development of ultrasound. M-mode measurements of right ventricular dimensions are, however, frequently not feasible and limitations became apparent, in particular the fact that dimensions were so heavily dependent on the angle traversed by the ultrasound beam across the ventricle.

Two-dimensional Imaging

Measurements of long and short-axis dimensions of right heart casts by two-dimensional imaging were quickly shown to be more accurate than M-mode techniques. Two-dimensional imaging allows estimation of the right ventricular dimensions, shape and wall thickness. In normal subjects, feasibility for assessment of right ventricular dimensions is high, with low inter-and- itraobserver variability. An eccentricity index, which is a measure of the degree of septal displacement, has been described. It is calculates as the ratio of the minor axis diameter of the left ventricle parallel to the septum to that perpendicular to it. Measuring this index at end-systole and end-diastole can provide a means of differentiating between right ventricular pressure and volume overload. Its clinical validity has been verified. Calculation of right ventricular area based on single plane echocardiographic methods correlate with right ventricular ejection fraction but assume a constant relationship between the dimensions of the ventricle in two planes. A combination of apical four-chamber and subcostal right ventricular outflow tract views is the most used. The value of two-dimensional echocardiography has perhaps been most clearly demonstrated in patients with pulmonary embolism. In this setting the feasibility is high. The echocardiographic features may be nonspecific or demonstrate dilatation of the proximal pulmonary arteries or disturbance of flow velocity in pulmonary Doppler recordings. Presence of thrombus in transit is required before other causes of right ventricular dilatation can be excluded, but normal right ventricular morphology is highly unlikely with a haemodynamically significant pulmonary embolism. Transoesopageal echocardiography has improved sensitivity and specificity compared with the transthoracic approach.

Doppler Echocardiography

With the introduction of Doppler echocardiography other parameters have been examined as measures of right ventricular performance. The widest application of Doppler to the right heart has been to estimate pulmonary artery systolic pressure by measuring the peak velocity of a tricuspid regurgitant jet and applying the modified Bernoulli equation. Although the relationship between pulmonary artery pressure and right ventricular function is complex and remains to be adequately elucidated, Doppler ultrasound is reliable in the detection of tricuspid regurgitation and a clearly defined continuous wave Doppler profile can be recorded in most patients. The application of echocardiogarphic contrast agents has further improved feasibility. The necessary estimation of right atrial pressure can be facilitated by a variety of means including clinical examination, tricuspid inflow parameters and inferior vena cava measurements. The tricuspid regurgitant profile on continuous wave Doppler can also be used to derive the rate of the right ventricular pressure rise in early systole which is a measure of right ventricular systolic function although measurements are influenced by pulmonary artery pressure.

Systolic time intervals such as duration the right ventricular pre-ejection period and ration of the pre-ejection period to the right ventricular ejection time have been investigated and found to correlate with similar intervals derived from tow-dimensional images and right ventricular ejection fraction. More recently pulmonary artery flow acceleration time has been investigated. Acceleration time is shortened in patients with pulmonary artery hypertension who may have a characteristic flow morphology phase with mid-systolic notching.

Diastolic function: Evaluation of the right ventricular diastolic function is conventionally based on the Doppler transtricuspid flow velocity profile. Variables measured include peak velocity of early filling(E velocity),peak velocity of late filling due to atrial contraction(A velocity), E/A ratio and deceleration time of early filling(Edt). The velocities across the tricuspid valve are significantly lower than across the mitral valve and tricuspid Edit is longer than mitral Edt. The tricuspid flow parameters do not appear to be as affected by age but respiration causes pronounced variability and measurement should be made at end-tidal or end-expiratory apnea. The normal filling pattern is affected by pre-load, afterload and compliance of the ventricular myocardium. In patients with pulmonary hypertension hypertrophic changes in the right ventricle may lead to an alteration in compliance with slowing of early right ventricular filling and augmentation of filling at atrial contraction. Edt is prolonged. Relevant information can also be derived by measuring the right ventricular isovolumetric relaxation time or from pulsed wave Doppler assessment of superior vena cava and hepatic venous flow. Right ventricular isovolumetric relaxation time is the period from pulmonary valve closure to tricuspid valve opening and is prolonged with abnormal relaxation and shortened with rapid relaxation or increased filling pressures. As could be predicted, changes in superior

vena cava and hepatic venous flow also occur during the respiratory cycle, both in health and disease, with significant variations as a result of changes in heart rate and loading conditions.

Three Dimensional Echocardiography

The advent of three-dimensional echocardiographic reconstruction removes the longstanding limitation imposed by standard imaging planes. Effectively, it eliminates the need for geometric assumptions of the complex right ventricular architecture and allows improved endocardial detection. The feasibility and reliability of three-dimensional echocardiographic imaging have been examined by in vitro and in vivo studies, and modern data collection and gating systems to minimize artefactual errors due to subject motion or respiration. Three-dimensional echocardiographic measurements of right ventricular volumes correlate closely with those of magnetic resonance imaging and permit reliable serial measurements. The accuracy and reproductibility of the technique improve the evaluation of the right ventricular hypertrophy. While three- dimensional echocardiography appears to be excellent for objective and accurate measurements of right ventricular geometry there is a paucity of information on its prognostic value, it is currently not widely available for routine use and time is required for post-acquisition reconstruction of the images.

Advances in Echocardiography of the Right Ventricle

Recently, the advent of more sophisticated imaging techniques has been of great benefit in more accurately quantifying right ventricular performance. Automated border detection methods have been employed in the assessment of global right ventricular function in patients with a variety of underlying pathologies. Estimation of changes in right ventricular dimensions based on this technique is in close agreement with contrast angiographic data. Colour kinesis can be used to quantitatively assess segmental right ventricular function and has been shown to be of value in a variety of pathologies affecting the right ventricle with excellent correlation between ventriculographic and colour kinesis measurements. Contrast echocardiography has been applied to the right ventricle in an attempt to overcome difficulties with endocardial border definition. In healthy subjects the correlation between echocardiographic and radionuclide derived right ventricular ejection fraction significantly increased and inter-observer variability improved with the addition of contrast. Tricuspid annular motion can be assessed easily using Doppler tissue imaging. An advantage is that measurement is independent of geometric assumptions and endocardial border tracing. This method has been accepted as a convenient means of quantitatively evaluating right ventricular systolic function and has been used as a diagnostic tool by number of groups. The sensitivity of tricuspid annular motion for the detection of early right ventricular dysfunction may be superior to more conventional imaging techniques and recent study has suggested that reduced systolic dysfunction as measured by radionuclide ventriculography. Intra-cardiac echocardiography is able to accurately delineate the entire right ventricular architecture in the invasive catheterization laboratory setting. Using a sequential catheter pull-back technique it has been demonstrated that right ventricular volume and function could be accurately assessed compared to a directly measured standard model.

Alternatives to Echocardiographic Evaluation of the Right Ventricle

Studies evaluating the usefulness of electrocardiography have been directed predominantly towards the detection of right ventricular hypertrophy and had low sensitivity and specificity. Angiocardiographic estimation of right ventricular volume is invasive and is not widely performed. Accurate measurements are reliant on the selection of appropriate orthogonal planes and accurate border tracing. A large variety of geometric figures have been used and many overestimate true volume probably due to problems with inclusion of right ventricular myocardium in heavily trabeculated regions of the ventricle. The use of radionuclide techniques to evaluate right ventricular function has been reviewed elsewhere. Both first pass and equilibrium techniques have been applied. Each has limitations and it is unlikely that the favourable mean inter-observer and inter-study variabilities for the estimation of left ventricular ejection fraction are applicable to the right ventricle. Magnetic resonance imaging provides a method of accurately visualizing the complex internal architecture of the right ventricular cavity and offers fast data acquisition. Time-volume curves of the right ventricle can be used to assess both systolic and diastolic function. It is now generally accepted that magnetic resonance imaging measurements are the gold standard for non-invasive estimation of right ventricular volume and wall mass but, unfortunately, availability is still limited and data is lacking on its prognostic value and use for serial assessment of right ventricular function.

Conclusion

Recent developments in ultrasound technology have overcome the limitations of simple M-mode and two-dimensional imaging and facilitated more accurate monitoring of disease progression. Competition from quantitative, highly reproducible techniques is emerging.

Magnetic resonance imaging has become the gold standard technique for evaluation of right ventricular volume and function but a balance able, accurately reflect right ventricular performance and are of proven prognostic value. Echocardiography provides a readily accessible tool for the evaluation of right ventricular function. It remains the first line investigation because of its ability to provide comprehensive information on right ventricular size, structure and function.

References

1. Ho SY, Nihoyannopoulos P. Anatomy, echocardiography and normal right ventricular dimensions. Heart 2006; 92(Suppl I): i2–i13. doi: 10.1136/hrt.2005.077875.

2. Innelli P, Esposito R, Olibet M, et al. The impact of ageing on right ventricular longitudinal function in healthy subjects: a pulsed tissue. Doppler study. Eur J Echocardiogr 2009; 10: 491-8.

3. McLaughlin VV, Archer SL, Badesch DB, et al. ACCF/AHA 2009 expert consensus document on pulmonary hypertension: a report of the American College of Cardiology Foundation Task Force on Expert Consensus Documents and the American Heart Association developed in collaboration with the American College of Chest Physicians; American Thoracic Society and the Pulmonary Hypertension Association. J Am Coll Cardiol 2009; 53:1573-619.

4. Sallach JA, Tang WHW, Borowski AG, et al. Right atrial volume index in chronic systolic heart failure and prognosis. JACC Cardiovasc Imaging 2009; 2: 527-34.

5. Fremont B, Pacouret G, Jacobi D, et al. Prognostic value of echocardiographic right/left ventricular end-diastolic diameter ratio in patients with acute pulmonary embolism: results from a monocenter registry of 1,416 patients. Chest 2008; 133: 358-62.

6. Otto C. The practice of clinical echocardiography. 3rd ed. Philadelphia : Saunders Elsevier; 2007.

7. Horton KD, Meece RW, Hill JC. Assessment of the right ventricle by echocardiography: a primer for cardiac sonographers. J Am Soc Echocardiogr 2009; 22: 776-92.

8. Papavassiliou DP, Parks WJ, Hopkins KL, et al. Three-dimensional echocardiography measurement of right ventricular volume in children with congenital heart disease validated by magnetic resonance imaging. J Am Soc Echocardiogr 1998; 11: 770-7.

9. Vogel M, Gutberlet M, Dittrich S, et al. Comparison of transthoracic three dimensional echocardiography with magnetic resonance imaging in the assessment of right ventricular volume and mass. Heart 1997; 78: 127-30.

10. Nesser HJ, Tkalec W, Patel AR, et al. Quantitation of right ventricular volumes and ejection fraction by threedimensional echocardiography in patients: comparison with magnetic resonance imaging and radionuclide ventriculography. Echocardiography 2006; 23: 666-80.

UDK: 616.133.33-007.64

ANEURYSMS OF THE ANTERIOR COMMUNICATING ARTERY

Chaparoski Aleksandar, Damjanovski S, Jovkovski S, Kostov M, Filipce V
University Clinic of Neurosurgery, Skopje, R. Macedonia

There are a lot of studies indicating the incidence of the cerebral aneurysms. Several large obductional studies show that 2-5% of population has cerebral aneurysms. The incidence is highest in 4th, 5th and 6th decade of life, and is lowest in the first three decades. In younger people the most common aneurysms, are those on ICA. Cerebral aneurysms are more frequent in women with ratio 2:1. Multiple aneurysms are found in 15-31% of the cases [1, 2].

Growth and rupture

Growth and rupture are explained mechanically and pathohistologically, based on structure of the wall, haemodynamics and extra mural factors. The axial blood flow, combined with permanent pulsing jet, are weakening the wall of the blood vessel, especially on its bifurcation, which leads to further growth and possible rupture of the aneurysms. In the same time, when the blood flow is exceeding normal velocity, there are occurrences of turbulences, which produce vibration with resonant effect. This effect is responsible for additional weakening of blood vessel wall. Intracranial pressure is the main extramural factor that stimulates faster rupture of the aneurysms. According to Normes decompression leads to rupture of the aneurysms. According to Carner the ruptures are most common on the fundus in 64% of the cases, on the lateral sacus in 10%, in the area of the neck only in 2% and unspecified in 24% of the cases. According to Valavanis the growth and delineation of the aneurysms depends from the structure of subarachnoidal cisterns. Namely, they are mainly built from calagenous trabecules which are connecting the blood vessel with the cisterns, the blood vessels to each other or connecting the walls of the cisterns between themselves. This brings to conclusion that aneurysms in different cistern might have different shape, size and direction of growth, even though the haemodynamics remains unchanged. The new technologies (3D CTA), enables easier following of the geometrical change of the unruptured sacular aneurysms, and its irregularity of the surface area, present the most important indicator for possible rupture [3, 4, 5].

Characteristics of the cerebral blood vessels

The arteries of central nervous system have origins from the large arteries of the neck and partially from the segmental branches of aorta and its branches. Cerebral arteries are entering the basal parts of the subarachnoidal space, distributing their branches both on surface and in the deep structures of the brain [3]. Cerebral arteries and their branches are situated in the subarachnoidal space, which formed from arachnoid membrane from one side and from pia mater from the other. Whole space is filled with cerebrospinal fluid. Some parts from this space are enlarged, representing subarachnoidal cisterns. Large arteries can be situated in one or more than one brain cisterns. For example arteria carotis interna (ICA) is situated in cysterna arteriae carotidis internae. Arteria basilaris is situated in cysterna prepontina and in cysterna interpeduncularis [3].

Brain arteries and their branches are fixed in subarachnoid space with arachnoidal trabecules. They are consisted of fibroblasts and their long extensions that are bonded dermozomes. Some of the trabecules are connecting arachnoid to pia and other are connecting the arachnoid with the adventitia of the blood vessels [3, 6].

In the subarachnoid space the arteries have their collaterals and terminal branches. Together they are forming the arterial network. Penetrant arteries and arterioles are rising from this arterial network penetrating in the brain parenchyma.

Structure of cerebral arteries wall

The wall of the cerebral arteries in consisted from 3 layers. The inner layer is called tunica intimae and is consisted of endothelium, sub endothelial space and lamina elastica interna. Tunica media is middle and thickest layer and contains smooth muscle cells connected with collagen and reticular fibers. Outer layer is called tunica adventitia. It contains fibroblasts, collagen fiber and nervous tissue [5].

Arteria cerebri anterior (ACA) rises laterally from the optic chiasm and is responsible for the vascularization dominantly of the medial part of the brain hemisphere. The artery is divided on proximal (A1) and distal (A2) segments. Proximal segment is beginning from the carotid artery to the anterior communicating artery (ACom). From the segment there are several branches such as rami hypothalamici providing vascularization for the rostral part of hypothalamus, arteria perforantes for the rostral parts of capsula interna and basal ganglia, and artery of Heubner (a. recurrents) for the vascularization of the same structures [2, 6, 7, 8].

Arteria communicans anterior (ACom) is short anastomotic blood vessel between the right and left ACA. There are several branches that are separating from ACom such as hypothalamic branches for the rostral part of hypothalamus as well as one larger branch of a. subcallosa that irrigates hypothalamus, septal area, corpus callosum and limbic cortex. Also a. mediana corporis callosi can be branched from ACom [2, 6].

Distal A2 segment of the ACA goes through interhemispheric fissure branching arteries mainly for the medial part of the hemisphere. In this segment besides rami olfactorii, rami gyri recti and artery of Heubner, there

are also several large lepromeningeal branches such as: a.orbifrontalis medialis, a. frontopolaris, a. frontalis interna anterior, media and posterior, a. paracentralis, a. parietalis superior, a. precunea [2, 6, 7, 8]

Cisterna lamina terminalis

In this cistern both A1 segments are situated as well as a. communicans anterior and proximal parts of A2 segments. Antero-inferior border is upper area of the optic chiasma, where it is connected with chiasmatic cistern. Rostrum of the corpus callosum is situated on the anterior-superior border. The postern border is lamina terminalis. On the lateral side the cistern is in communication with carotid cistern. In the olfactory area, arachnoid membrane is thicker. In center of the cistern there are fragile trabecular fibers which are connecting a. communicans anterior with lamina terminalis. Thick arachnoid fibers are also connecting the both A2 segments [2, 6].

Surgical treatment

Preoperative treatment

Following diagnostic procedures are made for every patient planned for operative treatment because of bleeding brain aneurysm on anterior communicating artery: CT scan of the brain, CT or Digital Subtractional Angiography. DSA is performed only in cases in which CT angiography is insufficient for the localization of the aneurysm and its relation to the surrounding structures (branches, perforators).

In our clinic barbiturates are applied in every patient. They are most efficient if they are applied before the period of temporary ischemia, which might be caused as a result of application of temporary clip. The effect of the barbiturates is proven for decreasing intracranial pressure by reducing the cerebral blood flow and cerebral metabolism [9, 10].

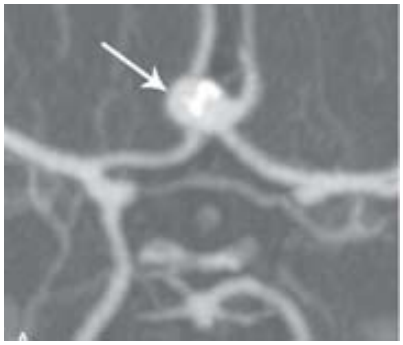

Fig. 1. Aneurism of a. communicans anterior

Pterional craniotomy

Firstly, arcus incision of the scalp is performed, in the area of the base of arcus zygomaticus (approximately 0.5 cm in front of the tragus), to the middle pupilary line. T e temporal muscle and its fascia are dissected and mobilized postero-basal for better presentation of the pterion. Then bone preparation is performed with three burr holes. Proximal part of linea temporalis is first and used as a key hole, the second is placed medially on squama frontalis and the third one on suturae squamosa. This enables better visualization of the fissurae Sylvi and upper temporal gyrus. Furthermore sphenoid ridge is drilled all the way through the lateral angle of fissurae orbitalis superior. The dura is cut in semicircle form [1, 2, 7, 11, 12, 13].

Vascular control

Vascular control is the highest priority, because it guarantees working under safe conditions. Dissection of the blood vessels starts from ICA, proceeding to ipsilateral A1 segment. Sometimes resection of gyrus rectus is needed. After that in largest number of cases exposition of the counter lateral A1 segment is possible. Dissection continues with exposition of the both A2 segments and both arteries of Heubner. After exposition of all these segments is done, neck of the aneurysm is shown. Eventual sacrificing of small perforators can result with serious consequences. Early evacuation of eventual intracerebral hematomas can provide extra space for manipulation [14, 15].

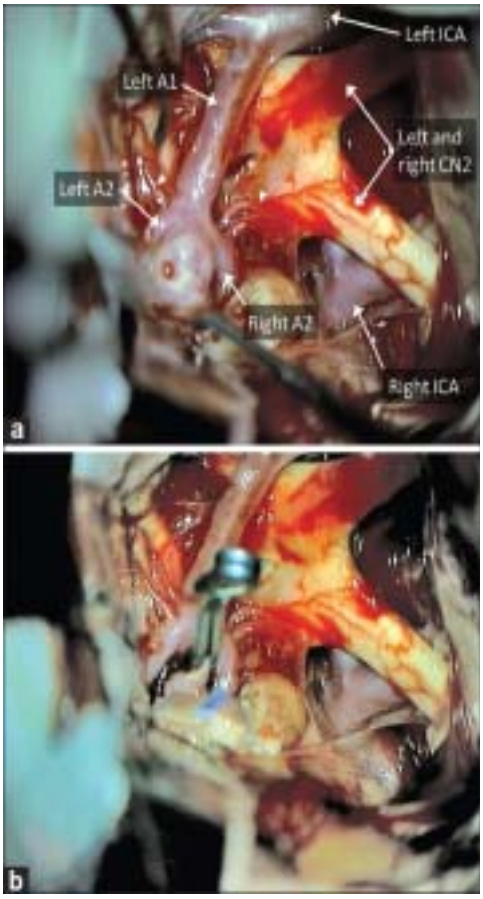

Fig. 2. Surgical clipping

Surgical clipping

The purpose of the intervention is excluding of the cerebral aneurysm from the blood circulation. One of the biggest problems is presence of the small perforators, which are frequently incorporated in the aneurysm neck. The size and form of the clip depend from the size and orientation of the aneurysm. Temporary clips are used for decreasing the intra aneurismal pressure. After the clipping any manipulation or traction of the blood vessels are unacceptable. Fenestrated clips are used for fibrosed or calcified aneurysms, because of the grater pressure produced by the tentacles of the clip. Residues from the neck can be clipped with additional clip. Alternatives for clipping of the neck are trapping parent occlusion or wrapping of the aneurysm [6].

Conclusion

The ACom aneurysms are one of the hardest for surgical treatment. Successful operative treatment is possible only with great knowledge of anatomy and precise surgical technique.

This principles together with basic principles of the vascular surgery, provides conditions for safe surgical clipping of the aneurysm without consequences in neurological status of the patient.

References

1. Andaluz N, Van Loveren HR, Keller JT, Zucarello M: Anatomic and clinical study of the orbitopterional approach to anterior communicating artery aneurysms. Neurosurgery 2003; 52 (5):1140-8.

2. Heros RC, Morcos JM. Neurosurgical education. Clin Neurosurg 2006; 53:26-37

3. Marinkovic S, Milisavljevic M, Antunovic V. Arterije mozga i kicmene mozdine: Anatomske i klinicke karakteristike. 1 ed. Beograd: Bit inzenjering; 2001.

4. Moret J, Pierot L, Boulin A, Castaings L, Rey A. Endovascular treatment of anterior communicating artery aneurysms using Guglielmi detachable coils. Neuroradiology 1996; 38 (8): 800-5.

5. Wolfe SQ, Baskaya MK, Heros RC, Tummala RP. Cerebral aneurisms learning from past and looking toward the future. Clin Neurosurgery 2006; 53: 153-78.

6. Yasargil MG. Microneurosurgery Vol I. Thieme Medical Publishers Inc: New York; 1987.

7. Figueiredo EG, Deshmukh P, Zabramski JM, Preul MC, Crawford N, Spetzler RF. The pterional-transsylvian approach: an analytical study. Neurosurgery 2006; 59 (4 Suppl 2): 263-9.

8. Hopf NJ, Perneczky A: Endoscopic neurosurgery and endoscope-assisted microneurosurgery for the treatment of intracranial cysts. Neurosurgery 1998; 43 (6):1330-6.

9. Lan Q, Gong Z, Kang D, Zhang H, Qian Z, Chen J, Huang H. Microsurgical experience with keyhole operations on intracranial aneurysms. Surg Neurol 2006; 66 (1): S2-9.

10. Pillai P, Sammet S, Ammirati M. Application accuracy of CT-based image-guided navigation of the temporal bone. Neurosurgery 2008; 63 (4): 326-33.

11. Figueiredo EG, Deshmukh P, Zabramski JM, et all. The pterional-transsylvian approach: an analytical study. Neurosurgery 2006; 59 (4 Suppl 2): 263-9.

12. Figueiredo EG, Deshmukh P, Zabramski JM, Preul MC, Crawford NR, Siwunawatn R, Spetzler RF. Quantitative anatomic study of three surgical approaches to the anterior communicating artery complex. Neurosurgery 2005; 56 (2 Suppl): 397-405.

13. Hsu FP, Clatterbuck RE, Spetzler RF. Orbitozygomatic approach to basilar apex aneurysms. Neurosurgery 2005; 56 (1): 172-7.

14. Kalavakonda C, Sekhar LN, Ramachandran P, Hechl P. Endoscope-assisted microsurgery for intracranial aneurysms. Neurosurgery 2002; 51 (5): 1119-26.

15. Mori K, Osada H, Yamamoto T, Nakao Y, Maeda M. Pterional keyhole approach to middle cerebral artery aneurysms through an outer canthal skin incision. Minim Invasive Neurosurg 2007; 50 (4):195-201.

UDK: 611.779:613.25

VISCERAL AND SUBCUTANEOUS FAT TISSUE DETERMINED BY ULTRASONOGRAPHY CORRELATED WITH ANTHROPOMETRIC PARAMETERS OF VISCERAL OBESITY

Ugrinska Ana[1], Trajkovska M[2], Miladinova D[1], Makazlieva T[1], Stefanova M[1]
Institute of Pathophysiology and Nuclear Medicine " Akademik Isak S Tadzer",
Medical Faculty, University " Ss. Kiril i Metodij" Skopje [1]
University Clinic for Gastroenterohepatology, Medical Faculty,
University " Ss. Kiril i Metodij" Skopje

Abstract

Obesity, defined as accumulation of excess body fat, represents major risk for a wide array of chronic diseases. The amount of visceral fat tissue represents a major risk factor associated with the metabolic syndrome. The amount of visceral fat is usually estimated by anthropometric parameters, although more precise measurements can be obtained by CT or MRI.

The aim of our study is to assess the correlation between the anthropometric parameters of visceral obesity and the visceral and subcutaneous fat tissue determined by ultrasound.

The study included 63 women with BMI between 23.6 and 50.2 kg/m2. Waist circumference, waist to hip and waist to thigh ratio were determined by standard methods. Ultrasound was used to perform measurement of subcutaneous fat tissue (SFT), defined as the thickness from the skin to the exterior wall of m. rectus abdominis, and visceral fat tissue (VFT) defined as distance between the aorta and interior surface of m. rectus abdominis measured 1 cm above the umbilicus.

The results from our study suggested that the waist circumference and waist to hip and waist to thigh ratio are well correlated with visceral fat tissue determined by ultrasound. The ratio between the SFT and VFT was correlated with waist to thigh ratio in overweight and normal weight subjects, but in obese subjects this ratio was not correlated to any of the anthropometric parameters and it seems useful to determine this ratio in these subjects by estimation of fat depots by ultrasound.

***Key words**: central obesity, visceral fat tissue, subcutaneous fat tissue*

Introduction

Obesity, defined as accumulation of excess body fat, represents major risk for wide array of chronic diseases. The distribution of the excess fat is also important in the pathogenesis of these chronic conditions.

Central obesity is one of the major pathogenic factors in the development of metabolic syndrome. The amount of visceral fat tissue (VFT) represents a major risk factor associated with the metabolic syndrome(1). Therefore the estimation of fat distribution is very important. Anthropometric measures such as waist circumference and waist to hip ratio (WHR) are easily obtained, but represent a crude estimation of central obesity and amount of VFT. More precise techniques such as CT and MRI measurement of VFT were developed over the past decades. However these techniques are not available in everyday clinical practice, nor are they applicable in large epidemiological trials. The ultrasonography is method that is more readily available and proved a good correlation in the assessment of VFT with CT which is considered a gold standard(2).

The aim of this study is to correlate the anthropometric parameters of visceral obesity in women with the visceral fat tissue and subcutaneous fat tissue (SFT) as determined by ultrasonography.

Material and methods

The study included 63 women, aged 21- 60 years with BMI range 23.6 – 50.2 kg/m2. The study group was selected from the participants of the project MONODIET which ran at the Institute of Pathophysiology and Nuclear Medicine, at the Medical Faculty in Skopje. The weight of the participants was obtained with digital scale with precision of 0.1 kg, with light indoor clothes and without shoes. The height was measured with a stadiometer to the nearest 0.5 cm.Waist circumference was measured with nonelastic plastic band over the umbilicus with subjects in a standing position. Hip circumference was measured between the anterior iliac spine and major trochanters. The thigh circumference was measured in the proximal end at the level that showed the largest circumference. The circumferences were measured to the nearest 0.5cm.Waist to hip ratio and waist to thigh ratio was calculated from the results of the measured circumferences, and the BMI was calculated using the values for the height and the weight.

The ultrasound measurements were performed at the University Clinic for Gastroenterohepathology at the Medical Faculty in Skopje. The measurements were performed with 3,5 MHz ultrasound probe one centimeter above the umbilicus without applying pressure to the abdominal wall. The distance between the aorta and the interior wall of musculus rectus abdominis was defined as representative of the amount of VFT, while the distance from the skin to the exterior wall of m. rectus abdominis was defined as SFT.

The subjects were divided in two groups with regard to the BMI. The first group comprised 24 normal weight or overweight subjects with BMI less than 30 kg/ m^2, and the second group had 39 obese subjects with

BMI greater than 30 kg/m^2. For the statistical analysis the Pearson correlation was used for the whole group and for the two subsets of patients divided by the BMI value. Probability values of $p < 0.05$ were considered statistically significant.

Results

The data obtained from the measurements of the fat tissues with ultrasonography for the whole group in correlation with anthropometric parameters are presented in tab.1.

The size of fat tissues 1 cm above the umbilicus was well correlated with BMI, waist and thigh circumferences. VFT showed stronger correlation with BMI and waist circumference than SFT. VFT showed correlation with the waist to hip ratio, and with waist to thigh ratio.

The ratio between SFT and VFT showed correlation only with waist to hip ratio, and weak correlation with waist to thigh ratio that didn't reach statistical significance.

The correlation between SFT and VFT and anthropometric parameters in subjects with BMI bellow 30 kg/m^2 are shown in table 2.

In this group of subjects SFT showed very strong correlation with BMI and thigh circumference. The strongest correlation of the VFT was with the waist circumference, W/H ratio and W/T ratio. The correlation of VFT with BMI was weaker than the one expressed by SFT. The SFT/VFT ratio showed correlation with thigh circumference and with W/T ratio.

Table 1. Correlation between fat depots, as determined by ultrasonography, and anthropometric parameters

	SFT		VFT		SFT/VFT ratio	
	r	p	r	p	r	p
BMI	0.37	<0.01	0.58	<0.01	-0.03	0.78
Waist Circumference	0.37	<0.01	0.63	<0.01	-0.10	0.3
Thigh Circumference	0.31	<0.01	0.33	<0.01	0.06	0.3
Hip Circumference	0.14	0.4	0.13	0.28	0.04	0.71
W/H ratio	- 0.019	0.8	0.52	<0.01	-0.3	<0.01
W/T ratio	0.094	0.46	0.39	<0.001	-0.19	<0.1

Table 2. Correlation between fat depots, as determined by ultrasonography, and anthropometric parameters in subjects with BMI bellow 30 kg/m^2

	SFT		VFT		SFT/VFT ratio	
	r	p	r	p	r	p
BMI	0.7	<0.001	0.42	<0.03	-0.17	0.4
Waist Circumference	0.27	0.19	0.62	<0.01	-0.38	0.06
Thigh circumference	0.46	<0.01	-0.39	0.05	0.5	< 0.01
Hip circumference	0.17	0.41	0.1	0.6	0.01	0.9
W/H ratio	0.18	0.3	0.66	<0.01	-0.45	0.02
W/T ratio	-0.07	0.7	0.77	<0.01	-0.58	<0.01

Table 3. Correlation between fat depots, as determined by ultrasonography, and anthropometric parameters in subjects with BMI above 30 kg/m^2

	SFT		VFT		SFT/VFT ratio	
	r	p	r	p	r	p
BMI	0.06	0.6	0.61	0.01	-0.18	0.2
Waist Circumference	0.06	0.6	0.6	0.01	-0.2	0.2
Thigh circumference	-0.07	0.6	0.4	0.01	-0.13	0.4
Hip circumference	0.03	0.84	0.06	0.6	0.02	0.8
W/H ratio	-0.17	0.2	0.41	0.01	0.27	0.09
W/T ratio	0.12	0.4	0.7	0.01	0.06	0.6

The correlation of SFT and VFT with anthropometric parameters in subjects with BMI greater than 30 kg/m^2 is presented in table 3.

The SFT in this subject group did not show correlation with any of the anthropometric parameters. The VFT on the other hand, presented with high correlation with BMI, waist and thigh circumference, W/H ratio and W/T ratio. The SFT/VFT ratio also did not correlate with the anthropometric parameters, except for the weak correlation with W/H ratio that did not reach statistical significance.

The hip circumference did not correlate with any of the anthropometric parameters in any of the groups.

Discussion

The estimation of the distribution of the fat tissue is very important in the assessment of the metabolic syndrome and cardiovascular risk. The most frequently used parameters are the anthropometrically derived ones like waist circumference, waist to hip and waist to thigh ratio. These parameters are easily obtained but they can't discriminate between the subcutaneous and visceral fat depots. The CT of the abdominal region has been established as gold standard for the assessment of fat distribution (3, 4). This method offers precise evaluation of various fat compartments. However, the CT is expensive and exposes the patients to ionizing radiation. There are several studies in the past decade that include the use of ultrasound as a more convenient method for the assessment of fat distribution. They all report good correlation of ultrasound method with CT (5, 6). However there is neither standardized method for the determination of fat distribution by ultrasound, nor are there standardized cut-off values. Our study has defined the thickness from the aorta to the interior wall of m. rectus abdominis as VFT, and the thickness from the skin to the exterior wall of the m. rectus abdominis as SFT. Both fat depots correlated well with BMI in the group as a whole. The SFT showed very high correlation with BMI (r 0.7, p< 0.0001) in the subgroup of subjects that had normal weight or were overweight, as oposed to the subgroup of obese subjects where the SFT did not correlated with BMI. On the other hand, VFT presented the highest correlation coefficient (r 0.61, p<0.001) with BMI in the subgroup of patients with BMI greater than 30 kg/m^2, although BMI was correlated with VFT in the group as a whole. It appears that BMI is influenced by the amount of subcutaneous fat in persons with normal or slightly elevated BMI, while in the group of obese subjects BMI is more influenced by the amount of visceral fat.

The waist circumference is considered to be one of the most important anthropometric parameters for the assessment of visceral obesity. There are number of studies that investigate the appropriate site for the measurement of this circumference and the proper cut-off values for visceral obesity(7, 8). The waist circumference represents the subcutaneous fat tissue and the visceral fat tissue. The study conducted by Roopkala et all confirmed that the waist circumference was the best predictor of the visceral fat accumulation in the abdomen when ultrasound was used as a method for the assessment of fat distribution (9). Our study showed high correlation of the waist circumference with VFT in all three groups (r 0.66, p<0.001), while the SFT showed weak correlation only when the group was analyzed regardless of the value for the BMI (r 0.37, p<0.01). These results suggest that the waist circumference is appropriate metric for the determination of the amount of visceral fat tissue.

The waist to hip and waist to thigh ratio showed correlation only with visceral fat tissue in all groups of subjects. The waist to hip ratio presented with higher correlation coefficient in the subgroup of subjects with BMI less than 30 kg/m^2 (r 0.66, P< 0.001) than in the subgroup of obese subjects (r 0.41, p<0.01). In the later subgroup the waist to thigh ratio seems to be better representative of visceral fat accumulation (r 0.77, p< 0.001).

The high proportion of visceral fat relative to the subcutaneous fat has been reported to predict more adverse metabolic profile in some studies (10). Therefore in our study we estimated the correlation of SFT/VFT ratio with anthropometric parameters. When the data from the whole group were analyzed only waist to hip ratio correlated with SFT/VFT (r - 0.3, p<0.01), while in the subset of subjects with BMI less than 30 kg/m^2 waist to thigh ratio emerged as better predictor of the ratio between SFT and VFT since the correlation coefficient reached – 0.58 (p<0.001).

Conclusions

The results from our study suggest that the waist circumference and waist to hip and waist to thigh ratio are well correlated with visceral fat tissue as determined by ultrasound. The ratio between the SFT and VFT was correlated with hip to thigh ratio in overweight and normal weight subjects, but in obese subjects this ratio was not correlated to any of the anthropometric parameters and it seems useful to determine this ratio in these subjects by the estimation of fat depots by ultrasound.

References

1. Jensen MD. Role of body fat distribution and the metabolic complications of obesity. The Journal of clinical endocrinology and metabolism 2008;93 (11 Suppl 1):S57–63.

2. Irooka MH, Umagi TK, Urose KK, Akanishi SN. A Technique for the Measurement of Visceral Fat by Ultrasonography: Comparison of Measurements by Ultrasonography and Computed Tomography. Medicine 2005;44 (8) 32-7.

3. Kvist H. Total and visceral volumes measurements with computed tomography men and women: predictive derived from in adult. Am J Clin Nutr 1988;48(6):1351-61.

4. Jang S, Lee CH, Choi KM, Lee J, Choi JW, Kim KA, et al. Correlation of fatty liver and abdominal fat distribution using a simple fat computed tomography protocol. World journal of gastroenterology: WJG 2011;17(28):3335–41.

5. Stolk RP, Wink O, Zelissen PM, Meijer R, van Gils a P, Grobbee DE. Validity and reproducibility of ultrasonography for the measurement of intra-abdominal adipose tissue. International journal of obesity and related metabolic disorders: Journal of the International Association for the Study of Obesity 2001;25(9):1346–51.

6. Gradmark AMI, Rydh A, Renström F, De Lucia-Rolfe E, Sleigh A, Nordström P, et al. Computed tomography-based validation of abdominal adiposity measurements from ultrasonography, dual-energy X-ray absorptiometry and anthropometry. The British journal of nutrition . 2010; 104(4):582-8.

7. Heshmat R, Khashayar P, Meybodi HR a, Homami MR, Larijani B. The appropriate waist circumference cut-off for Iranian population. Acta medica Indonesiana . 2010;42(4):209–15.

8. Bosy-Westphal A, Booke CA, Blocker T, Kossel E, Goele K, Later W, et al. Measurement Site for Waist Circumference Affects Its Accuracy As an Index of Visceral and Abdominal Subcutaneous Fat in a Caucasian Population. J Nutr 2010; 140(5):954-61.

9. Roopakala MS, Suresh A, Ashtalakshmi, Srinath, Ashok, Giridhar, Anand, Silvia WD. Anthropometric measurements as predictors of intraabdominal fat thickness. Indian J Physiol Pharmacol. 2009;53(3):259-64.

10. Taksali SE, Caprio S, Dziura J, Dufour S, Calý AMG, Goodman TR, et al. High visceral and low abdominal subcutaneous fat stores in the obese adolescent: a determinant of an adverse metabolic phenotype. Diabetes. 2008;57(2):367-71.

UDK: 616-002-022.782.11:616.132.2

CHLAMIDIA PNEUMONIAE INFECTION ASSOCIATED WITH CORONARY HEART DISEASE

Grdanoska Tatjana[1], Branko Jaglikovski[3], Beti Zafirova[4], Ljubica Georgievska-Ismail[2], Nikola Panovski[1]
[1]Institute of Microbiology and Parasitology, [2]University Clinic of Cardiology, [4]Institute of Epidemiology, [5]University Clinic of Infectious Diseases, Faculty of Medicine, University "Ss Cyril and Methodius", [3]AVICENA Laboratory, Skopje, Republic of Macedonia

Abstract

Atherosclerosis is a complex chronic disease comprising numerous factors that contribute to formation of atherosclerotic plaques. Recently, it has been suggested that chronic infections might be associated with CHD (5, 6), especially those that are due to *Chlamydia pneumoniae*, *Helicobacter pylori* and cytomegalovirus (CMV).

Aim

The aim of this investigation was to determine the frequency of immune response to *Chlamydia pneumoniae* in patients with acute coronary syndrome (ACS), patients with chronic coronary artery diseases (CAD), and healthy individuals who were the control group.

Material We used sera taken from three groups of subjects: 64 patients with coronary artery syndrome (ACS) comprising patients with unstable angina pectoris, myocardial infarction without elevation of ST segment, myocardial infarction with elevation of ST segment; 53 patients with coronary artery disease (CAD) and a group of 36 conditionally healthy individuals - the control group.

Results In the group of patients with acute coronary disease, the largest number and percentage of subjects (57 or 49.1%) had hsCRP antibody titer higher than 3 mg/L. Positive IgA antibodies were registered in only one subject from CG (titer 32) and in 21 (17.95%) patients with coronary disease, of whom 15 were low positive and 6 high positive. In the ACS group 15 (23.44%) patients were seropositive for these antibodies, 12 being with low seropositivity and the remaining 3 patients with high seropositivity. In the CCAD group 6 (11.32%) patients were seropositive for IgA antibodies, of whom 3 with low and 3 with high seropositivity. In the ACS group 33 or more than half of the subjects were seropositive for IgG antibodies. In the CCAD group seropositive for IgG antibodies were 20 (31.7%) subjects. . Regarding seropositivity in both subgroups of the study group, antibodies to cHeat Shock Protein-60 were detected in 9 (14.1%) patients with ACS and in 6 (11.3%) patients with CCAD.

Conclusion Our results have shown that increased IgA antibody titers for *C. Pneumoniae*, increased CRP values are predictors for coronary events, especially when their levels are persistently increased and not transitory.

Key words:*Chlamidia pneumoniae*, atherosclerosis, acute coronary syndrome, chronic coronary artery diseases

Introduction

Coronary heart disease (CHD) is one of the leading causes of death. In asymptomatic patients younger than 65 years, with initial myocardial infarction, the mortality rate was 80% (2). The disease is usually manifested as angina pectoris or myocardial infarction. The most common cause of CHD is atherosclerosis.

Atherosclerosis is a complex chronic disease comprising numerous factors that contribute to formation of atherosclerotic plaques (3). The exact mechanism of its onset is unknown, but generally it is accepted as a response to the damage of blood vessels endothelium (4). Several factors can cause damage, including:

- circulatory stress (hypertension),
- metabolic stress (hypercholesterolemia),
- immunologic disorder.

Damage causes lipoprotein infiltration, monocyte migration, increased thrombocyte adhesiveness, activation of active phase reactants (CRP, fibrinogen, sialic acid), inflammatory factors and growth hormone releasing factors. Proliferation of intimal smooth muscle cells and macrophages results in accumulation of lipids (*foamy cells*), which on the other hand form fat traces by constant accumulation. The final product is atherosclerotic plaque, which causes narrowing of the blood vessel lumen and compromising blood circulation and CHD symptoms.

Recently, it has been suggested that chronic infections might be associated with CHD (5, 6), especially those that are due to *Chlamydia pneumoniae*, *Helicobacter pylori* and cytomegalovirus (CMV). The mechanism that defines association of these organisms and CHD is their *direct effect* on the arterial vessels [(endothelial damage (7), proliferation of smooth muscle cells (8-10), local inflammation (7)], or *indirect effects* that are transmitted through circulation [chronic inflammation (11-17), cross-reactive antibodies (18-20), changes in the known cardiovascular risk factors (11, 21, 22)].

The aim of this investigation was to determine the frequency of immune response to *Chlamydia pneumoniae* and classic markers of myocardial damage: troponin, creatine kinase isoenzyme MB (CK-MB), myoglobin, hsCRP in patients with acute coronary syndrome (ACS), patients with chronic coronary artery diseases (CAD), and healthy individuals who were the control group.

Material and methods

We used sera taken from three groups of subjects: 64 patients with coronary artery syndrome (ACS) comprising patients with unstable angina pectoris, myocardial infarction without elevation of ST segment, myocardial infarction with elevation of ST segment; 53 patients with coronary artery disease (CAD) and a group of 36 conditionally healthy individuals - the control group.

Mean age of the control group of individuals was 59.03 ±10.2 years, of ACS patients 61.38 ± 10.15 years, and of CAD patients 62.8 ± 10.15 years.

Patients' diagnosis was made in line with the guidelines for evidence-based medicine at the Cardiology Clinic.

Analysis of patients' sera for detection of specific antichlamydial antibodies, detection of eventual anti-cHSP-60 antibodies as well as determination of inflammatory markers' levels - hsCRP and markers of myocardial injury (creatine kinase isoenzyme MB, troponin) was done with serological analysis at the Institute of Microbiology and Parasitology, Medical Faculty, Skopje.

Analysis for presence of elevated specific IgA and IgG antibodies to *C. pneumoniae* was done with Sero FIA tm-Chlamydia IgA, IgG (Savyon Diagnostics, Israel) MIF for detection of antichlamydial antibodies. This test is a semi-quantitative assay for detection of the three classes of antibodies of the three chlamydia species: *C. pneumoniae, trachomatis* and *psitacci* concomitantly in samples of human sera. This method is a world recognized for detection of specific antibodies. Recombinant enzyme immunoassay for quantitative detection of IgG antibodies - cHSP60-IgG- ELISA medac test was used for detection of antibodies to chlamydial Heat Shock Protein-60.

Analysis of patients' sera for presence of markers for myocardial damage (myoglobin, troponin, creatine kinase isoenzyme - CK-MB) along with determination of **hs**CRP level was done on the Immulite system, DPC (Diagnostic Products Corporation), Los Angeles, USA. The process is fully automated in the Immulite system.

Interpretation of the results

All subjects were examined for presence of elevated levels of specific IgA and IgG antibodies to *C. pneumoniae* using the world recognized reference method, the microimmunofluorescence method (MIF). Fluorescence presence in defined sera solutions of the subjects was a sign of a positive result.

CRP values in relation to cardiovascular events are interpreted as follows:

- value of **< 1 mg/l** is considered to be a low risk for cardiovascular disease;
- value of **3 mg/l** is considered to be a medium risk for cardiovascular disease;
- value of **> 3 mg/l** is considered to be a high risk for cardiovascular disease.

Myglobin level higher than **25 ng/ml** was considered to be elevated. **Creatine kinase isoenzyme MB** level higher than **5.7 ng/ml** was considered to be elevated. If IgG antibody titer to **cHSP60** was 1:50 it was considered to be negative and if it was equal or higher than 1:50 it was considered to be positive.

Statistical analysis

Statistical analysis of data was done using the statistical program SPSS (Statistical Package for Social Sciences), version 13. The final results of our analyses are expected to be completed within a year.

Results

We present the results obtained by statistical analysis of the data.

Table 1. Examined groups

Examined groups	Number	**%**
Control group (CG)	36	23,53
Coronary artery disease (CAD)		
Acute coronary syndrome (ACS)	64	41,83
Chronic coronary artery disease (CCAD)	53	34,64
Total	153	100

Table 2 and Figure 1 present the distribution of subjects from the analyzed groups regarding **hsCRP** antibody levels, analyzed as normal, low positive and high positive.

Table 2. Anti hsCRP levels in patients with ACS and CCAD and healthy subjects

Anti hsCRP		**CG**	**ACS**	**CCAD**	**Total**
Number	<1.0 mg/l	19	10	20	49
%		52.78	15.63	38.46	
Number	1.1 – 3.0 mg/L	7	15	14	36
%		19.44	23.44	26.92	
Number	>3 mg/L	10	39	18	67
%		27.78	60.94	34.62	
Total	All groups	36	64	52	152

CG/ACS Chi-square= 16.3 df=2 p=0,0029
CG/CCAD Chi-square =1.71 df=2 p=0,41
ACS/CCAD Chi-square =9.97 df=2 p=0,006

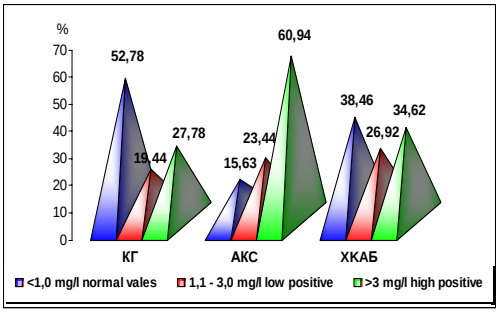

Fig. 1. Anti hsCRP levels in patients with ACS and CCAD and healthy subjects

Predominant subjects in the CG group (19 or 52.8%) were those with anti-hsCRP antibody titer less than 1.1 mg/L. In the group of patients with acute coronary disease, the largest number and percentage of subjects (57 or 49.1%) had hsCRP antibody titer higher than 3 mg/L. In the group of subjects with chronic coronary disease 39 (60.9%) patients had higher titer than 3 mg/L, whereas in the group of subjects with chronic coronary disease the most common finding was normal titer (20 or 38.5%).

Tested difference in the distribution of subjects with normal, low positive and high positive hsCRP antibodies was statistically significant between CG and patients with ACS, as well as between ACS and CCAD patients.

Table 3. IgA levels in patients with ACS, chronic CAD and healthy subjects

IgA		CG	ACS	CCAD	Total
Number	Negative	35	49	471	31
%		97,22	76,56	88,68	
Number	Positive	1	12	3	16
%	1: 32	2,78	18,75	5,66	
Number	High	0	3	3	6
%	positive	0,00	4,69	5,66	
	1:64				
Total	All groups	36	64	53	153

Chi-square=7.32 df=1 p=0.0068 CG/ACS
Yates correct. d=1.14 df=1 p=0.28 CG/CCAD

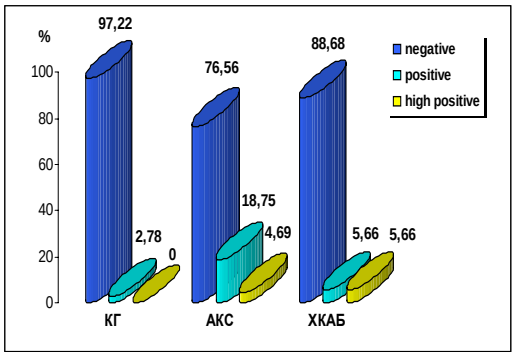

Fig. 2. IgA levels in patients with ACS, chronic CAD and healthy subjects

Table 3 and Figure 2 present the distribution of healthy subjects and patients with coronary disease regarding seropositivity for **antichlamydial IgA antibodies**. Positive antibodies were registered in only one subject from CG (titer 32) and in 21 (17.95%) patients with coronary disease, of whom 15 were low positive and 6 high positive. In the ACS group 15 (23.44%) patients were seropositive for these antibodies, 12 being with low seropositivity and the remaining 3 patients with high seropositivity. In the CCAD group 6 (11.32%) patients were seropositive for IgA antibodies, of whom 3 with low and 3 with high seropositivity.

There was a statistically significant difference between CG subjects and CCAD patients as well as between CG subjects and ACS patients due to more frequent detection of IgA class antibodies in patients with acute coronary events.

In the group of healthy controls 14 (38.88%) had **IgG** antibodies for *Chlamydia pneumonia*, among whom in 7 (19.4%) the titer was >1:64 and in the other 7 patients it was elevated (>1:128/256). Seropositive for IgG antibodies were 53 (45.3%) patients with coronary disease, of whom 22 (18.8%) were presented with high seropositivity.

In the ACS group 33 or more than half of the subjects were seropositive for IgG. Twenty (31.2%) had antibody titer >1:64 and 13 (20.3%) had antibody titer >1:128/256.

In the CCAD group seropositive for IgG antibodies were 20 (31.7%) subjects, of whom the majority (11 or 20.75%) were with low seropositivity and only 9 (16.9%) with high seropositivity.

Tested differences regarding IgG antibodies between healthy subjects and patients with coronary disease, between healthy subjects and patients with acute coronary disease and chronic coronary disease, as well as between patients with acute and chronic coronary disease were statistically non-significant (Table 4, Figure 3).

Table 4. IgG levels in patients with ACS, chronic CAD and healthysubjects

IgG		CG	ACS	CCAD	Total
Number	Negative	22	31	33	86
%		61.11	48.44	62.26	
Number	Positive	7	20	11	37
%	1:64	19.44	31.25	20.75	
Number	High positive	7	13	9	27
%	1: 128/256	19.44	20.31	16.98	
Total	All groups	36	64	53	153

CG/ACS Chi-square=1.49 df=1, p=0.22
CG/CCAD Chi-square = 0.01 df=1, p=0.91
ACS/CCAD Chi-square = 2.24 df=1, p=0.13

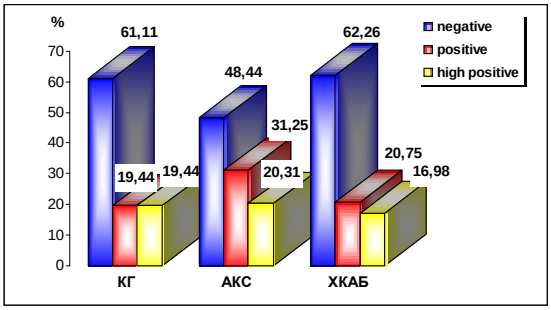

Fig. 3. IgG levels in patients with ACS, chronic CAD and healthy subjects

Table 5. Anti-cHeat Shock levels in patients with ACS, chronic CAD and healthy subjects

Anti-cHeat-Shock		CG	ACS	CCAD
Number	Negative	33	55	47
%		91.67	85.94	88.68
Number	Positive	3	9	6
%		8.33	14.06	11.32
Total	All groups	36	64	53

CG/CCAD Yates = 0.01 df=1, p=0.92
ACS/CCAD Chi-square = 0.19 df=1, p=0.66

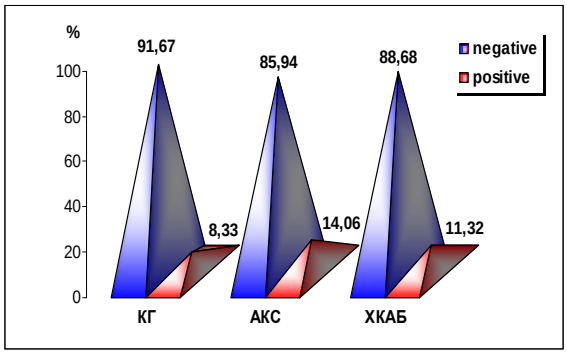

Fig. 4. Anti-cHeat Shock levels in patients with ACS, chronic CAD and healthy subjects

Seropositivity for chlamydial **cHeat Shock Protein-60** was registered in 3 (8.3%) control subjects and in 15 (12.8%) patients with CCAD. Regarding seropositivity in both subgroups of the study group, antibodies to cHeat Shock Protein-60 were detected in 9 (14.1%) patients with ACS and in 6 (11.3%) patients with CCAD.

Distribution of subjects with negative and positive anti-cHeat Shock Protein-60 between CG and CAD group, between CG and ACS group, between CG and CCAD, as well as between ACS group and CCAD was statistically not significant (Table 5, Figure 4).

Univariate analysis has confirmed the following significant risk predictors for acute coronary disease (ACS): anti-hsCRP antibodies and IgA antibodies for *Chlamydia pneumoniae* (Table 6).

Multivariate model for Binary regression analysis has confirmed hsCRP antibody levels higher than 3 mg/L to be independent significant factors or predictors for ACS.

Discussion

Risk factors for onset of coronary heart diseases (CHD) may be **modifying**: diet, smoking, hypertension, hyperlipidemia, diabetes mellitus, alcohol, poor physical activity, stress, or **non-modifying**: age, sex, race, genetic inheritance. Correction is possible only in modifying factors.

Subjects with **hsCRP** levels higher than 3 mg/L were at 12.05-fold significantly greater risk for coronary disease than subjects with hsCRP levels lower than 1 mg/L.

Our results are in agreement with those reported by Kiechl et al. (2001) (9), where the association between chronic infection and risk for onset of atherosclerosis was increased by higher CRP levels (>1mg/L). In the study conducted by Gattone et al. (2001) (3) concomitant seropositivity for *C. pneumoniae* and CMV was associated with increased CRP levels and risk for myocardial infarction. Today atherosclerosis is recognized as an inflammatory disease (Ross, 1999) (17) and several prospective studies have shown that CRP is a strong independent predictor for future coronary events (Rifai & Ridker 2001, Ridker *et al.* 2002) (15, 16). Subjects in our investigation with hsCRP levels ranging from 1.1 mg/L to 3 mg/L had a 4-fold increased risk for coronary disease compared to subjects with hsCRP levels less than 1 mg/L. On the other hand, subjects with hsCRP levels higher than 3 mg/L had a 7.4-fold significantly increased risk for coronary disease compared to subjects with levels less than 1 mg/L.

Several theories advocate for the direct effect influence on the contact with microorganisms. Microorganisms have the ability to bind to the endothelial cells' plasma membrane, penetrating into the cells, damaging them and altering their functionality. Microorganisms that have already entered into the

Table 6. Logistic regression analysis (Binary logistic regression) for ACS

Risk predictors	Univariate analysis		
	OR	95% CI	
hsCRP			
hsCRP (1)	4.070	1.252	13,243
hsCRP (2)	7.410	2.635	20.837
cHeat-Shock	1.8	0.455	7.127
IgA	10.714	1.352	84.925
IgG	1.673	0.729	3.837

* Sig. Dependent variable: healthy/ACS patients

endothelial cells might stay in a latent shape and might be reactivated during endothelial injury. It is believed that they increase the accumulation of smooth muscle cells and change the cellular lipid metabolism. According to another theory, microorganisms contribute to endothelial damage by realizing toxins.

Diagnosis of infection caused by *C. pneumoniae* is established with serologic tests for detection of IgM, IgG and IgA specific antibodies with the microimmunofluorescence (MIF) or ELISA test. Identification of *C. pneumoniae* -specific DNA is performed with PCR- reaction. MIF, the test we used in this investigation, is the most sensitive and most specific test since it enables differentiation between active and past infection according to the detected antibody class (5). Positive result is considered if there is a 4-fold rise in specific antibody titers (IgG>32, IgM>16, IgA>16) (5). Detection of IgA class correlates with chronic infection

In our investigation positivity for specific chlamydial IgA antibodies found in ACS patients significantly increased the risk (for 10.7 times) for acute coronary disease.

Several studies support the theory that elevated IgA antibody titers are a better marker for *C. pneumoniae* chronic infection than the IgG antibody titers. IgA titer is more strongly associated with CHD and is an increased risk for further coronary events (Saikku *et al.*1992, Miettinen *et al.* 1996, Mayr *et al.* 2000, Kiechl *et al.* 2001, Danesh *et al.* 2002) (18, 11, 10, 6, 2).

Persistent infection of the microorganism leads to chornic stimulation of inflammatory factors, the concentration of acute-phase reactants is increased as well as factor II, which are known predictors of CHD.

Two theories suggest an association between *C. pneumoniae* and CHD. *The first theory* takes into consideration production of chlamydial lipopolysaccharide immune complexes (8, 9) that are due to chronic Chlamydia infection. Circulating immune complexes may be responsible for tissue injury. *The second theory* explores intracellular capability of *C. pneumoniae* and its detection in coronary atherosclerotic plaques (19, 7, 12, 14, 1, 13. Microorganism incorporation into macrophages may result in chronic infection of atherosclerotic lesion thereby contributing to onset of atherosclerosis.

Conclusion

Our results have shown that increased IgA antibody titers for *C. Pneumoniae*, increased CRP values are predictors for coronary events, especially when their levels are persistently increased and not transitory. Coronary risk is associated with increased antibody titers and increased CRP levels. In conclusion, chronic infection and autoimmunity are associated with cardiovascular events in the examined subjects.

References

1. Campbell LA, O'Brien ER, Cappuccio AL, et al. Detection of *Chlamydia pneumoniae* TWAR in human coronary atherectomy tissues. J Infect Dis 1995;172:585-8.

2. Danesh J, Whincup P, Lewington S, Walker M, Lennon L, Thomson A, Wong YK, Zhou X & Ward M (2002) Chlamydia pneumoniae IgA titres and coronary heart disease. Prospective study and meta-analysis. Eur Heart J 23: 371–75.

3. Gattone M, Iacoviello L, Colombo M, Castelnuovo AD, Soffiantino F, Gramoni A, Picco D, Benedetta M & Giannuzzi P (2001) Chlamydia pneumoniae and cytomegalovirus seropositivity, inflammatory markers, and the risk of myocardial infarction at a young age. Am Heart J 142: 633–640.

4. Grayston JT, Campbell LA, Kuo CC, et al. A new respiratory tract pathogen: *Chlamydia pneumoniae* strain TWAR. J Infect Dis 1990;161:618-25.

5. Grayston JT, Kuo CC, Wang SP, Altman J. A new Chlamydia psittaci strain, TWAR, isolated in acute respiratory tract infections. N Engl J Med 1986;315:161-8.

6. Kiechl S, Egger G, Mayr M, Wiedermann CJ, Bonora E, Oberhollenzer F, Muggeo M, Xu Q, Wick G, Poewe W & Willeit J (2001) Chronic infections and the risk of carotid atherosclerosis: prospective results from a large population study. Circulation 103: 1064–70.

7. Kuo CC, Shor A, Campbell LA, Fukushi H, Patton DL, Grayston JL. Demonstration of *Chlamydia pneumoniae* in atherosclerotic lesions of coronary arteries. J Infect Dis 1993;167:841-9.

8. Leinonen M, Linnanmaki E, Mattila K, et al. Circulating immune complexes containing chlamydial lipopolysaccharide in acute myocardial infarction. Microbiol Pathol 1990;9:67-73.

9. Linnanmaki E, Leinonen M, Mattila K, Nieminen MS, Valtonen V, Saikku P. *Chlamydia pneumoniae* — specific circulating immune complexes in patients with chronic coronary heart disease. Circulation 1993;87:1130-4.

10. Mayr M, Kiechl S, Willeit J, Wick G & Xu Q (2000) Infections, immunity, and atherosclerosis: associations of antibodies to Chlamydia pneumoniae, Helicobacter pylori, and cytomegalovirus with immune reactions to heat-shock protein 60 and carotid or femoral atherosclerosis. Circulation 102: 833–9.

11. Miettinen H, Lehto S, Saikku P, Haffner SM, Rönnemaa T, Pyörölö K & Laakso M (1996)

Association of Chlamydia pneumoniae and acute coronary heart disease events in non-insulin dependent diabetic and non-diabetic subjects in Finland. Eur Heart J 17: 682–8.

12. Muhlestein JB, Hammond Eh, Carlquist JF, et al. Increased incidence of chlamydia species within the coronary arteries of patients with symptomatic atherosclerotic versus other forms of cardiovascular disease. J Am Coll Cardiol 1996;27:1555-61.

13. Ong G, Thomas BJ, Mansfield AO, Davidson BR, Taylor-Robinson D. Detection and widespread distribution of *Chlamydia pneumoniae* in the vascular system and its possible implications. J Clin Pathol 1996; 49:102-6.

14. Ramirez JA. Isolations of *Chlamydia pneumoniae* from the coronary artery of a patient with coronary atherosclerosis. Ann Intern Med 1996;125:979-82.

15. Ridker PM, Rifai N, Rose L, Buring JE & Cook NR (2002) Comparison of C-reactive protein and low-density lipoprotein cholesterol levels in the prediction of first cardiovascular events. N Engl J Med 347: 1557–65.

16. Rifai N & Ridker PM (2001) High-sensitivity C-reactive protein: a novel and promising marker of coronary heart disease. Clin Chem 47: 403–11.

17. Ross R (1999) Atherosclerosis—an inflammatory disease. N Engl J Med 340: 115–26.

18. Saikku P, Leinonen M, Tenkanen L, Linnanmäki E, Ekman MR, Manninen V, Mänttäri M, Frick MH & Huttunen JK (1992) Chronic Chlamydia pneumoniae infection as a risk factor for coronary heart disease in the Helsinki Heart Study. Ann Intern Med 116: 273–8.

19. Shor A, Kuo CC, Patton DL. Detection of *Chlamydia pneumoniae* in coronary arterial fatty streaks and atheromatous plaques. S Afr Med J 1992;82:158-61.

UDK: 616.36-006.311

PEDUNCULATED LIVER TUMOR: CAPILLARY HEMANGIOMA SURROUNDED BY FOCAL CIRRHOSIS, A CASE REPORT

Trajkovska Meri [1], Shumkovski A [2], Popova-Jovanovska R [1], Janevska D [1], Brzanov N [2]
Clinic of Gastroenterohepatology [1], Clinic of Digestive Surgery [2], Medical Faculty, Skopje, Republic of Macedonia

Abstract

Capillary liver hemangioma is a frequent finding during routine ultrasound examination, while hemangioma with focal cirrhosis, in a form of isolated liver tumor is rather rare. The finding of pedunculated liver tumor morphologically defined as a combination of cirrhotic liver tissue surrounding capillary hemangioma, is a unique case in our clinical practice.

A case of 44-years-old female patient, with left liver lobe tumor incidentally found by ultrasound, is presented. The unexpected microscopic finding of cirrhotic tissue in the tumor specimen obtained with fine needle biopsy under ultrasound control, was confirmed by second biopsy. Because etiological, clinical and biochemical findings supporting the diagnosis of cirrhosis were absent, another fine needle biopsy of the right liver lobe was performed, revealing a normal liver histology. Since contrast enhanced Computed Tomography (CT) confirmed the presence of pendulous tumor, the patient underwent abdominal surgery and tumor resection. Histological analysis of surgical specimen revealed the presence of capillary hemangioma surrounded by cirrhotic liver tissue.

The presence of liver tumors can be easily detected by "imaging methods" such as ultrasound and contrast-enhanced CT, but only biopsy specimen can determine the real nature of the lesion. Microscopic finding obtained from operative specimen compared to histological finding of specimen obtained by percutaneous fine needle biopsy is superior in determining the diagnosis of focal liver lesions.

Key words: liver tumor, focal cirrhosis, FNH, capillary hemangioma, histology

Introduction

The hepatic hemangioma is the most common benign tumor of the liver with the prevalence of 5-20% [1]. Hepatic hemangioma can occur any time, but it is considered as most frequent in people between their 30s-50s; women are more affected then men (60-80%). In the etiology of hemangiomas vascular malformations are thought to be the major problem, although correlation between hemangioma genesis and female hormones has been described, but disputed.

Hemangiomas are usually an incidental finding during imaging study of the abdomen performed for other reasons, and they cause no symptoms except the large ones (>5cm in diameter) which may cause mechanical complaints or coagulopathy [2, 3]. Most hemangiomas are small and due to absence of malignant transformation require no treatment. Sometimes follow-up is all that is advised.

Focal cirrhosis is described as a different entity among numerous focal lesions which can be detected in liver parenchyma. This lesion can occur in both sexes, usually solitary, but also multiple lesions can be found, varying in diameter from few millimeters to several centimeters. Focal cirrhosis has been most frequently recognized by the surgeons as an incidental finding at laparotomy, with completely normal appearance of the residual liver parenchyma. It has been discussed that it's a peculiar reaction of the liver to the injury, or it might have been congenital in origin. In one study single or multiple hemangiomas were detected in addition to the solitary cirrhotic nodule [4]. Recently focal cirrhosis has been described as focal nodular hyperplasia (FNH) of the liver parenchyma, but with still controversial pathogenesis of the lesion. It has been suggested that vascular anomaly preceded the development of FNH in terms that atrophy occurred in poorly perfused areas, with secondary development of nodules in well-perfused areas. More evidence suggested the role of oral contraceptives and endogenous estrogens in the growth of FNH [5, 6, 7].

The clinical importance of focal cirrhosis distinguishes this entity from solitary malignant hepatic masses, such as metastatic nodules or primary hepatocellular carcinoma (HCC).

A case report

A forty-four-year-old woman referred to Gastroenterology outpatient department, complaining of allergy and an occasionally mild abdominal discomfort. She had no history of alcohol or drug abuse (including oral contraceptives), neither any positive physical

findings. She has already been through numerous examinations, but no exact reason for her condition was revealed. Routine blood testing, liver and renal functional biochemistry, abdominal ultrasound, as well as different allergy tests were in normal range.

During repeated ultrasound examination, solid tumor mass 5 cm in diameter was found pending from the left liver lobe. The patient was admitted to the hospital for determining the diagnosis. Fine-needle aspiration biopsy of the tumor was performed under ultrasound guidance. Histology revealed four pieces of hepatic parenchyma, containing connective tissue and chronic inflammatory infiltrate, as well as cholangiole proliferations, surrounding hydropically degenerated hepatocytes arranged in nodules. Biopsy finding suggested a cirrhotic process.

Regarding patient's general condition and absence of clinical and biochemical signs indicating cirrhosis, she underwent several more tests. Serological viral markers for hepatitis B and hepatitis C, as well as immunological screen (anti-nuclear, anti-mitochondrial, anti-smooth muscle, anti-LKM antibodies) were negative. Serum iron and copper levels were in normal range. Gastroscopy excluded any signs of portal hypertension, while colonoscopy revealed a small pedunculated polyp (less then 1 cm), which was removed during the procedure. Tumor markers (Alfa-1-fetoprotein, CEA, CA19-9, CA-125, CA72-4) were in normal range. Finally, contrast enhanced computed tomography (CT) was performed. The CT finding confirmed the diagnosis of left liver lobe tumor.

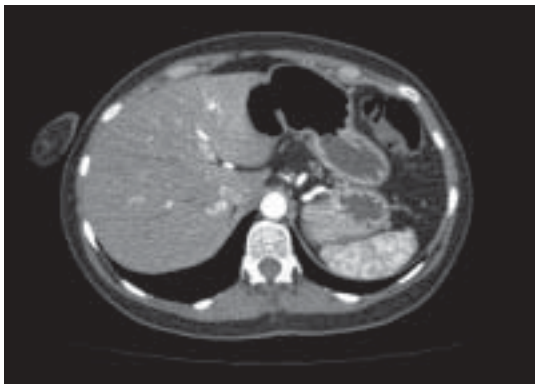

Fig. 1. CT scan of normal liver parenchyma

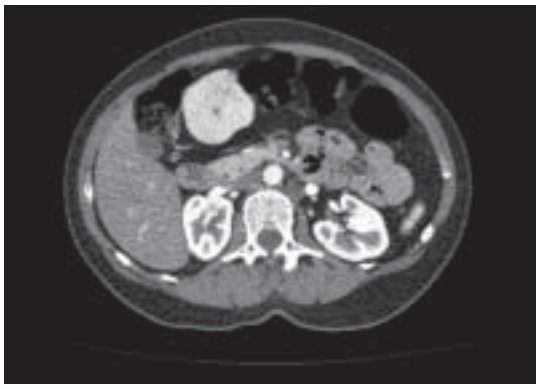

Fig. 2. CT scan of pedunculated left liver lobe tumor

In order to exclude any histological mistake, a second fine-needle biopsy of the tumor and a fine needle biopsy of the right liver lobe were also performed. The biopsy specimen from the tumor confirmed the diagnosis of cirrhotic liver, while the biopsy from the right lobe revealed a normal hepatic parenchyma, and this added to the diagnostic dilemma.

Atypical presentation and difficulty in diagnosis has made mandatory surgical exploration and resection of the lesion. The patient was transferred to the surgical department and during open surgery, except tumor, pending on massive tissue pendulum from the third liver segment, otherwise completely normal hepatic parenchyma was seen. Surgical resection of the third segment together with the tumor was made.

The macroscopically delivered pathological specimen tagged as "part of the left lobe" was 7.5 x4.5x4 cm in diameter. Part of the specimen revealed hemorrhagic zone 4x4 cm in diameter, while in the rest of the tissue a nodular structure of hepatic parenchyma was expressed.

Fig. 3. Macroscopic appearance of surgically resected tumor

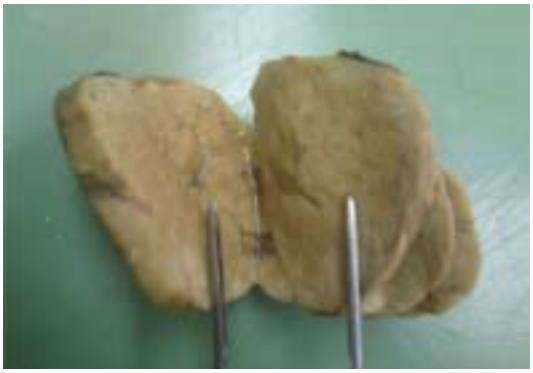

Fig. 4. Macroscopic appearance of focal cirrhosis (FNH)

Fig. 5. Macroscopic appearance of capillary hemangioma

The microscopic examination of the part described as hemorrhagic zone, depicted typical architecture of capillary hemangioma built from a multiple vascular channels limited by a single layer of endothelial cells.

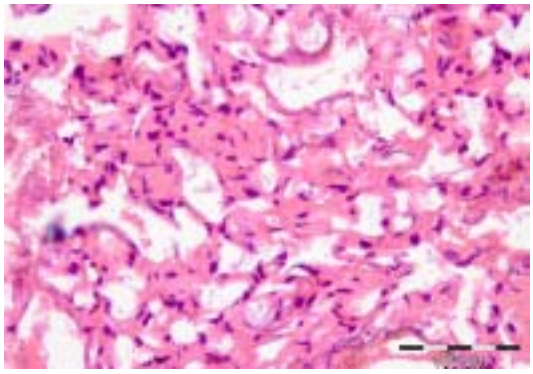

Fig. 6. Microscopic appearance of capillary hemangioma

The microscopic examination of the part described as nodular tissue revealed a hepatic parenchyma consisisting of porto-portal and centro-portal fibrous bridging, surrounding hyperplasic hepatic nodules. Chronic inflammatory infiltration accompanied by small bile ducts proliferation in portal spaces, was also expressed. The finding was typical for liver cirrhosis.

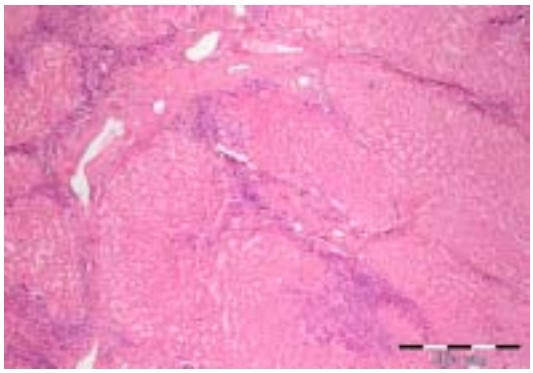

Fig. 7. Microscopic appearance of focal cirrhosis with fibrous septa and regenerative nodules

Our patient left the hospital uneventful, and came on a routine control a month later, in excellent condition with normal biochemistry and ultrasound findings.

Discussion

Hemangiomas are the most common benign liver tumors and may present as solitary lesions, or multiple only in 10% of patients. Hemangiomas are commonly seen at posterior liver segments, mostly in peripheral and subcapsular locations. Classified as small (capillary), or large (cavernous) vascular spaces, sometimes showing hyalinization and calcifications inside, they have no malignant potential. Hemangiomas can be easily diagnosed by imaging modalities, starting with real-time ultrasound, contrast-enhanced CT and Magnetic Resonance Imaging (MRI) (specificity of 90-100%, sensitivity of 90%). Technetium-99m labeled red-blood cells scintigraphy can be diagnostic for hemangiomas larger than 2 cm. Percutaneous biopsy is considered when the results of non-invasive test are inconclusive. Histology reveals large vascular spaces limited by a single layer of endothelial cells of a well-defined tumor. Blood flow inside these channels is extremely slow which explains the absent signal on color-Doppler ultrasound imaging [8].

Liver hemangiomas are divided in three groups: small (<1.5cm), medium (1.5-5cm) and large (>5cm) sized.

When small, they are usually asymptomatic, medium and large can cause symptoms, pain due to capsular stretch, infarction, or from pressure on adjacent structures such as the bowel. Bleeding or rupture of hemangioma can also occur. However, the treatment of large hemangiomas is still a matter of debate, except when they cause consumptive coagulopathy (Kasabach-Merritt syndrome) which is an absolute indication for surgical resection [9,10].

Although liver hemangiomas are easily recognized with imaging modalities in normal liver parenchyma, this finding becomes difficult to diagnose in cases of steatosis or liver cirrhosis. Detection and characterization of focal masses within a cirrhotic liver is challenging for ultrasonographers as well as for radiologists. The distinction from regenerative and dysplastic nodules, and especially from primary HCC is the most important task [11, 12].

Small hemangiomas which are fibrotic or hyalinized can be difficult to distinguish in cirrhotic liver. It has been recently reported that small hemangiomas and malignant hepatic lesions are difficult to be distinguished at multiphase helical CT [13,14]. In such cases percutaneous fine-needle biopsy under ultrasound guidance should be considered [15].

Focal nodular hyperplasia (FNH) and hemangioma are benign and generally asymptomatic hepatic tumors that are increasingly being discovered as incidental findings with the use of imaging tests. Recently in the literature, there is number of reports describing coexistence of these two kinds of tumors in the same liver. In one study 20% of the patients had FNH with one or more associated hepatic hemangiomas, while in another even in 23% of patients association between hemangioma and FNH was found [16, 17].

In our case report, there was an unusual association between focal cirrhosis (FNH) and capillary hemangioma. The hemangioma was surrounded by cirrhotic tissue, which condition aggravated the diagnostic procedure, leading to necessity of surgical intervention. Neither imaging procedures, nor percutaneous fine-needle aspiration biopsy could provide accurate diagnosis. Surgical excision of the tumor mass and patohistology from the specimen were mandatory for providing diagnosis.

Knowledge and recognition of this association is important, because the presence of liver masses with variable imaging characteristics sometimes can be falsely interpreted, which may potentially lead to inappropriate further evaluation and therapy.

However, resection of presumed benign liver tumors is justified, especially when preoperative diagnosis is not firmly established [18].

References

1. Weimann A, Ringe B, Klempnauer J, Lamesch P, Gratz KF, Prokop M, Maschek K, Tusch G, Pichlmayr R. Benign liver tumors: differential diagnosis and indications for surgery. World J Surg 1997; 21:983-90.

2. Caseiro Alves F, Brito J et al. Liver hemangioma: common and uncommon findings and how to improve the differential diagnosis. Eur Radiol 2007; 17:1544-54.

3. Erdogan D, Buschr OR, van Delden OM et al. Management of liver hemangiomas according to size and symptoms. J Gastroenterol Hepatol 2007; 22:1953-8.

4. Benz J, Bagenstoss AH. Focal cirrhosis of the liver: its relation to so-called hamartoma (adenoma, benign hepatoma) Cancer July 1953; 6:743-55.

5. Yi Pan, Zhao-Ming Wang, Ling-Jun Mou, Xiao-Dong Teng, Zhou-Jun Zheng, Li-Xiong Jing. Focal nodular hyperplasia of the liver pathological analysis of 11 cases. Hepatobiliary Pancret Dis Int 2004; 3(2):199-203.

6. Wanles IR, Wawdsley C, Adams R. On the pathogenesis of Focal Nodular Dysplasia of the liver. Hepatology 1985; 5:1194-200.

7. Nakamuta M, Ohashi M, Fukutomi T, Tanabe J, Hiroshige K, Nakashima O et al. Oral-contraceptive dependent growth of focal nodular hyperplasia. J Gastroenterol Hepatol 1994; 9:521-3.

8. Deitrich CF, Mertens JC et al. Contrast enhanced ultrasound of histologically proven liver hemangiomas. Hepatology 2007; 45:1139-45.

9. Yoon SS, Charny CK, Fong Y, Jarnagin WR at al. Diagnosis, management and outcomes in 115 patients with hepatic hemangioma. J Am Coll Surg 2003; 197:392-402.

10. Hanazaki K, Kajikawa S , Matsushita Am Monma T, Hiraguri M et al. Giant cavernous hemangioma of the liver, is the tumor size a risk factor for hepatectomy? J Hepatobiliary Pancreat Surg 1999; 6:410-3.

11. Roncalli M, Roz E, Coggi G, Di Rocco MG et al. The vascular profile of regenerative and dysplatic nodules of the cirrhotic liver: implications for diagnosis and classification. Hepatoogy 1999; 30:1174-8.

12. Lim JH, Cho JM, Kim EU, Park CK. Dysplastic nodules in liver cirrhosis : evaluation of hemodynamics with CT during arterial portography and CT hepatic arteriography. Radiology 2000; 214:869-74.

13. Cheng HC, Tsai SH, Chang CY. Hyalinized liver hemangioma mimicking malignant tumor at MR imaging (letter) AJR Am J Roentgenology 1995; 165:1016-7.

14. Kim T, Federle MP, Baron RL, Peterson MS, Kawanori Y. Discrimination of small hepatic hemangiomas from small hypervascular malignant tumors with two phase helical CT. Radiology (in press).

15. Caturelli E, Pompili M, Bartolucci F, Siena DA, Sperandeo M et al. Hemangioma like lesions in chronic liver disease: diagnostic evaluation in patients. Radiology 2001; 220(2):337-42.

16. Vilgrain V, Uzan F, Brancatelli G, Federle MP, Zappa M, Menu Y. Prevalence of hepatic hemangioma in patients with Focal Nodular Hyperplasia: MR Imaging Analysis. Radiology 2003; 229:75-9.

17. Mathieu D, Zafrani ES, Anglade MC, Dhumeaux D. Association of Focal Nodular Hyperplasia and hepatic hemangioma. Gastroenterology 1989; 97(1):154-7.

18. Belgithi R, Pateron D, Panis Y, Vilgrain V, Flejou VF, Benhamou JP, Fekete F. Resection of presumed benigned liver tumors. Br J Surg 1993; 80(3):380-3.

UDK: 616.711.1-006.2

MAXILLARY FOLLICULAR CYST WITH MESIODENS – CASE REPORT

Evrosimovska Biljana[1], Velickovski B[1], Zabokova-Bilbilova E[2], Dimova C[3]

[1]Department of Oral Surgery, "Ss. Cyril and Methodius University", Faculty of Dentistry, Skopje, Macedonia
[2]Department of Pedodontic Dentistry, "Ss. Cyril and Methodius University", Faculty of Dentistry, Skopje, Macedonia
[3] Faculty of Medical Sciences, Study of general Stomatology, University "Goce Delcev", Stip, Macedonia

Abstract

Previous studies have shown that follicular cysts are the most frequent cystic lesions around supernumerary teeth. Most often (in more than 90% of cases), they develop around the crown of a mesiodens in the upper jaw.

Follicular cysts may grow to a large size before they are identified. Most are diagnosed upon investigation of a tooth that has failed to erupt, or as an incidental radiographic finding, as they are usually not painful unless secondarily infected. Many patients first become aware of the cyst as a slowly enlarging swelling.

The purpose of this report is to describe a case of a large follicular cyst located in upper jaw with mesiodens in it.

Anyway, the most applied approach for the surgical removal of follicular cysts is enucleation of the entire cyst including both the epithelial layer and the capsule and removal of the associated tooth with appropriate management of the resultant dead space.

The prognosis for most histopathologically diagnosed follicular cysts is excellent, recurrence being a rare finding. In all dentigerous cysts, the microscopic features must be determined, to rule out its transformation in an ameloblastoma or, to squamouscell carcinoma.

Cooperation of a dentist, an oral surgeon, a pathologist, and other specialists can lead to early diagnose and prevention of further growth of a follicular jaw cyst, thus preventing substantial bone damage.

Key words: follicular cyst, mesiodens, therapy

Introdaction

Anomalies in tooth number, in which qualify hyperodontia is a result of increased proliferation of the tooth bud and is often hereditary during development, or the enamel organ divides into two or more parts during development [1].

Supernumerary teeth may have a typical shape with all morphological characteristics of normal teeth (*dens supernumeratus)* or an atypical shape, such as the rudimentary remains of the tooth bud *(dens accessorius)*. Most frequently supernumerary teeth are lateral incisors, the third premolar (parapremolar) and the fourth molar (paramolar) [2].

Of all atypical supernumerary teeth, the most frequent is mesiodens. It may be of different shape, but most often is conical [3].

In certain cases, where the supernumerary teeth are located deep (high) in the alveolar ridge and do not jeopardize the eruption and sequence of permanent teeth; they may stay undiagnosed for many years. In these cases, they are usually diagnosed by chance, during an X-ray examination for other reasons or when they cause certain complications [3].

Previous studies have shown that follicular cysts are the most frequent cystical lesions around supernumerary teeth. Most often (in more than 90% of cases), they develop around the crown of a mesiodens in the upper jaw [4, 5].

In terms of involved tissues, odontogenic cysts can be designated as follicular cysts, which enclose the crown of an unerupted tooth by expansion of its follicle and are attached to the neck of the tooth [6].

Usually, follicular cysts begin to develop through an accumulation of fluid between the remnants of the enamel organ and the subjacent tooth crown shortly after complete formation of the crown [7].

The expansion of follicular cysts is related to a secondary increase in cyst fluid osmolality as a result of passage of inflammatory cells and desquamated epithelial cells into the cyst lumen [8].

Follicular cysts may grow to a large size before they are identified. Most are diagnosed upon investigation of a tooth that has failed to erupt, or as an incidental radiographic finding, as they are usually not painful unless secondarily infected. Many patients first become aware of the cyst as a slowly enlarging swelling [9, 10].

Radiographically the cyst appears in association with the crown of unerupted tooth as well defined unilocular pericoronal radiolucency with a well corticated sclerotic margin, unless it becomes secondarily infected [11].

The histological features of follicular cysts may vary greatly depending mainly on whether or not the cyst is inflamed. In the non-inflamed dentigerous cyst, a thin epithelial lining may be present with the fibrous connective tissue wall loosely arranged. In the inflamed follicular cyst, the epithelium commonly demonstrates hyperplastic rete ridges, and the fibrous cyst wall shows an inflammatory infiltrate [12].

Different variants of the dentigerous cyst have been identified including the eruption cyst, lateral follicular cyst, and the inflammatory follicular cyst [13, 14].

The follicular cyst may enlarge and extend posteriorly to involve major portions of the ramus, or anteriorly into the body of the mandible to involve roots of adjacent teeth. It can also expand into the antrum displacing involved teeth posteriorly or toward the orbital floor [11].

The purpose of this report is to describe a case of a large follicular cyst located in upper jaw with mesiodens in it.

Case report

A 17 year old mail patient came to the Clinic of oral surgery by the University dental clinical centre "Sts. Pantelejmon" in Skopje by suggestion of his dentist. Patient reported pail from the right palatal side of the maxilla for a period of few days. Intraoral clinical examination revealed sing of soft tissue swelling with cortical plate expansion from the palatal side of the upper jaw in region from papillae incisive to canine (Fig. 1). Luxation of the right lateral incisive was observed.

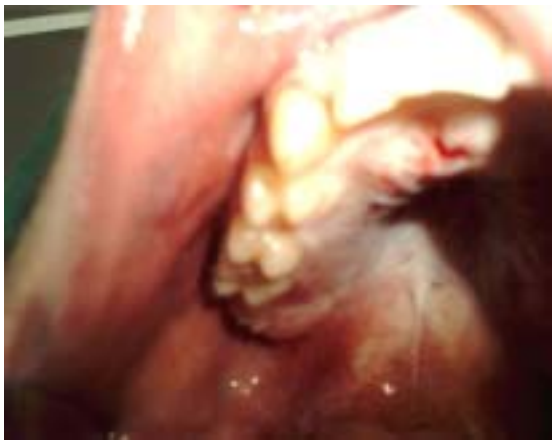

Fig. 1. Intraoral finding from the palatal side of the maxillae

Diagnosed orthopantomograph X-ray showed a large, circular well-defined and unilocular radiolucent are surrounding the supernumerary tooth localized between central and lateral incisor of the right side of the maxillae (Fig. 2).

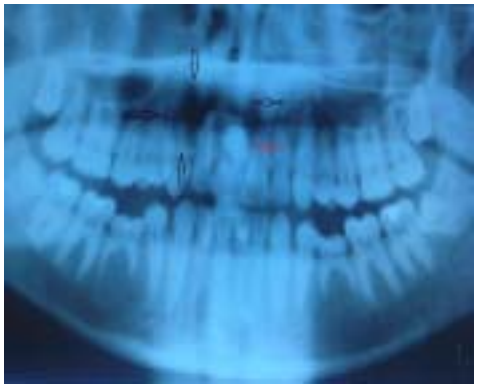

Fig. 2. Orthopantomograph X-ray (black pointer shows the dimension of the follicular cyst and the red pointer shows the supernumerary tooth)

The apices of the first and second incisive and canine appeared to project into the lumen of the cystic cavity, and they were not resorbed.

The clinical and radiological examination implied that, most probable, this was the case of a follicular cyst developed around the mesiodens.

There was a negative family history of dental anomalies or craniofacial, dermal or skeletal dysmorphologies.

After curing the primary inflammation with ordination of the antibiotics the surgical removal of the cyst was done.

According to the X-Ray and because of the localization of the prominence from the palatal side of the upper jaw, surgical approach was made from this area. In local anesthesia, mucoperiosteal flap was made from the papillae of maxillary first premolar of the right side through the margo gingivae of the canine, lateral and central incisive, avoiding papillae incisive and crossing contra lateral side until lateral incisive. There was a resorbtion of the palatal bone due to previous inflammation of the cyst. When mucoperiosteal lambo was lift, cyst and the supernumerary tooth revealed.

The cyst was completely detached from the bone and removed in a single piece together with the mesiodens through the cavity made with osteotomy. After this mucous membrane of the nose floor was show (Fig. 3, 4, 5).

After the removal of the cystical sac and wound debridement, large defect was filled with bone substituent

Fig. 3. Removed mucoperiosteal lambo with revealed and detached cyst from the bone with supernumerary tooth in it

Fig. 4. Supernumerary tooth (mesiodens)

Fig. 5. Removed follicular cyst

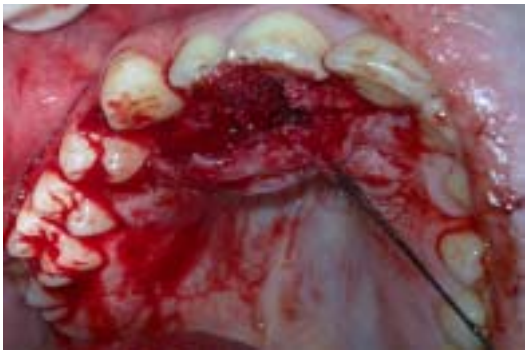

Fig. 6. Bone substituent (BioOss) filled the cystic cavity

(BioOss) in order to enhance bone restoration (Fig. 6). The flap was repositioned and sutured with single sutures.

After surgical removal, the material for pathohistological analysis was sent for analysis to the Institute of Pathology of the Faculty of Medicine, University St. Ciril and Methody in Skopje.

Macroscopic examination showed existence of cystic formation with dimensions 2 x 1.8 cm and thickness of the cyst wall of 0.2 x 0.3 cm, with present mesiodens. In the cyst lumen, granular necrotic cell debris was noticed. In four slices, the material was histopatologicly examinated.

According to microscopic intersections, the cyst wall showed edematous connective fibrous tissue, covered with multilayer flat cell epithelium. In some parts the epithelium was papilomatous proliferated, with mucoid changes of the stroma and rare lymphocyte infiltration, plasma cells and macrophages filled with haemosiderin pigment from previous haemoragie. The peripheral lining was with few bone trabecules. The histopathological examination corresponds with monolocular follicular cyst in the maxilla.

A standard protocol was conducted postoperatively, with cold compresses, antibiotic coverage, mushy food and adequate oral hygiene. The sutures were removed after seven days.

Radiographic examination a month after extraction revealed the circular radiolucent area had become smaller and that new bone had formed (Fig. 7).

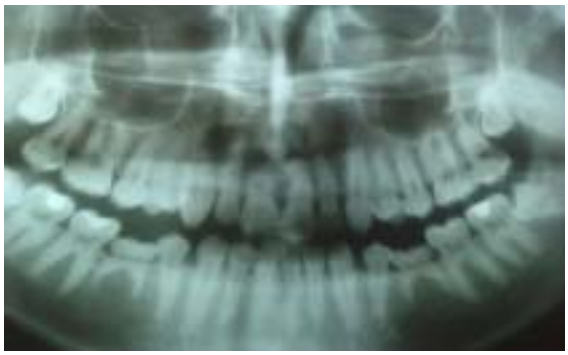

Fig. 7. Control orthopantomograph X-ray made after one month of intervention

Disscusion

Many follicular cysts are small asymptomatic lesions that are discovered serendipitously on routine radiographs, although some may grow to considerable size causing bony expansion that is usually painless until secondary infection occurs [8, 15].

These cysts can grow to very large size and can cause displacement of teeth, or in few cases it may remain relatively small. The age range varies widely, from 5 to 57 years [12, 16].

Research of Šarac Z et al. [17] showed that follicular cysts were diagnosed to almost the same number of male and female patients, so the opinion that a follicular jaw cyst occurs more frequently in male patients was not confirmed.

Follicular cysts, which occur in children, grow much faster. The larger the cyst gets, the smaller is its annual growth in diameter [18]. Ten years is required for a cyst to grow two centimeters in diameter [6].

If a radiolucent cystic lesion is discovered, then prompt referral for assessment and early surgical intervention is warranted. If it is hoped that the tooth will erupt, then marsupulization of the cyst may be appropriate. This will allow free drainage of the liquid content of the cyst, shrinkage of the cyst sac, and new bone formation [19].

When supernumerary teeth cause some orthodontic anomalies, it is necessary to extract them as soon as they are diagnosed. They are removed surgically and, in the case of a mesiodens, it is usually a simple intervention with a palatal approach, where the mesiodens is most often located [20].

However, if the tooth is located extremely deep (high) so that it jeopardizes the eruption of permanent teeth and their location in the dental arch, and the extraction might be accompanied with certain complications (the injury of adjacent erupted and unerupted teeth, nose, a large bony defect), then this intervention is delayed until adulthood. The reason for the delay is the fact that these interventions are stressful for children and they should be avoided, if unnecessary. It is advised to make control X-rays in regular intervals in order to detect cystical formations around such teeth or root resorption of adjacent teeth. In the event of these complications, it is advised to undertake a careful extraction with an adequate approach in order to preserve adjacent teeth and bone. The approach depends on the size and localization of the cystical lesions, as well as the condition of adjacent teeth and patient's age. Larger defects may be filled with any of bone substituents in order to enhance prosthodontic rehabilitation [3].

Anyway, the most applied approach for the surgical removal of follicular cysts is enucleation of the entire cyst including both the epithelial layer and the capsule and removal of the associated tooth with appropriate management of the resultant dead space [20].

Large follicular cysts may be treated with marsupialization when enucleation and curettage might otherwise result in neurosensory dysfunction or predispose the patient to an increased chance of pathological fracture [15, 21, 22].

If follicular cysts remain without appropriate treatment, they can become increasingly large in size and continue to expand uninhibited. This makes future management strategies more complex, increases the risk of pathological bone fracture, and compromises adjacent dento-alveolar structures. Follicular cysts appear to have a greater tendency to cause root resorption of adjacent teeth compared to radicular cysts or odontogenic keratocyst [10]. This may be derived from the potential of the dental follicle, from which the cyst originates, to resorb the roots of the deciduous teeth [23].

Transformation of the epithelial lining of the cyst into an ameloblastoma is also possible, as is rare carcinomatous transformation [24].

It is crucial then that the clinician fully investigate all teeth that fail to erupt at the expected time, and promptly initiate appropriate assessment and management of suspected cystic lesions [11].

If a supernumerary tooth is left undiagnosed and untreated in a timely manner, it may, in older age, cause various complications and prevent an adequate prosthodontic rehabilitation [3].

The prognosis for most histopathologically diagnosed follicular cysts is excellent, recurrence being a rare finding. In all dentigerous cysts, the microscopic features must be determined, to rule out its transformation in an ameloblastoma or, to squamouscell carcinoma.

Cooperation of a dentist, an oral surgeon, a pathologist, and other specialists can lead to early diagnose and prevention of further growth of a follicular jaw cyst, thus preventing substantial bone damage.

References

1. Beloica D i saradnici; Dechja stomatologija-praktikum, Kuca štampe, Zemun 2006.

2. Beloica D i saradnici. Decja stomatologija, Drasler Partner. Beograd 2005.

3. Tomic S, Jankovic S, Smrekic B, Đordjevic S. The consequences of an untimely diagnosed mesiodens - case report. Serbian Dental J 2007; 54.

4. Kusukawa J, Irie K, Morimatsu M, Koyanagi S, Kameyama T: Dentigerous cyst associated with a deciduous tooth: A case report. Oral Surgery, Oral Medicine Oral Pathology 1992; 73: 415–8.

5. Lustman J, Bodner L.; Dentigerous cyst associated with supernumerary teeth. Int J Oral Maxillofac Surg 1980; 17: 100.

6. Soames JV, Southam JC: Cysts of the jaws and oral soft tissues. In: Oral Pathology, 2nd Ed. Soames JV, Southam JC, Eds. Oxford: Oxford University Press 1993; 69-87.

7. Lautenschläger G, Gallina M, Ferreira O, Lara V. Primary Failure of Tooth Eruption Associated with Secondarily Inflamed Dental Follicle: Inflammatory Follicular Cyst? Braz Dent J 2007; 18(2): 144-7.

8. Browne RM, Smith AJ: Pathogenesis of odontogenic cysts. In: Investigative Pathology of the Odontogenic Cyst. CRC Press Boca Raton 1991; 88–109.

9. Murakami A, Kawabata K, Suzuki A, Murakami S, Ooshima T. Eruption of an impacted second premolar after marsupialization of a large dentigerous cyst: case report. Pediatric Dentistry 1995; 17: 5.

10. Shear M. Dentigerous (follicular) cyst. In: Wright, ed. Cysts of the oral regions. 3 rd ed. Oxford: Pergamon Press 1992; 75-98.

11. Farah CS, Savage NW. Pericoronal radiolucencies and the significance of early detection. Australian Dental Journal 2002; 47: (3):262-5.

12. Mhaske S, Ragavendra T R, Doshi J J, Nadaf I. Dentigerous Cyst associated with impacted permanent maxillary canine. People's Journal of Scientific Research 2009; 2 (2).

13. Prabhu NT, Rebecca J, Munshi AK. Dentigerous cyst with inflammatory etiology from a deciduous predecessor – report of a case. J Indian Soc Pedod Prev Dent 1996; 142: 49-51.

14. Wood NK, Goaz PW, Schwartz LJ. Pericoronal radiolucencies. In: Wood NK, Goaz PW, eds. Differential diagnosis of oral lesions. 3rd edn. St Louis: Mosby 1985; 357-78.

15. Johnson LM, Sapp JP, McIntire DN: Squamous cell carcinoma arising in a dentigerous cyst. Journal of Oral & Maxillofacial Surgery, 1994; 52: 987–90.

16. Shear M, Speight P: Cysts of the Oral and Maxillofacial Regions. 4th Edn; Blackwell Publishing Ltd 2007; 59-78.

17. Šarac Z, Periè B, Filipoviè-Zore I, Æabov T, Bioèiæ J. Follicular Jaw Cysts, Coll. Antropol 2010; 34(1): 215–9.

18. Shear M, Seward GR. Cysts of the oral region. Wright, Oxford, 1992.

19. Killey HC, Kay LW, Seward GR. Benign cystic lesions of the jaws, their diagnosis and treatment. Churchil Livingstone, Edinburgh, 1997.

20. Seward G. Treatment of cysts. In: Shear M, ed. Cysts of the oral regions. 3 rd ed. Oxford: Wright 1992; 227-56.

21. Banderas JA, Gonzalez MA, Ramirez F, Arroyo A. Bilateral mucous cell containing dentigerous cysts of mandibular third molars: Report of an unusual case. Archives of Medical Research 1996; 27: 327-9.

22. Kne•eviæ KA, Kne•eviæ G, Periæ B, Grgureviæ J. Marsupilization in the treatment of jaw cysts. Acta Stomatol Croat 2010; 44 (1): 53-60.

23. Struthers P, Shear M. Root resorption produced by ameloblastomas and cysts of the jaws. Int J Oral Surg 1976; 5: 128-32.

24. Regezi JA, Sciubba JJ. Cysts of the oral region. In: Regezi JA, Sciubba JJ, eds. Oral pathology; clinical pathologic correlations. 3rd ed. Philadelphia: WB Saunders Company 1999; 288-322.

INFORMATION FOR AUTHORS

These guidelines are in accordance with the "Uniform Requirements for Manuscripts Submitted to Biomedical Journals". (Complete document available at www.icmje.org)

Manuscripts are accepted for processing if neither the article nor any essential part, tables or figures, has been or will be published or submitted elsewhere before presenting in Acta Morphologica. This restriction does not apply to abstracts or press reports related to scientific meetings.

The Editors will consider both invited and uninvited review articles. Authors should detail how their work differs from existing reviews on subject in cover letter.

Manuscripts/General Guidelines

The manuscript should conform the guidelines set forth in the "Uniform Requirements for Manuscripts Submitted to Biomedical Journals", 5th edition, New Engl J Med 1997; 336 (4): 309–315.

Manuscript must contain no more than 5000 words. A cover letter signed by all authors should identify the person (post address, telephone number, and e-mail address) responsible for negotiations. Each author must sign a statement attesting that he or she fulfills the authorship criteria of the Uniform Requirements. Each author must significantly contribute to the submitted work.

Form of Manuscript

Three copies of each manuscript, along with a disk (see "Instructions for Electronic Manuscript Submission"), must be submitted in English, in double-spaced typewritten form with a 5-cm (2-inch) left margin. (Do not use "erasable" bond.) The text should be written in following sequence: Introduction, Methods, Results, Discussion, Acknowledgement, References, Tables, Illustrations and Figure Legends, Structured Abstract with key words and Condensed Abstract.

Page 1 should bear an article title, name(s) of the author(s) and institution where the work was done and a person whom proofs and reprint request should be sent, with complete address (including postal codes), telephone number and e-mail address (address for correspondence).

Tables should be typed neatly, each on a separate sheet, with title above and any notes below. All abbreviations should be explained. Do not provide duplicite information in tables and figures.

Illustrations should be submitted as clear glossy prints (two duplicate sets may be photocopied), with lettering large enough to be legible if reduced. The maximal final size of any figure in the printed journal will be 20 by 28 cm (8.25x11 inch). **On the back of each figure**, the name of author and the figure number should be writen, with the top indicated by an arrow. Each figure should have a separate, fully explicit legend; all parts of the figure and all abbreviations and symbols should be clearly defined. **Figure legends** should be typed on separate pages; figure numbers must follow their reference in text.

Drug names. Generic names should be used; trade names may be given in parentheses in the first mention, and generic names should be used thereafter.

Abbreviations. The list of abbreviations given in "Uniform Requirements for Manuscripts Submitted to Biomedical Journals" (section References) should be followed. For additional abbreviations, consult the CBE Style Manual (available from the Council of Biology Editors, 9650 Rockville Pike, Bethesda, Maryland 20814, U.S.A.) or other standard sources.

References

The journal complies with the reference style given in "Uniform Requirements for Manuscripts Submitted to Biomedical Journals". References should be cited in text by number and numbered in order they are cited. The reference should by written in double-spaced form at the end of the text, following the sample formats given below. For the abbreviations of journal names, refer to the List of Journals Indexed in Index Medicus (available from the Superintendent of Documents, U.S. Government Printing Office, Washington, D.C. 20402, U.S.A., DHEW Publication No. NIH 83-267; ISSN 0093-3821).

Provide all names of authors when fewer than seven: when seven or more, list the first three and add et al. Provide article titles and inclusive pages. The author is responsible for the accuracy of reference data.

Article:

1. Greenblatt DJ, Abernethy DR, Shader Jr RI. Pharmacokinetic aspects of drug therapy in the elderly (commentary).

Ther Drug Monit 1986; 8 (6): 249-55.

Book:

2.Mitchell JR, Horning MG, (editors). Drug metabolism and drug toxicity. 2nd ed. New York: Raven Press; 1984.

Chapter of book:

3. Kutt H, Pippenberg CE et al. Plasma clearance of nor-methsuximide in a uremic patient. 223-226. In: Levy RH, Pitlick WH, Meijer J, (editorss). Metabolism of antiepileptic drugs. New York: Raven Press; 1984. pp-1-25.

Internet:

Greenblatt DJ, Abernethy DR, Shader Jr RI. Pharmacokinetic aspects of drug therapy in the elderly (commentary). Ther Drug Monit 1986; 8 (6): 249-55. Available from:http://www.med.monash.edu.au/medical

Structured Abstract

A structured abstract should be provided on a separate page with no more than 250 words, presenting essential data in five paragraphs introduced by separate headings in following order: Objectives, Background, Methods, Results, Conclusion. Complete sentences should be used. All data in the structured abstract must be present also in the submitted text or tables. Three to five key words should be added. Terms from Index Medicus should be used.

Condensed Abstract (for table of contents)

A condensed abstract of no more than 50 words should be provided for the expanded table of contents, stressing clinical implications. Do not include data which are not present in the text or tables.

Proofs

Proof must be returned within 3 days; late return may cause a delay in publication. Please check text, tables, legends, and references carefully.

Instructions for Electronic Manuscript Submission

The preferred storage medium is a 3.5 inch disk in MS-DOS compatible format.

Each submitted disk must be clearly labeled with the name of the author, article title, journal title, type of the equipment used to generate the disk, word processing program (including version number), and filenames.

The manuscript submitted on a disk must be in the final corrected version and must agree with the final accepted version of the submitted paper manuscript. The submitted disk should contain only the final version of the manuscript. Delete all other material from the disk. Please follow the general instructions on style/arrangement and, in particular, the reference style as given in “Instruction to Authors”.

Note, that while the paper version of the manuscript must be presented in the traditional double spaced format, the electronic version will be typeset and should not contain extraneous formatting instructions. Do **not** use tabs or extra space at the beginning of a paragraph or for list entries. Do **not** indent runover lines in references. **Turn off** line spacing. Do **not** specify page breaks, page numbers, or headers. Do **not** specify typeface.

Take care to enter “one” (1) and lower case “el” (1)“, as well as “zero” (0) and capital “oh” (O) correctly.

Please note the following conventions on dashes: Use a single hyphen with space before it for a minus sign, use a double hyphen (with space before and after) to indicate a “long dash” in text, and a triple hyphen (with no extra space) to indicate a range of numbers (e.g. “23–45”).

Non-standard characters (Greek letters, mathematical symbols, etc.) should be coded consistently throughout the text. Please make a list and provide a listing of the used codes.

Authors agree to execute copyright transfer forms as requested. Authors should express all measurements in conventional units, with Systéme International (SI) units given in parentheses throughout the text. Conventional units should be used in figures and tables, with conversion factors given in legends or footnotes.

In electronic manuscript submission **text editor Word 6 or higher** is recommended (editor T602 is possible). Text should be **aligned left (not justified), without hyphenation, without bullets, numbering and underlines**, without extra hard returns at the end of line (only at the end of paragraphs). **One type of Word paragraph** should be used throughout the text. Word graphic experiments should not be used.

Word tables : do not use vertical lines, unless it is necessary. Provide tables as a separate file (do not place in text).
Excel graphs : provide as Excel file.

Word graphs : provide as a separate Word file (do not place in text!)

Table and graph legends should be provided separately at the end of the text.

Graphs should be processed for black and white print. **Graphs printed on laser or ink printers could not serve as templates– always provide original electronic files !**

Figures : provide original or scan. Scan to **600-800 dpi !** – set to B/W or line art.

Figures – black and white photos – provide high-quality original or scan to **350 dpi** !

Figures – color photos — provide high-quality original or scan to **350 dpi** !

Figures scanned to 72 or 96 dpi are not suitable for print !

On principle, **do not place scans in text !** Always provide original figures in tif or jpg format (with minimal compression). Placing scan in Word text causes a loss of quality!

Figure legends should be provided as a separate text file.

Do not place figures in PowerPoint – this application is meant for presentations and it is not possible to use it as a template for print !

Figures from digital camera should not be placed in text. Provide them in **tif** or **jpg** format (with minimal compression)!

Transciption of Macedonian Cyrillic Alphabet into English Latin

A a	A a	N n	N n
B b	B b	W w	Nj nj
V v	V v	O o	O o
G g	G g	P p	P p
D d	D d	R r	R r
\ |	G g	S s	S s
E e	E e	T t	T t
@ ‘	Zh zh	] }	K k
Z z	Z z	U u	U u
Y y	Dz dz	F f	F f
I i	I I	H h	Kh kh
J j	J j	C c	Ts ts
K k	K k	^ ~	Ch ch
L l	L l	X x	Dzh dzh
Q q	Lj Lj	[{	Sh sh
M m	M m		

On the basis of ISO Recomandation R-9-1968 International List of Periodical Title Abbreviations (1970)

EKSKLUZIVNA IZJAVA ZA OBJAVUVAWE NA AVTORITE KOI PODNESUVAAT TRUD
AN EXCLUSIVE STATEMENT FOR PUBLICATION IS NESSESARY WHEN SUBMITTING AN ARTICLE FOR PUBLICATION

Potvrduvam deka nitu eden materijal od ovoj rakopis ne e prethodno objaven ili daden za objavuvawe vo bilo koj vid, osven izvadok (apstrakt) od 400 zbora ili pomalku.

I hereby confirm that the materials of this manuscript have neither been previously published nor handed for publishing, except the abstract of 400 words or less.

SOGLASNOST ZA PRENOS NA PE^ATARSKI PRAVA
TRANSFER OF COPYRIGHT AGREEMENT

Pe~atarski prava na trudot so naslov:
Copyright to the article entitled:

_____

_____

koj }e se objavi vo spisanieto Acta Morphologica, se prenesuvaat na Acta Morphologica, no avtorite go zadr ‘ uvaat slednovo:

to be published in the journal Acta Morphologica is hereby transferred to the Acta Morphologica, but this authors reserve the following:

1. Site prava na sopstvenost osven pe~atarskite, kako pravoto na patent
   All proprietary rights other than copyright, such as the patent right.

2. Pravoto za upotreba na del ili site delovi od ovoj trud za svoja li~na rabota
   The right to use all of the parts of the article in future works of their own.

Ime i prezime
First and last name

Potpis
signature

_____
_____
_____

VA@I SAMO PO PRIFA]AWE NA TRUDOT
VALID ONLY AFTER THE ACCEPTANCE OF THE ARTICLE